Fischer-Type Carbene Complexes of Tris(1,4-phenylene)amines and Tri(2-furyl)phosphine

Nora-ann Weststrate,[†] Israel Fernández,*[,‡] David C. Liles,[†] Nina van Jaarsveld,[†] and Simon Lotz*[,†]

[†]Chemistry Department, University of Pretoria, 0028 Pretoria, South Africa

[‡]Departamento de Química Orgánica I, Facultad de Ciencias Químicas, Universidad Complutense de Madrid, 28040 Madrid, Spain

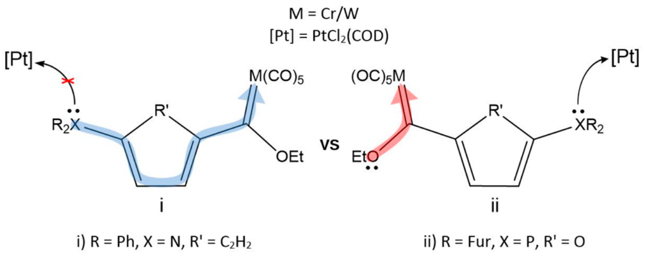

ABSTRACT: Novel chromium and tungsten mono- and multiethoxycarbene complexes were synthesized from tris(4-bromophenyl)amine and tri(2-furyl)phosphine substrates. A comparative study between the amine and phosphine multicarbene complexes revealed small differences between the respective compounds. In solution, an equilibrium situation was observed between the mono- and bis-carbene complexes of tri(2-furyl)phosphine. The monocarbene amine ligand differs from the analogous phosphine ligand in the way the heteroatom lone pair electrons are able to interact with the carbene functionality. Unlike for the phosphine, the greater electron delocalization of the amine affected the coordination ability of the ligand when reacted with $[Pt(COD)Cl_2]$. These properties of the monocarbene-carrying ligands were confirmed and supported by solid state structural studies, spectroscopic data, and density functional theory (DFT) calculations.

INTRODUCTION

It is already 50 years since the discovery of the first transition metal alkoxycarbene complex by Fischer and Maasböl[1] which kick-started research in areas associated with the metal−carbon double bond in particular and organometallic chemistry in general. Applications until now have been mostly devoted to organic transformations and template reactions of mononuclear Fischer carbene complexes.[2−8] In recent years, research in organometallic chemistry has shifted toward the synthesis and properties of macromolecules and applications of metal−organic frameworks, dendrimers, nanoparticles, polymers, etc.[9−12] Lately, Fischer carbene functionalities in small multicarbene−metal and multimetal−carbene complexes have come to the forefront and have been reported for biscarbene rods,[13−16] small clusters, or structured carbene macromolecules.[17−22] However, they lack the potential to impact in the above areas of material research because of challenging aspects associated with the synthesis of Fischer multicarbene complexes.[23] As a result, the incorporation of a large number of Fischer carbene functionalities into transition metal macromolecular frameworks remains largely unexplored.

In this study, our approach was first to synthesize Fischer carbene complexes as substituents of common ligands such as amines or phosphines to investigate the effect multiple Fischer carbene complexes will have on each other and on the electron lone pair on the amine-N and phosphine-P. Second, we wished to transport the Fischer carbene functionality into the vicinity of the coordination sphere of other metals via the ligand heteroatom, in effect exploring electronic and steric features of amine-N and phosphine-P ligands in alkoxycarbene complexes that play a role when Fischer carbene complexes are "piggybacked" into larger macromolecules. Two ligands were chosen which contain aromatic substituents known to stabilize electrophilic Fischer carbene carbons via π-electron delocalization,[24] namely, tris(4-bromophenyl)amine ($N(C_6H_4Br)_3$) and tri(2-furyl)phosphine ($PFur_3$). The triarylamine backbone has been known for being used as dyes in photonsensitizers and electroactive materials when attached to appropriate substituents[25−27] and displays charge transfer and reversible redox properties with metal-containing substituents.[28] Tris(4-bromophenyl)amine has three halogenated sites where site-specific carbene synthesis can be executed.[29] The particular phosphine that was chosen contains furyl groups which are known to be able to readily form Fischer carbene complexes at the acidic sites of the ring (position 2 and 5).[30] Even though a furyl group is known to be an electron-withdrawing group due to the influence of the oxygen atom in the ring, it is also an electron rich system due the presence of 6 π-electrons in a 5-membered ring.[31] The tri(2-furyl)phosphine ligand itself plays an important role as an ancillary ligand in coordination chemistry and in catalysts that facilitate metal−organic synthesis.[32] Thus, making use of the acidic properties of the protons at the 5-positions of the furyl rings, $PFur_3$ is ideal for Fischer carbene synthesis.

The carbene carbon atom is linked to the nitrogen or phosphorus atom via a π-conjugated phenylene or furylene linker and can affect the bonding properties of the nitrogen or phosphorus atoms in two possible ways (Figure 1). First, the strong electron-withdrawing properties of the pentacarbonyl-

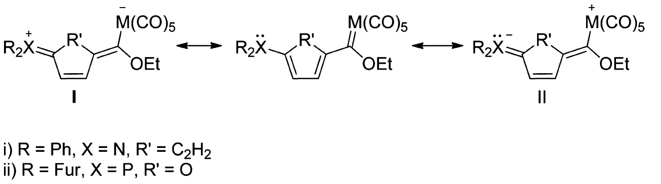

Figure 1. Illustration of movement of electron density between the heteroatom and the carbene carbon affording extreme resonance structures **I** and **II**.

metal−carbene moiety[33−36] can drain electron density away from the heteroatom via the π-conjugated spacer unit (**I**). This decrease in the availability of the LP electrons on the heteroatom will weaken the potential bonding properties of the ligand's donor-atom. Thus, the movement of electron density toward the carbene carbon can decrease the electron deficiency at the carbene carbon atom, which will have a stabilizing effect on the carbene carbon and lessen its reactivity.[37] Alternatively, coordination by the heteroatom to a second transition metal (**II**) can move electron density away from the carbene carbon enhancing the carbene's electrophilicity and reactivity.

RESULTS AND DISCUSSION

Amine Ligands. The lithium−halogen exchange reactions of triarylamines are readily achievable at low temperatures with *n*BuLi. Lithiation of $N(C_6H_4Br)_3$ and subsequent addition of group 6 metal carbonyls (Cr/W) gave the corresponding metal acylates which, after treatment with the alkylation agent Et_3OBF_4, yielded the neutral carbene complexes **1**−**3** (Scheme 1). The reaction afforded all three carbene complexes in addition to small amounts of the butylcarbene complex. The products were separated and isolated with a silica gel column in the sequence **1**, **2**, and **3**.

To maximize the yields for the synthesis of the multicarbene complexes, it was found that a stepwise addition of the second and third equivalents of *n*BuLi followed by metal carbonyl addition is required. Addition of three equivalents of the alkylating agent afforded the neutral mono-, bis-, and triscarbene complexes with the triphenyleneamine core, **1**, **2**, and **3**, respectively (Scheme 1).

The complexes that were isolated were bright orange with color intensity increasing with the number of $M(CO)_5$ units attached to the original amine by carbene complex formation. The differences in the optical properties of the three different compounds are small compared to the notable differences in moving from the known monocarbene complex, $[M\{C(OEt)\text{-}Fur\}(CO)_5]$, to the corresponding biscarbene complex, $[\{(CO)_5MC(OEt)\}_2Fur']$ (Fur′ = furylene), which changes from red to purple.[14,30] In several instances, one or two bromine atoms were replaced by a hydrogen atom, which complicated the ^1H NMR spectra of **1**. For instance, **1a**′ (the complex is analogous to **1a** with bromine atoms replaced by hydrogen atoms in 30% yield) was isolated and found to form on the addition of excess amounts of Et_3OBF_4 during the alkylation step of the synthesis. The isolated carbene complexes were characterized by spectroscopic methods and the molecular structures confirmed by single X-ray crystallography for **1a**′, **1b**, and **2b** (see below).

NMR analysis of complexes **1**−**3** focuses on changes in the chemical shifts of the protons and carbons with an increase of carbene substituents. The chemical shift values in the ^1H NMR spectra of the α-protons is indicative of the deshielding and electron-withdrawing properties of the carbene substituent. These chemical shifts are found furthest downfield and become more shielded on moving from **1** (**a**, 7.66; **b**, 7.75 ppm) to **2** (**a**, 7.47; **b**, 7.63 ppm) to **3** (**a**, 7.38; **b**, 7.57 ppm) in the ^1H NMR spectra. The downfield shifts of the aromatic protons of the rings with the carbene complex substituents in **1**(**a**,**b**)−**3**(**a**,**b**) are in general smaller (6.57−7.75 ppm) than that found in phenyleneamine ester compounds (7.21−8.03 ppm)[38] and even more so for that recorded for a nitro substituent in the 4-position of phenyleneamines (6.95−9.10 ppm).[39] The ^{13}C NMR spectra of the compounds reveal that the carbene carbon signals move downfield as the number of carbene substituents on the molecule increase: **1** (**a**, 332.6; **b**, 308.6 ppm), **2** (**a**, 337.9; **b**, 311.1 ppm), **3** (**a**, 337.9; **b**, 312.6 ppm). In the ^{13}C NMR spectra, metal−carbonyl resonances are metal-sensitive but are insensitive to the number of carbene substituents and

Scheme 1. Synthesis of Triphenyleneamine Mono(1)-, Bis(2)-, and Triscarbene(3) Complexes

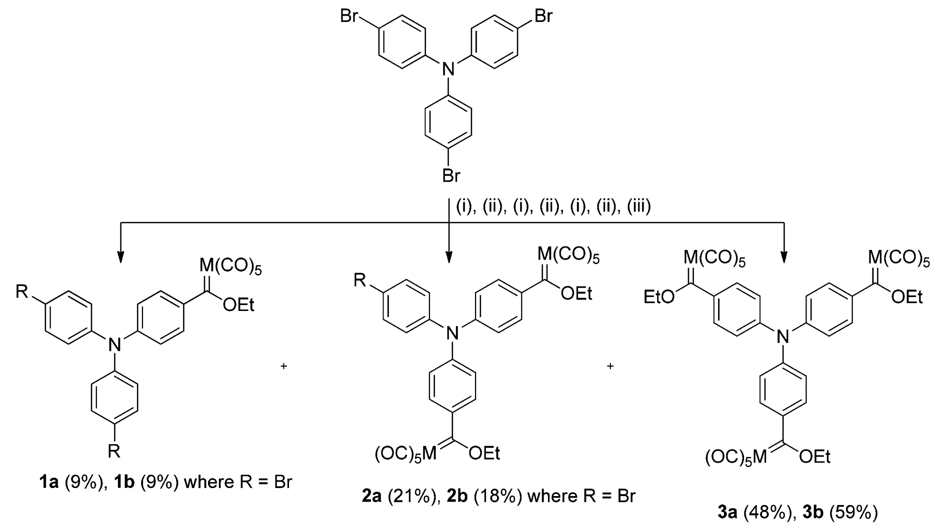

1a (9%), **1b** (9%) where R = Br

2a (21%), **2b** (18%) where R = Br

3a (48%), **3b** (59%)

M = Cr(**a**), W(**b**)

(i) 1.2 eq *n*BuLi, THF, -78°C, (ii) 1 eq $M(CO)_6$, -50°C, (iii) 3.9 eq Et_3OBF_4, CH_2Cl_2

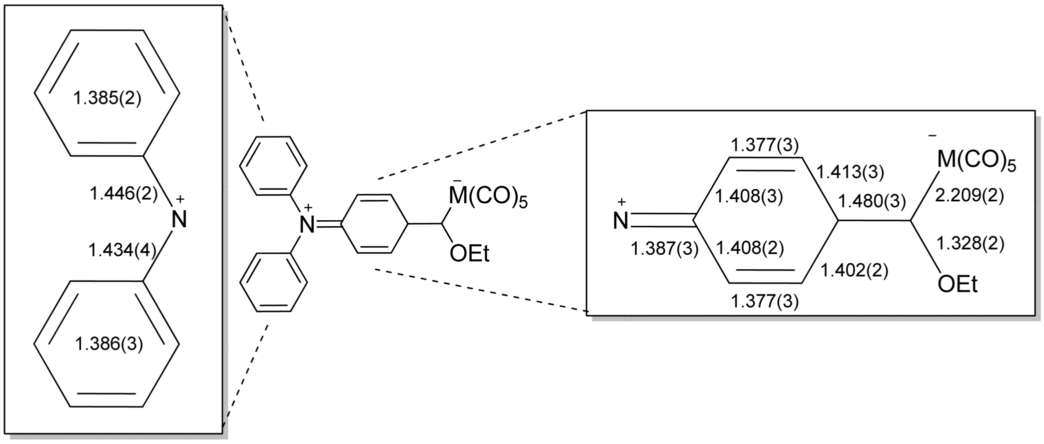

Figure 2. Selected bond lengths of **1a**′ showing alternating longer−shorter bond distances in the phenylene linker between the amine-N and carbene-C atoms.

give similar δ-values for **1**, **2**, and **3**. The same is true for the vibrational frequencies in the IR spectra of **1**, **2**, and **3**.

A comparative study of the bond distances in the solid state structures of **1a**′, **1b**, and **2b** indicate extended conjugated systems that stretch from the amine nitrogen to the carbene carbon atom (Figure 2). Compound **1a**′ reveal angles involving the central nitrogen atom that deviate only slightly from 120°, which indicates that the nitrogen lies in a flat plane with the phenylene carbons and the carbene carbon atom in the 4-position (Figure 3). The bond angles around the nitrogen atom closely resemble an sp^2-hybridized atom with the lone pair in a p-orbital. The latter is favorably oriented perpendicular to the plane of the ring to participate in the π-interaction with the bridging 1,4-phenylene π-cloud and the empty p_π-orbital of the carbene carbon atom.

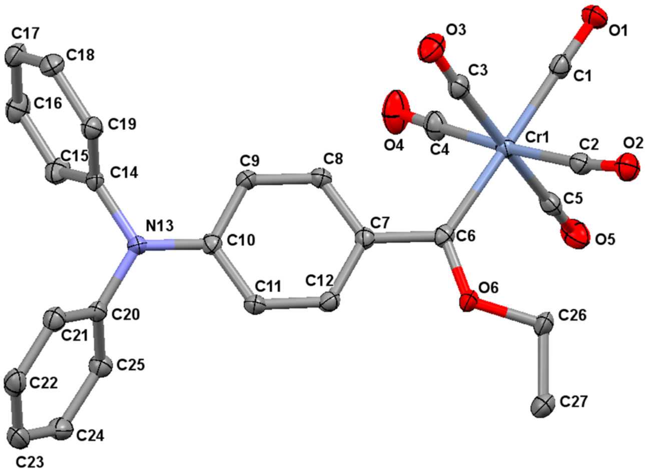

Figure 3. Solid-state structure of **1a**′. Ellipsoids were set at 50% probability; hydrogen atoms were omitted for clarity. (See Figure 2 for important bond lengths.)

The torsion angles of C9−C10−N13−C14 and Cr1−C6−C7−C8 are small with values of −4.4(2)° and 0.9(2)°, respectively. By contrast, Mills and Redhouse found that for $[(CO)_5Cr\{C(OMe)Ph\}]^{40}$ (**A(a)**) the phenyl plane was roughly perpendicular to the p_π-orbital of the carbene carbon (101.1°). This implies that the π-electron system of the carbene and ring in **A(a)** did not interact. Another difference between compound **1a**′ and **A(a)** is the angle around the carbene carbon atom with angle values for Cr-$C_{carbene}$-O of 126.9(1)° (**A(a)**: 134(2)°), for the C_{Ph}-$C_{carbene}$-O of 105.9(1)° (**A(a)**: 104(2)°), and for C_{Ph}-$C_{carbene}$-Cr of 127.2(1)° (**A(a)**: 122(1)°). Selected bond and torsion angles of **1a**′ are listed in Table 1.

The delocalization of the nitrogen lone pair via the bridging phenylene is manifested in alternating longer and shorter bond distances in the benzene ring, while this is not the case for C−C bond distances of the two unsubstituted phenyl rings which are all the same. The bond between the nitrogen and the phenyl ring, C10−N13 (1.378(3) Å), is significantly shorter compared to that of the other nitrogen−carbon(phenyl) bonds, C14−N13 (1.446(2) Å), and C20−N13 (1.434(3) Å).

We have further compared complexes **1a**′ and **A(a)** with the help of density functional theory (DFT) calculations.[41] The most relevant bond distances and corresponding Wiberg bond indices (WBI's) are shown in Figure 4. In good agreement with the structural analysis commented above, our calculations reveal that the presence of the nitrogen atom in **1a**′ provokes a clear shortening of the $C_{carbene}$−C_{aryl} bond (the corresponding

Table 1. Selected Bond Angles (deg) and Torsion Angles (deg) for 1a′

bond angles (deg)		torsion angles (deg)	
atoms	angles	atoms	angles
Cr1−C6−O6	126.9(1)	Cr1−C6−C7−C8	0.9(2)
Cr1−C6−C7	127.2(1)	O6−C6−C7−C12	−1.9(2)
O6−C6−C7	105.9(1)	C7−C8−C9−C10	0.8(3)
C10−N13−C14	120.5(1)	C8−C9−C10−N13	179.3(2)
C10−N13−C20	122.6(1)	C9−C10−N3−C14	−4.4(2)
C14−N13−C20	116.3(1)	C12−C11−C10−N13	−180.0(2)

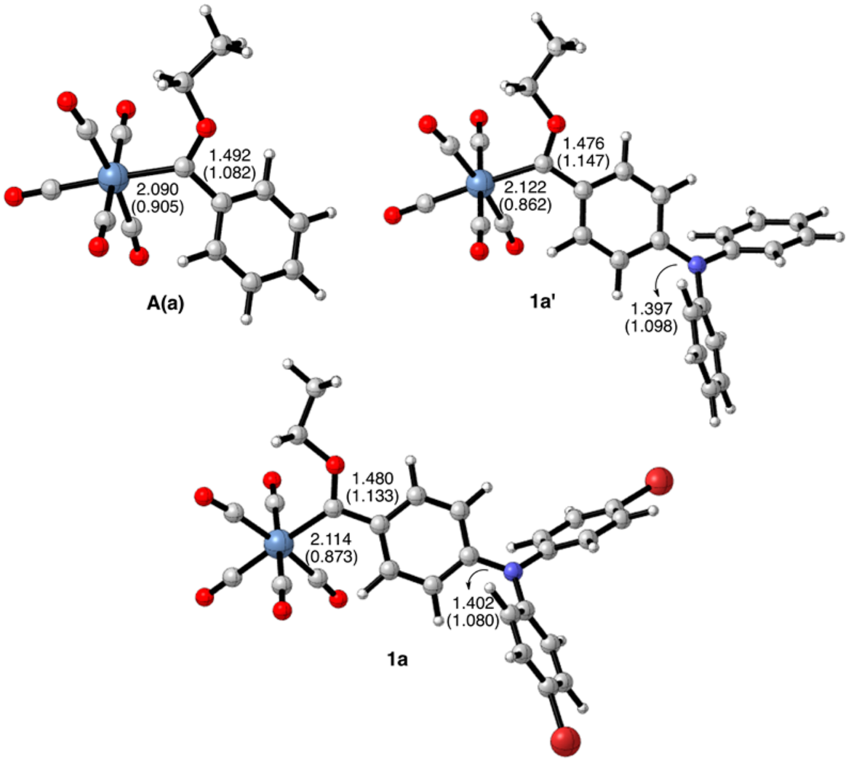

Figure 4. Fully optimized geometries of complexes **A(a)**, **1a′**, and **1a**. Bond distances are given in angstroms (corresponding Wiberg Bond Indices in parentheses). All data have been computed at the B3LYP/def2-TZVP level.

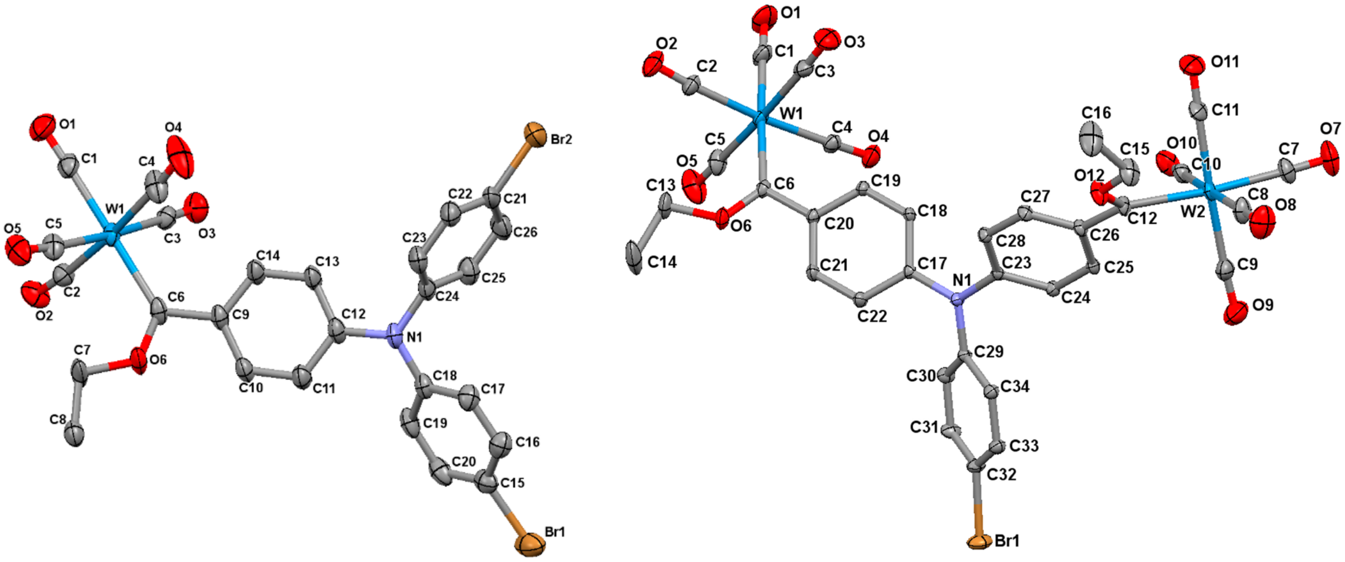

Figure 5. Solid-state structure of **1b** and **2b**. Ellipsoids were set at 50% probability; hydrogen atoms were omitted for clarity.

WBI increases from 1.082 to 1.147 from **A(a)** to **1a′**) with the concomitant lengthening of the Cr−C$_{\text{carbene}}$ bond (the corresponding WBI decreases from 0.905 to 0.862 from **A(a)** to **1a′**). The same trend is found for complex **1a** (see Figure 4). This is due to the delocalization of the nitrogen atom LP into the system, which increases the contribution of the resonance structure depicted in Figure 2 in the description of the ground state of **1a′** (and **1a**). Indeed, the second order perturbation theory (SOPT) of the natural bond orbital (NBO) method indicates a clear stabilizing delocalization of the LP of the nitrogen atom into the π^* moiety of the adjacent aryl fragments. Interestingly, for **1a′** this delocalization is clearly stronger into the aryl fragment directly attached to the pentacarbonyl-carbene moiety (associated SOPT energy, $\Delta E^{(2)}$, of −30.2 kcal/mol) than into the other phenyl substituents ($\Delta E^{(2)}$ = −14.1 and −13.6 kcal/mol, respectively). This is a direct consequence of the well-known strong electron-withdrawing ability of the $(CO)_5M{=}C$ group, which behaves in a manner similar to that of a Lewis acid complexed carbonyl function.[33−35,42] Similar SOPT energies have been computed for the analogous complex **1a** ($\Delta E^{(2)}$ = −31.2 kcal/mol vs −14.8 and −15.1 kcal/mol).

In Figure 5, the solid state structures of **1b** and **2b** are shown and in general correspond with the structural features of **1a′**.

The bond distances and angles around the nitrogen and carbene carbon atoms in **1b** and **2b** correspond well with those found for **1a**′ taking into account the difference in size of the W and Cr atoms. These data support previous conclusions about the delocalization of the nitrogen lone pair over the phenylene rings toward the carbene carbon atoms and the bond angles around the nitrogen and carbene carbon atoms. When comparing **1b** and **2b**, the above effects are observed for two carbene−phenylene−nitrogen fragments rather than one. Further, the torsion angle, W1−$C_{carbene}$−C_{ipso}−C14 in **1b** has a value of 11.2(4)°, while the corresponding bonds have torsion angles of 33.3(4)° and 29.8(4)° in **2b**, indicating the loss of planarity of **1b** and **2b** between the phenyl ring and carbene carbon atom, which we ascribed to less π-interaction. A general trend of the same nature was observed in the solid state structures of **1b** and **2b** (Figure 5). Particularly, they exhibit similar $C_{carbene}$−C_{aryl} bond lengths (ranging from 1.480 to 1.486 Å) thus confirming the partial double-bond character of this bond as a consequence of the delocalization of the LP of the nitrogen atom. The most significant difference between these structures and **1a**′, excluding the presence of the bromine substituents at the 4-positions of the rings, are the N−C_{phenyl} with carbene substituent bond lengths. In **1a**′, the bond length is 1.387(3) Å, while the value for the same bond in **1b** is 1.398(4) Å and respective values of 1.410(3) and 1.416(3) Å in **2b**. This can be ascribed to the lower electron-withdrawing ability of the $(CO)_5$W-carbene fragment as a consequence of the higher W → $C_{carbene}$ π-backdonation (as compared to Cr → $C_{carbene}$) and to the distribution of the nitrogen LP into two carbene moieties (in **2b**).

The bond distances and angles around the nitrogen and carbene carbon atoms in **1b** and **2b** correspond well with those found for **1a**′ taking into account the difference in the sizes of W and Cr atoms. These data support previous conclusions about the delocalization of the nitrogen lone pair over the phenylene rings toward the carbene carbon atoms and the bond angles around the nitrogen and carbene carbon atoms. When comparing **1b** and **2b**, the above effects are observed for two carbene−phenylene−nitrogen fragments rather than one. Further, the torsion angle, W−C_{ipso}−$C_{carbene}$−O, in **1b** has a value of 11.2(4)°, while the same bonds have torsion angles of 33.3(4)° and 29.8(4)° in **2b**, indicating less π-interaction between phenyl ring and the carbene complex and loss of planarity of **1b** and **2b** between the phenylene ring and carbene carbon.

A "push−pull" feature between the π-donor nitrogen lone pair and the π-acceptor carbene carbon of complexes **1**−**3** should display different electronic properties when compared to those of the parent $[(CO)_5Cr\{C(OMe)Ph\}]$ (**A(a)**). The UV−vis spectra of compounds **1**−**3** and **A(a)** (see Figure 6 and Table 2) exhibit three distinct low-lying bands centered at 456−476 nm, 370−382 nm, and 240 nm, which can be tentatively assigned to a spin-forbidden metal-ligand charge-transfer (MLCT) absorption, a spin-allowed ligand-field (LF-1) absorption, and one additional ligand-field (LF-2) transition, respectively, according to previous studies on related alkoxycarbene complexes.[43−46] While the intense LF band remains practically unaltered in complex **A(a)** (λ_{max} = 252 nm), the corresponding MLCT band appears at a much shorter wavelength (λ_{max} = 403 nm). This indicates that the delocalization of the LP of the nitrogen atom into the carbene moiety induces a strong bathochromic shift in the MLCT band ($\Delta\lambda_{max}$ = 50−75 nm), as found in related push−pull Fischer carbene complexes.[42,47]

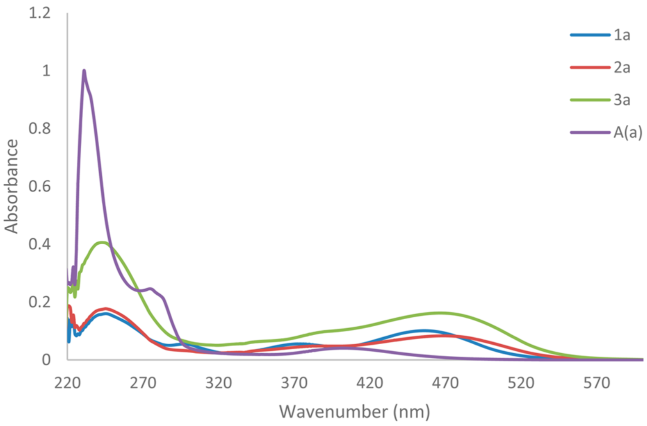

Figure 6. UV/vis spectra of compounds **A(a)** and **1a**−**3a** at a fixed concentration of 0.00001 M in CH_2Cl_2.

Time-dependent density functional theory (TD-DFT) calculations were effected on complexes **A(a)** and **1a** to gain insight into the nature of the MLCT absorption. The computed vertical excitation energies concur reasonably well with the experimental data (see Table 2). These calculations ascribe the MLCT absorption in **A(a)** to the promotion of one electron from the HOMO−1 (a doubly occupied chromium-d atomic orbital) to the LUMO, which is mainly located at the p_z atomic orbital of the carbene carbon atom (see Figure 7). Similarly, the MLCT band in **1a** is ascribed by the TD-DFT calculations to the HOMO−1 → LUMO vertical transition; however, in this case this transition overlaps with the intense (according to the corresponding computed oscillator strength) HOMO → LUMO absorption. As shown in Figure 7, whereas the HOMO−1 of **1a** is also located at the transition metal and the LUMO at the carbene carbon atom, the HOMO can be considered as the LP of the nitrogen atom. Therefore, the broad absorption observed in the range of 456−476 nm for complexes **1**−**3** is the result of a combination of a MLCT transition (resulting from the HOMO−1 → LUMO vertical transition) and a LF transition (resulting from the HOMO → LUMO vertical transition).

Phosphine Ligands. The deprotonation reaction of tri(2-furyl)phosphine by *n*BuLi was accomplished by the same methodology as that for the multicarbene synthesis with N(4-$C_6H_4Br)_3$. The acidity of the proton at the 5-position of the ring is sufficient for deprotonation followed by metal acylate formation after the addition of chromium or tungsten hexacarbonyl to give the carbene precursors. Alkylation with Et_3OBF_4 in the last step afforded **4**−**6** in reasonable to good yields (Scheme 2). A stepwise procedure was again employed to optimize the yields of **5** and **6**. Complex **5** was the least stable and afforded in solution **4** and $PFur_3$.

In addition to the major products **4**, **5**, and **6**, three other carbene complexes, **7**, **B**, and **C** were unexpectedly formed during the reaction and could be isolated and characterized from the reaction mixture (Scheme 3). The formation of **7**, 2-monocarbene $[M\{C(OEt)Fur\}(CO)_5]$[30] complex (**B**), and 2,5-biscarbene complex $[\{M(CO)_5(C(OEt)\}_2Fur']$[30] (**C**) can be explained by the presence of excess *n*BuLi in the reaction mixture. A plausible interpretation involves a furyl metal acylate intermediate (**I**) being subjected to a nucleophilic displacement reaction by the butyl group of *n*BuLi. It was assumed that in **I**

Table 2. Comparison of the UV/Vis Excitation Energies (in nm) of Compounds 1−3[a]

	LF-2	LF-1	MLCT
A(a)	232		403 *(377, 0.214, HOMO−1→LUMO)*[b]
1a	245	372	456 *(468, 0.067, HOMO−1→LUMO)*[b] *(440, 0.695, HOMO→LUMO)*[b]
2a	245	382	467
3a	243	388	467
1b	244	372	457
2b	239	378	476
3b	241	370	475

[a] The first value corresponds to experimental data (recorded at room temperature in CH_2Cl_2 with a concentration of 0.00001 M). In parentheses, the first value corresponds to the computed PCM(CH_2Cl_2)-TD-B3LYP/def2-TZVP vertical excitation energy, and the second value is the corresponding oscillator strength. [b] Time-dependent (TD)-DFT vertical transition assigned to the observed band.

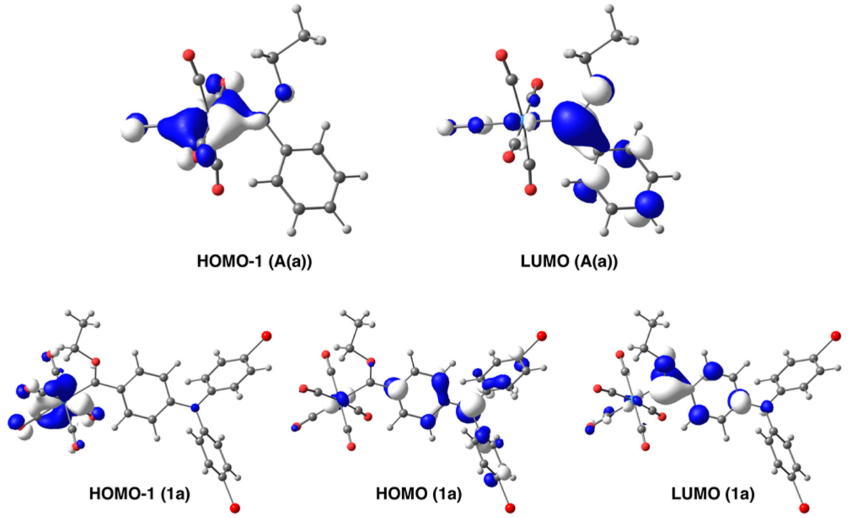
HOMO-1 (A(a)) LUMO (A(a))

HOMO-1 (1a) HOMO (1a) LUMO (1a)

Figure 7. Computed molecular orbitals of complexes **A(a)** (top) and **1a** (bottom) (isosurface value of 0.05 au).

Scheme 2. Synthesis of Trifuryl Mono (4)-, Bis (5)-, and Triscarbene (6) Complexes with 3 Mol Equiv *n*BuLi and $M(CO)_6$

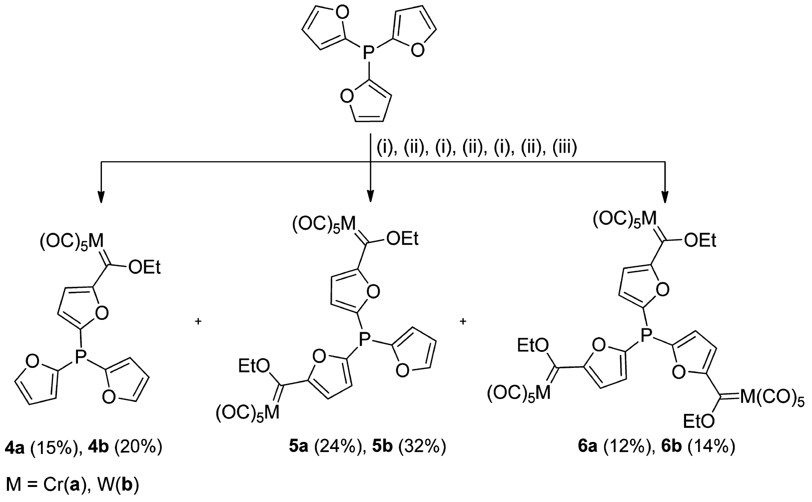

4a (15%), **4b** (20%) **5a** (24%), **5b** (32%) **6a** (12%), **6b** (14%)

M = Cr(**a**), W(**b**)

(i) 1 eq *n*BuLi, THF, -78°C, (ii) 1 eq $M(CO)_6$, -60°C, (iii) 3 eq Et_3OBF_4, CH_2Cl_2

the P-furyl bonds are weakened allowing for their cleaving during *n*BuLi addition. The resulting intermediates are the butyl-phosphine metal acylate (**II**), which is the precursor of **7**, and a lithiated furyl compound (**III**), which after subsequent alkylation gives the red furylcarbene complex, **B**. Deprotonation by a second equivalent *n*BuLi of **III** gives **IV** while **I** gives **V**, which are the precursors of the purple furylene biscarbene complex **C**.

Assignments of the furyl ring proton signals in the ^1H NMR spectra were based on the chemical shifts, their patterns and the magnitude of ^{31}P-coupling constants displayed by a particular ring proton in the ^1H and ^{13}C NMR spectra. The protons furthest downfield in the ^1H NMR spectra were assigned to the proton in the 5-position of the unsubstituted furan rings. Small downfield shifts were observed in the ^1H NMR spectra of the furyl rings for the protons in going from $PFur_3$[32] to **4**. The ^1H

Scheme 3. Formation of Products 7, B, and C from Precursor Metal Acrylates of 4 and 5 in the Presence of 3 Mol Equiv *n*BuLi/M(CO)$_6$

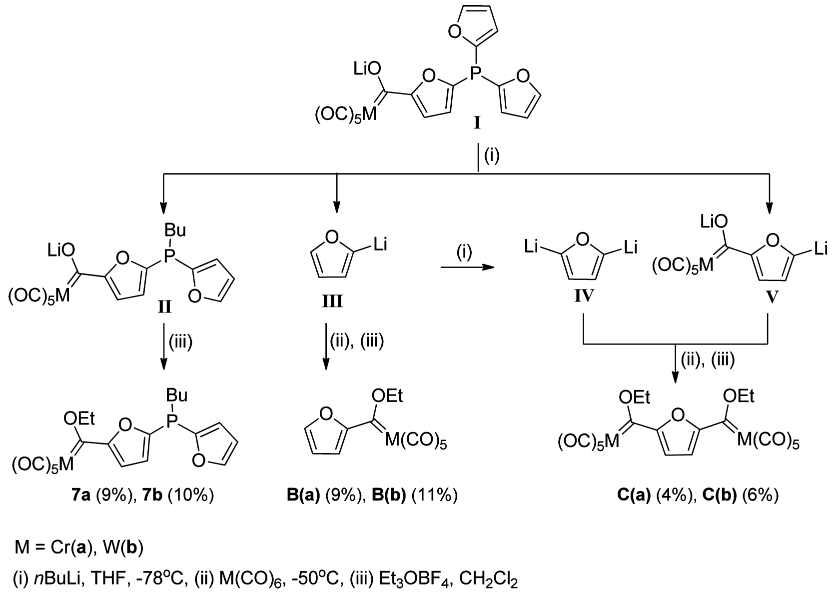

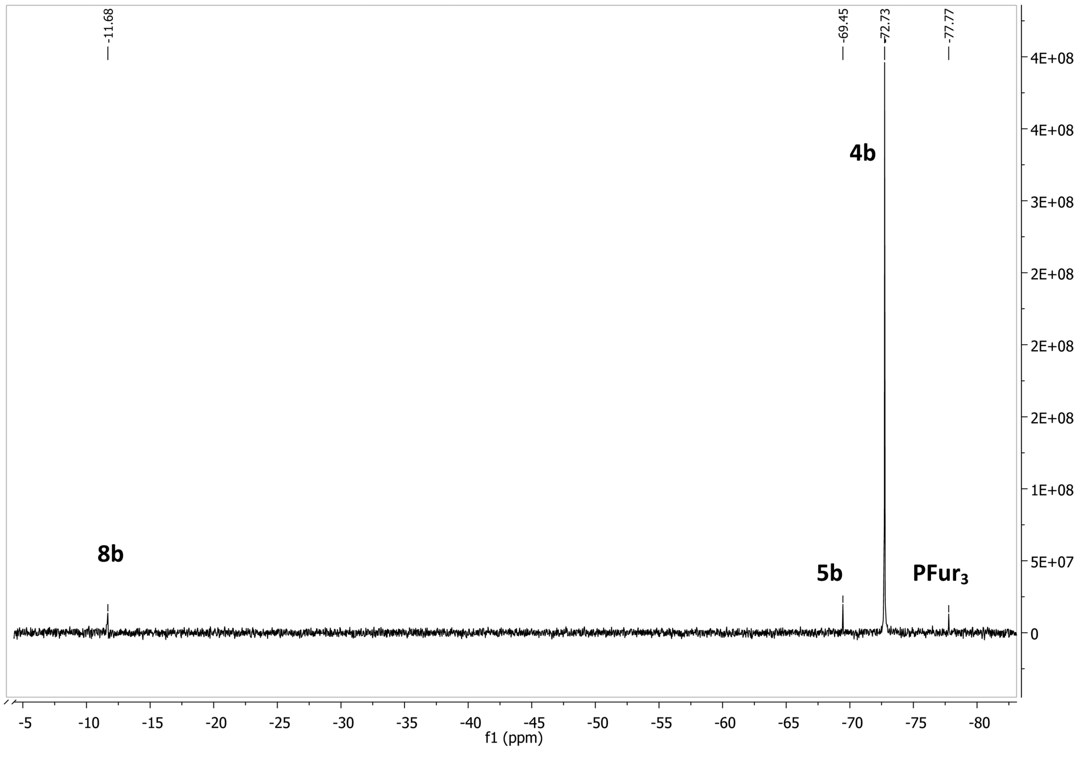

Figure 8. ^{31}P NMR spectrum of **4b** in CDCl$_3$ solution.

NMR chemical shifts for the protons of the furyl rings with or without carbene substituents and the ethoxycarbene substituents generally remained approximately the same in spite of the number of carbene substituents increasing from one (4) to two (5) to three (6). This was supported by similar values found for the resonances in the ^{1}H and ^{13}C NMR spectra for the WC(OEt)Fur-unit[30] and the complexes **4b**–**6b**. The carbene carbon chemical shifts in the ^{13}C NMR spectra are insensitive on increasing the number of carbene substituents and remain the same. The ^{31}P NMR resonances move slightly downfield as the number of carbene substituents increase in the complexes from one to two to three; however, there is a negligible difference between the chromium and tungsten resonances of the respective compounds (**4**, Cr −72.8, W −72.7 ppm; **5**, Cr −69.6, W −69.4 ppm; **6**, Cr −63.5, W −63.2 ppm). From this data, it is clear that the carbene moiety as a substituent does not significantly affect the bonding properties of the phosphorus atom of the phosphine.

Furthermore, measurement of the NMR spectra of both **4a** and **4b** in CDCl$_3$ over time revealed the presence of three other compounds excluding the major product (illustrated in the ^{31}P NMR spectrum of **4b** in Figure 8). In addition to the major

Scheme 4. Equilibrium between 4 and 5 in Solution

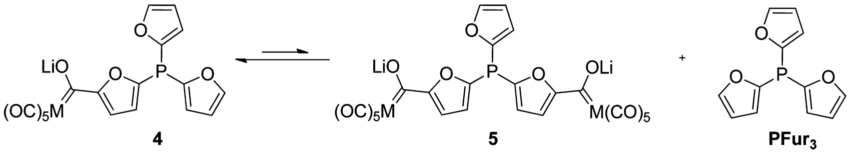

product **4b** (−72.8 ppm), small amounts of **5b** (−69.5 ppm) and PFur$_3$ at −77.8 ppm (upfield from the reported value of −76.8 ppm)[31] as well as a downfield peak at −11.7 ppm (*vide supra* **8b**) are observed. The formation of the minor product, **5**, is interesting and can be explained by a reaction of **4** to form **5** and PFur$_3$, which are always present in any solution of **4** (Scheme 4). The equilibrium between **4** and **5** in solution lies far to the left (Scheme 4), based on ^{31}P NMR peak intensities.

The ^{1}H NMR spectrum of **4b** displays two sets of signals of different intensities (**4b**:**8b**, 19:1) and at distinctly different chemical shift values for all the signals. Since the chemical shifts of PFur$_3$, **4b**, and **5b** are very similar, the dramatic downfield shift of the final signal in the ^{31}P NMR is indicative of a phosphine phosphorus atom coordinated to a second transition metal (**8b**, Figure 9). A duplication of the M(CO)$_5$-pattern of bands for the carbonyl vibrational frequencies was observed in the IR spectrum and clearly indicates the different bonding properties of carbene (**4b**) and phosphine ligands (**8b**). The observation that phosphines can displace carbonyl ligands *in situ* to afford coordination compounds is not new, and examples involving a Fischer carbene complex are known.[17,48−50]

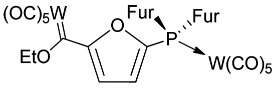

8b

Figure 9. Coordination of **4b** to form a bimetallic compound **8b**.

The solid state structure of **4b** shows a trigonal pyramidal arrangement of substituents around the phosphorus atom, while the electron lone pair takes up the fourth position (Figure 10). The metal−carbene bond is slightly out of the plane of the furyl ring with the W1−C6−C9−O7 torsion angle at 8.4(2)°. A comparative study among the solid state structures of **4b**, PFur$_3$, and **B**(**b**) (Table 3) provides an indication of the overall effect that the Fischer carbene substituent has on the properties of the phosphine. The most significant differences are found in the bond distances of the furan ring attached to the carbene substituent compared to the distances of the other furan rings, which are the same as those for PFur$_3$. These differences become greater as one approaches the carbene carbon and are indicative of a localized stabilization of the carbene carbon by this furan ring. There are three striking differences between the solid state structures of **B**(**b**) and **4b**: first, the planar arrangement of substituents around the carbene carbon in **B**(**b**) (W−C6−C5−C4: 0.00(6)°) compared to a corresponding torsion angle of 8.4(2) for **4b**; second, a remarkable difference in the bond lengths of the $C_{carbene}$−O(Et) bond and the $C_{carbene}$−C_{furyl} bond of **4b** and **B**(**b**) reveals an alternate way of stabilization of the carbene carbon in the two compounds;[49] and third, the presence of much longer C−O distances in the furan ring of **B**(**b**) compared to those of **4b**.

Again, we have further compared compounds **4b**, **B**(**b**), and PFur$_3$ with the help of DFT calculations. As shown in Figure 11, the W=$C_{carbene}$ and $C_{carbene}$−C_{Fur} distances remain practically unaltered when comparing compound **4b** to the analogous [(CO)$_5$W=C(OEt)Fur] complex, **B**(**b**). This confirms that the metal−carbene fragment is not affected by the presence of the phosphine fragment. Notably, the P−C_{Fur} distance containing the carbene substituent is slightly longer in **4b** than in PFur$_3$ (as found in the solid state), which provides

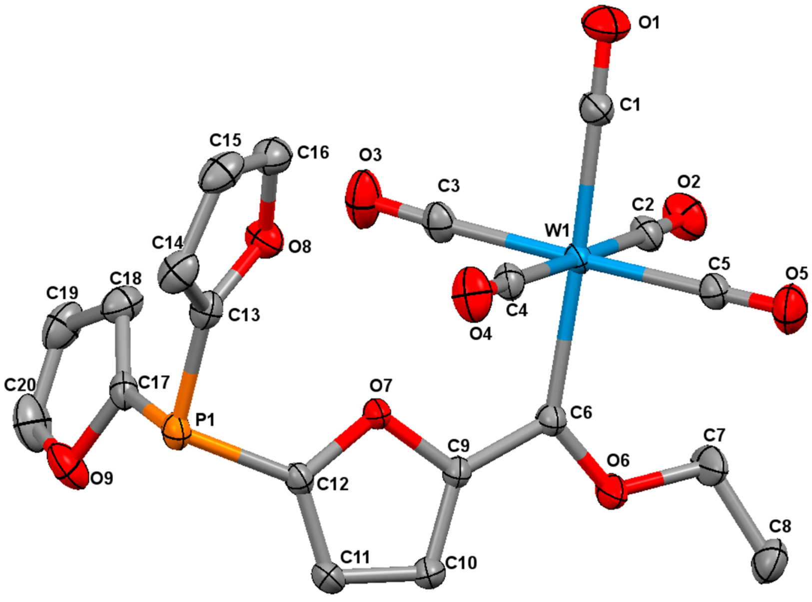

Figure 10. Solid-state structure of **4b**. Ellipsoids were set at 50% probability; hydrogen atoms were omitted for clarity.

Table 3. Comparison of Furan Ring Bond Distances[a] of $PFur_3$,[48] 4b, and B(b)[49]

Bond	**$PFur_3$**[a]	**4b**[a]		**B(b)**
	Bond distances (Å)	Bond distances (Å)		Bond distances (Å)
	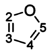	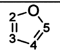	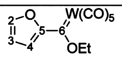	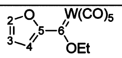
P – C2	1.802(1)[a]	1.801(3)[a]	1.812(2)	–
O1 – C2	1.380(2)[a]	1.378(3)[a]	1.366(2)	1.449(19)
C2 – C3	1.357(2)[a]	1.358(4)[a]	1.366(3)	1.133(23)
C3 – C4	1.426(2)[a]	1.422(4)[a]	1.412(2)	1.420(7)
C4 – C5	1.338(2)[a]	1.333(4)[a]	1.366(2)	1.355(8)
C5 – O1	1.370(2)[a]	1.372(4)[a]	1.376(2)	1.424(9)
C5 – C6	-	-	1.460(2)	1.353(11)
C6 – W	-	-	2.171(2)	2.199(3)
C6 – OEt	-	-	1.327(2)	1.406(1)
W–CO_{cis}	-	-	2.049(4)[a]	2.042(7)[a]
W–CO_{trans}	-	-	2.031(2)	2.009(4)

[a] The average taken for similar rings in the same structure.

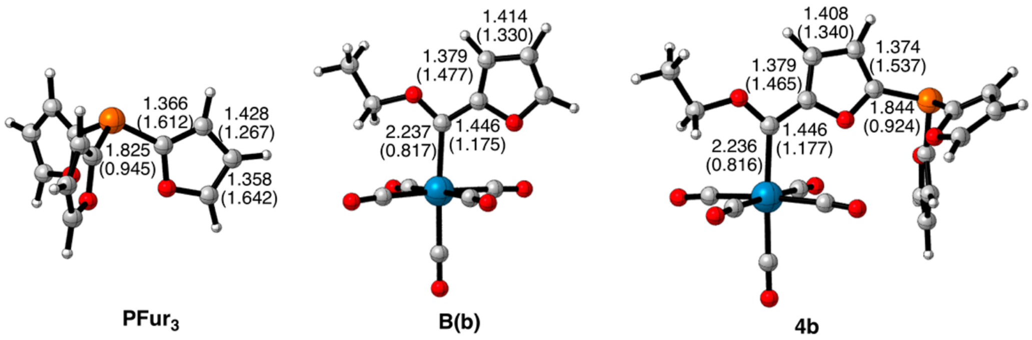

Figure 11. Optimized geometries of $PFur_3$ and complexes **4b** and **B(b)**. Bond lengths are given in angstroms. Corresponding Wiberg bond indices are given in parentheses. All data were computed at the B3LYP/def2-TZVP level.

further support for the lack of direct conjugation between the LP and the carbene moiety.

Interestingly, as a consequence of the π-conjugation between the furyl substituent and the electrophilic carbene carbon atom in **4b** (which significantly alters the C—C and C—O distances of the furyl group attached to the carbene), the delocalization of the phosphorus LP into the adjacent σ^*(C—O) molecular orbital observed in the free $PFur_3$ is reduced in complex **4b** (associated SOPT-energy, $\Delta E^{(2)} = -9.7$ kcal/mol in $PFur_3$ vs $\Delta E^{(2)} = -8.2$ kcal/mol in **4b**; Figure 12). This indicates that the phosphorus LP in complex **4b** is even more available than in the free phosphine, thus increasing its electron-donating ability. On the basis of these findings, we anticipated that the otherwise reactive Fischer carbene moiety would more than likely remain intact during coordination of the phosphine-carrying carbene to other metals.

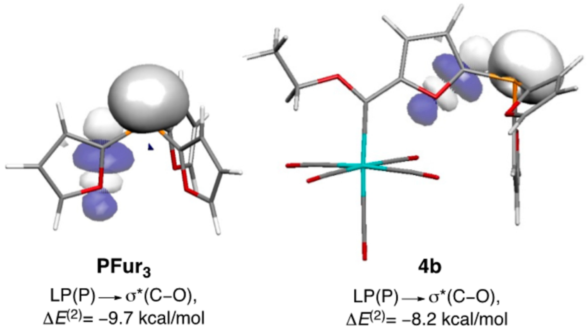

Figure 12. NBO-molecular orbitals responsible for the delocalization of the phosphorus lone-pair.

The wavelengths of the absorption maxima of the phosphine series are listed in Table 4. The values did not reveal any significant differences between the compounds, again illustrating the absent effect of the increasing number of carbenes on the molecular system of each compound. Not surprisingly, there is a clear difference between the wavelengths of the LF and MLCT transfers of the two different metals, with average values of 319 and 330 nm for the LF transition as well as 477 and 455 nm for the MLCT transition of the respective chromium and tungsten analogues.

TD-DFT calculations were effected on complex **4b** to gain insight into the nature of the MLCT absorption. In this case, our calculations ascribe the MLCT absorption to the promotion of one electron from the HOMO−1 to the LUMO. As shown in Figure 13, the HOMO−1 is mainly centered at a d atomic orbital of tungsten, whereas the LUMO is centered at the p_z atomic orbital of the carbene carbon atom. Strikingly, no contribution of the LP of the phosphorus atom in

Table 4. Comparison of the Main UV/Vis Excitation Energies of Compounds 4−6[a]

	LF-2	LF-1	MLCT
4a			483
5a		313	475
6a		325	473
4b	285	336	453 *(444, 0.296, HOMO−1→LUMO)*[b]
5b	286	326	457
6b	282	326	455

[a] The first value corresponds to experimental data (recorded at room temperature in CH_2Cl_2 with a concentration of 0.00001 M). In parentheses, the first value corresponds to the computed PCM-(CH_2Cl_2)-TD-B3LYP/def2-TZVP vertical excitation energy, and the second value is the corresponding oscillator strength. [b] Time-dependent (TD)-DFT vertical transition assigned to the observed band.

this absorption was found, which sharply contrasts with the situation in amine-carrying complexes **1**−**3**. Therefore, it can be safely concluded that whereas the LP of the nitrogen atom is not available for coordination in complexes **1**−**3**, the scenario is completely different for the phosphine-carrying complexes **4**−**6**, where the LP of phosphorus is even more available than in the parent phosphine PFur$_3$.

Coordination Properties of 1b and 4b. To investigate the coordination ability of the amine-N (**1b**) and phosphine-P (**4b**) ligands, we proceeded to test their coordinative properties to another metal center. The coordinative properties of the ideal carbene-carrying ligand should be such that it would be capable of piggybacking a fragile Fischer carbene functionality into the vicinity of the coordination sphere of the second metal center (without affecting the identity of either the ligand or the accompanying carbene complex). On the basis of the above structural data, features, and theoretical calculations, we anticipated that the phosphine ligand **4b** compared to the amine **1b** should be the better host of a carbene substituent. A platinum fragment as acceptor was chosen because it is widely used as a node in organometallic frameworks.[51−54]

The COD ligand in [Pt(COD)Cl$_2$] was displaced by two molecules of **4b** to give **9b** after stirring for 18 h in CH_2Cl_2 in high yields (Scheme 5). By contrast, the analogous reaction with 2 mol equiv of **1b** did not give the corresponding platinum−bisamine−carbene complex. Spectroscopic measurements of the product mixture revealed the presence of carbene transfer and carbene−carbene coupling products. The formed products support the catalytic role of the platinum metal center. It is well-known that platinum and palladium complexes can participate in carbene transfer reactions and carbene−carbene coupling reactions.[55−57]

The coordination of **4b** to Pt resulted in downfield shifts of the ^{31}P NMR resonances to −35.3 ppm with a (^{195}Pt{^{31}P}) coupling of 1847 Hz for **9b**. The ^{1}H NMR resonances of the furyl rings, particularly the furyl group with the carbene substituent, did show a downfield shift with values of 7.11 (**4b**: 7.01) and 6.96 (**4b**: 6.65) ppm for the furylene linker, while significant shifts were also observed in the ^{13}C NMR. Interestingly, the carbene carbon atom remains practically unaltered (δ = 284.0 ppm in **4b** vs 286.4 in **9b**). The above results indicate that the coordination of the phosphorus atom to the platinum center affects the properties of the phosphine ligand without modifying the electronic properties of the carbene moiety.

The molecular structure of **9b** comprises two molecules of **4b** coordinated, via the phosphorus atoms, in cis-positions of a square planar Pt complex, in spite of their bulkiness (Figure 14). The averaged C_{Fur}−P−C_{Fur} angle increases marginally in the order 101.3(1)° in **4b** to 102.9(1)° in PFur$_3$ and 104.4(2)° and 103.2(3)° in **9b**, while the angles for P−Pt−P and Cl−Pt−Cl angles in **9b** are 94.4(1)° and 87.7(1)°, respectively. The bond distances within the larger molecule show the same general trends as was observed for **4b**. The two different ligands of **4b** within the **9b** are, however, not exactly the same. For example, the bond distances of the two C_{furyl}−$C_{carbene}$ bonds have values of 1.468(8) and 1.449(8) Å and respective W−$C_{carbene}$ bond distances of 2.160(5) and 2.183(6) Å. A reasonable explanation for the observation is the steric hindrance, which is illustrated in the solid state structure of **9b** in Figure 14.

CONCLUSIONS

In conclusion, we have demonstrated that the multiple carbene moieties present in compounds **2**, **3**, **5**, and **6** function independently of each other and are stable compounds. Further, we have shown how a common ligand such as a phosphine (PFur$_3$) can be used to carry a reactive Fischer carbene moiety into the coordination sphere of a second transition metal (Pt). Through theoretical calculations we showed that in **4b**, the phosphine's coordinating abilities to other metals become stronger, while the carbene carbon atom's bonding properties are hardly affected. The fact that in **4b**, unlike for **1b**, no inter- or intramolecular template reactions involving the carbene unit occurred in the presence of the platinum metal suggested that phosphines could successfully act as carbene-carrying agents. This was confirmed by the synthesis of **9b**, which can be considered as the first step of a carbene-

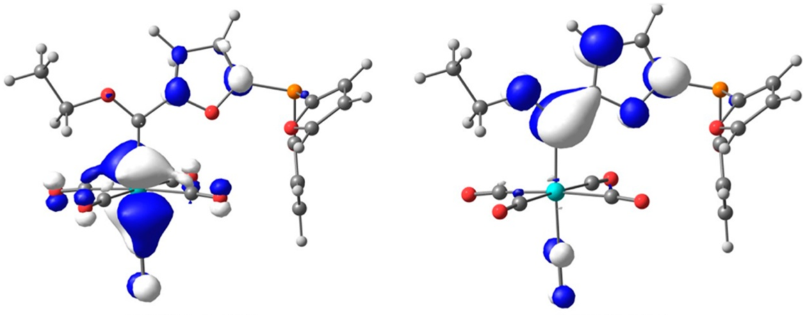

HOMO-1 (4b)

LUMO (4b)

Figure 13. Computed molecular orbitals of complex **4b** (isosurface value of 0.05 au).

Scheme 5. Substitution of COD in $[Pt(COD)Cl_2]$ by 4b to Form 9b

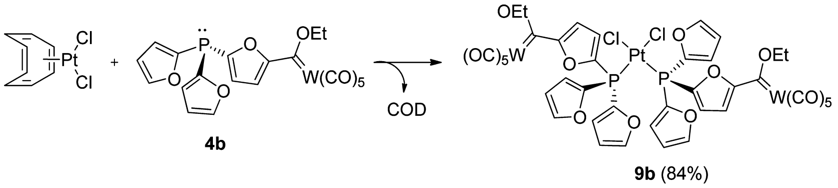

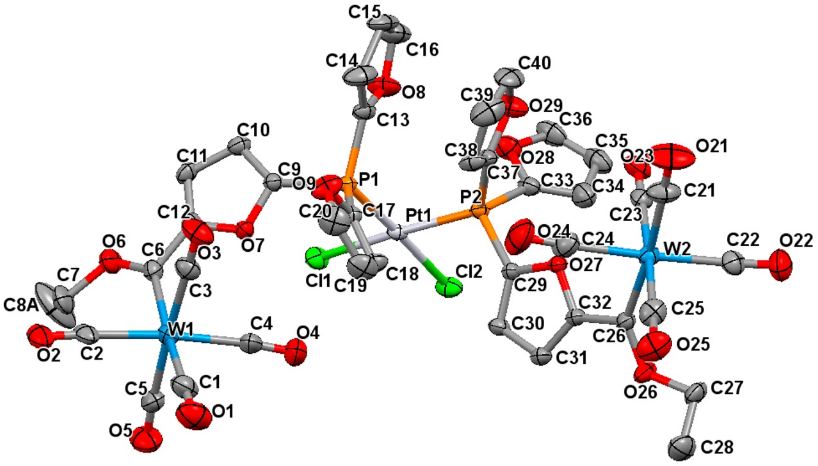

Figure 14. Solid-state structure of **9b**. Ellipsoids were set at 50% probability; hydrogen atoms were omitted for clarity.

loading process preceding coordination studies on larger molecules or surfaces. Hence, conditions were met to use phosphine ligands as agents to piggyback Fischer carbene complexes into small macromolecules with potential application in metal organic frameworks and networks.

EXPERIMENTAL SECTION

General. Tris(4-bromophenyl)amine, tri(2-furyl)phosphine, $Cr(CO)_6$, $W(CO)_6$, and $K_2[PtCl_4]$ were purchased from Sigma-Aldrich and Strem Chemicals and used as received. $[Pt(COD)Cl_2]$ was prepared from $K_2[PtCl_4]$ by the procedure of Clark and Manzer,[58] while Et_3OBF_4 was prepared according to the literature procedure by Meerwein.[59] All operations were performed using standard Schlenk techniques under an atmosphere of nitrogen or argon. Silica gel 60 (particle size 0.0063−0.200 mm) was used as resin for all separations in column chromatography. Anhydrous THF and hexane were distilled over sodium metal and dichloromethane over CaH_2. All other reagents were used as received from commercial suppliers. NMR spectra were recorded on Bruker Ultrashield Plus 400 AVANCE 3 and Bruker Ultrashield 300 AVANCE 3 spectrometers using $CDCl_3$ and C_6D_6 as solvents at 25 °C. The NMR spectra were recorded for ^1H at 400.13 and 300.13 MHz, ^{13}C at 100.163 and 75.468 MHz, and ^{31}P at 161.976 and 121.495 MHz. The chemical shifts were recorded in ppm, using deuterated solvent signals for internal references. For $CDCl_3$ and C_6D_6, respectively, δH at 7.2400 and 7.1500 ppm, and δC at 77.000 and 128.000 ppm, and the ^{31}P NMR spectra were referenced to the deuterated lock solvent which had been referenced to 85% H_3PO_4. Infrared spectroscopy was performed on a PerkinElmer Spectrum RXI FT-IR spectrophotometer with a NaCl cell, using hexane as solvent. X-ray crystallography was performed at 20 °C on a Siemens P4 diffractometer fitted with a Bruker 1 K CCD detector using graphite-monochromated, Mo−Kα radiation by means of a combination of phi and omega scans. UV/visible Spectroscopy was measured in a range of 200.0 to 1100 nm in a quartz cell with CH_2Cl_2 as reference and measured on a PerkinElmer Lamda 25 instrument with a Dell Ortiplex 760 Intel Celeron CPU. Mass spectral analyses were performed on a Synapt G2 HDMS by direct infusion at 5 μL/min with positive electron spray as the ionization technique. The m/z values were measured in the range of 400−1500 with methanol as solvent.

*Synthesis of $[\{M(CO)_5C(OEt)C_6H_4\}NPh_2]$ (M = Cr **1a**; W **1b**), $[\{M(CO)_5C(OEt)C_6H_4\}_2NPh]$ (M = Cr **2a**; W **2b**), and $[\{M(CO)_5C(OEt)C_6H_4\}_3N]$ (M = Cr **3a**; W **3b**).* nBuLi (0.80 mL, 1.50 M, 1.20 mmol) was added to a cold solution (−78 °C) of tris(4-bromophenyl)amine (0.48 g, 1.00 mmol) dissolved in dry THF (30 mL). Upon lithiation, one equivalent $M(CO)_6$ [($Cr(CO)_6$: 1.00 mmol, 0.22 g) ($W(CO)_6$: 1.00 mmol, 0.35 g)] was immediately added and allowed to stir until all of the metal carbonyl was dissolved (45 min). The lithiation and reaction with $M(CO)_6$ steps were repeated twice more. After the third lithiation and metal acylate formation, the solvent was removed *in vacuo*, and the residue dissolved in a minimum amount of CH_2Cl_2. Et_3OBF_4 (0.57 g, 3.0 mmol) dissolved in CH_2Cl_2 (30 mL) was added to the cold (−40 °C) reaction mixture. The resulting solution was filtered through silica gel, washed with CH_2Cl_2, and the solvent removed under vacuum. The fractions were isolated from a silica gel column using hexane and dichloromethane mixtures. The products were concentrated under reduced pressure, yielding three bright orange products. By changing the molar equivalents of nBuLi and $M(CO)_6$ added, the yields of the major products can be controlled (Table 5). Compound **1a**′ was isolated in a yield of 30% (0.37 g) when 1 equiv of nBuLi and $M(CO)_6$ were added subsequently followed by 2 equivs of alkylation agent (all under the above specified reaction conditions).

Table 5. Reaction Yields for n Subsequent Steps[a]

	$n = 1$		$n = 2$		$n = 3$	
	mass	yield	mass	yield	mass	yield
1a	0.21 g	32%	0.05 g	8%	0.06 g	9%
2a	0.16 g	20%	0.33 g	40%	0.17 g	21%
3a			0.16 g	16%	0.47 g	47%
1b	0.32 g	41%	0.09 g	11%	0.07 g	9%
2b	0.26 g	24%	0.84 g	43%	0.20 g	18%
3b			0.30 g	22%	0.82 g	59%

[a] nBuLi and $M(CO)_6$ were added to 1.00 mmol tris(4-bromophenyl)amine under specified reaction conditions (M = Cr(a), W(b)).

Crystals for **1a′**, **1b**, and **2b** were obtained from a CH_2Cl_2 solution layered with hexane after slow diffusion of hexane into the solution. Scheme 6 illustrates ^1H and ^{13}C NMR numerical assignments of compounds **1**−**3**.

Scheme 6. Numerical Proton and Carbon Assignments

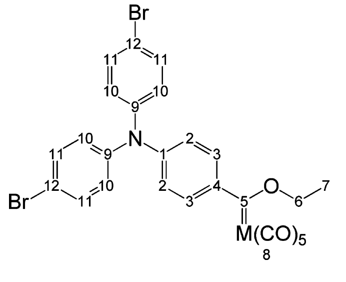

1a: $C_{26}H_{17}O_6NCrBr_2$. ^1H NMR (C_6D_6, 300 MHz) δ 7.66 (d, 9.0 Hz, 2H, H3), 6.98 (d, 7.2 Hz, 4H, H11), 6.93 (d, 7.1 Hz, 4H, H10), 6.78 (d, 9.0 Hz, 2H, H2), 4.71 (q, 7.1 Hz, 2H, H6), 1.04 (t, 7.0 Hz, 3H, H7). ^{13}C NMR ($CDCl_3$, 75 MHz) δ 332.6 (C5), 223.8 (C8, *trans*), 217.2 (C8, *cis*), 152.1 (C4), 146.0 (C9), 144.5 (C1), 130.0 (C2), 129.7 (C11), 126.3 (C10), 125.1 (C12), 118.0 (C3), 76.5 (C6), 15.2 (C7). IR (cm^{-1}, hexane): 2056(m), 1984(w), 1950(s), 1944(vs). ESI-MS (15 V, positive mode, m/z): calcd for $[M + H]^+$ 649.8906; found, 649.8812.

1a′: $C_{26}H_{19}O_6NCr$. ^1H NMR (C_6D_6, 400 MHz) δ 7.66 (d, 7.9 Hz, 2H, H3), 6.98 (d, 6.9 Hz, 4H, H11), 6.93 (d, 6.6 Hz, 4H, H10), 6.87 (m, 2H, H12), 6.78 (d, 8.1 Hz, 2H, H2), 4.71 (q, 6.9 Hz, 2H, H6), 1.04 (t, 6.8 Hz, 3H, H7). ^{13}C NMR ($CDCl_3$, 126 MHz) δ 332.3 (C5), 223.8 (C8, *trans*), 217.2 (C8, *cis*), 152.1 (C4), 146.0 (C9), 144.4 (C1), 130.1 (C2), 129.7 (C11), 126.3 (C10), 125.1 (C3), 117.9 (C12), 76.4 (C6), 15.2 (C7). IR (cm^{-1}, hexane): 2056(m), 1984(w), 1950(s), 1944(vs). ESI-MS (15 V, positive mode, m/z): calcd for $[M]^+$ 493.0617; found, 493.0610.

1b: $C_{26}H_{17}O_6NWBr_2$. Mp: 125 °C. ^1H NMR (C_6D_6, 300 MHz) δ 7.75 (d, 9.1 Hz, 2H, H3), 7.08 (d, 8.9 Hz, 4H, H11), 6.57 (d, 9.1 Hz, 2H, H2), 6.44 (d, 8.9 Hz, 4H, H10), 4.61 (q, 7.0 Hz, 2H, H6), 1.03 (t, 7.0 Hz, 3H, H7). ^{13}C NMR ($CDCl_3$, 75 MHz) δ 308.6 (C5), 203.1 ($^1J_{\{W\}C}$ = n.o., C8, *trans*), 198.0 ($^1J_{\{W\}C} = 63.1$ Hz, C8, *cis*), 151.4 (C4), 146.9 (C1), 145.8 (C9), 132.8 (C12), 131.6 (C3), 129.9 (C11), 127.6 (C10), 119.2 (C2), 79.3 (C6), 15.0 (C7). IR (cm^{-1}, hexane): 2064(m), 1988(w), 1950(vs). ESI-MS (15 V, positive mode, m/z): calcd for $[M + H]^+$ 781.9010; found, 781.9045.

2a: $C_{34}H_{22}O_{12}NW_2Br$. ^1H NMR (C_6D_6, 300 MHz) δ 7.47 (d, 7.5 Hz, 4H, H3), 6.99 (d, 6.9 Hz, 2H, H11), 6.87 (d, 6.9 Hz, 2H, H10), 6.79 (d, 7.7 Hz, 4H, H2), 4.66 (q, 7.0 Hz, 4H, H6), 1.03 (t, 7.0 Hz, 6H, H7). ^{13}C NMR ($CDCl_3$, 126 MHz) δ 337.9 (C5), 223.8 (C8, *trans*), 216.8 (C8, *cis*), 149.9 (C4), 147.3 (C1), 145.4 (C9), 130.0 (C11), 128.5 (C3), 126.9 (C10), 126.0 (C12), 121.6 (C2), 76.9 (C6), 15.2 (C7). IR (cm^{-1}, hexane): 2057(m), 1987(w), 1950(vs). ESI-MS (15 V, positive mode, m/z): calcd for $[M+K]^+$ 857.8773; found, 857.8750.

2b: $C_{34}H_{22}O_{12}NW_2Br$. Mp: 152 °C. ^1H NMR (C_6D_6, 300 MHz) δ 7.63 (d, 8.8 Hz, 4H, H3), 7.09 (d, 8.8 Hz, 2H, H11), 6.68 (d, 8.9 Hz, 4H, H2), 6.48 (d, 8.6 Hz, 2H, H10), 4.60 (q, 7.0 Hz, 4H, H6), 1.03 (t, 7.0 Hz, 6H, H7). ^{13}C NMR ($CDCl_3$, 101 MHz) δ 311.1 ($^1J_{\{W\}C} = 52.2$ Hz, C5), 203.1 ($^1J_{\{W\}C} = 58.7$ Hz, C8, *trans*), 197.6 ($^1J_{\{W\}C} = 63.5$ Hz, C8, *cis*), 150.0 (C4), 148.9 (C1), 144.4 (C9), 133.2 (C11), 131.4 (C12), 130.7 (C3), 128.2 (C10), 121.8 (C2), 79.6 (C6), 15.0 (C7). IR (cm^{-1}, hexane): 2066(m), 1984(w), 1948(vs). ESI-MS (15 V, positive mode, m/z): calcd for $[M]^+$ 1082.9349; found, 1082.9327.

3a: $C_{42}H_{27}O_{18}NCr_3$. ^1H NMR (C_6D_6, 400 MHz) δ 7.38 (d, 8.4 Hz, 6H, H3), 6.79 (d, 8.8 Hz, 6H, H2), 4.64 (q, 6.6 Hz, 6H, H6), 1.03 (t, 6.6 Hz, 6H, H7). ^{13}C NMR ($CDCl_3$, 75 MHz) δ 337.9 (C5), 223.8 (C8, *trans*), 216.6 (C8, *cis*), 148.8 (s, C4), 148.7 (C1), 127.8 (C3), 123.3 (C2) 76.6 (C6), 15.2 (C7). IR (cm^{-1}, hexane): 2057(m), 1983(w), 1949(vs). calcd for $[M + H]^+$ 989.9522; found, 989.9447.

3b: $C_{42}H_{27}O_{18}NW_3$. ^1H NMR (C_6D_6, 300 MHz) δ 7.57 (d, 8.8 Hz, 6H, H3), 6.77 (d, 8.8 Hz, 6H, H2), 4.60 (q, 7.0 Hz, 6H, H6), 1.04 (t, 7.1 Hz, 6H, H7). ^{13}C NMR ($CDCl_3$, 101 MHz) δ 312.6 ($^1J_{\{W\}C} = 52.1$ Hz, C5), 203.2 ($^1J_{\{W\}C} = 57.6$ Hz, C8, *trans*), 197.5 ($^1J_{\{W\}C} = 64.3$ Hz, C8, *cis*), 150.2 (C4), 149.3 (C1), 130.1 (C3), 123.3 (C2) 79.8 (C6), 15.0 (C7). IR (cm^{-1}, hexane): 2058(m), 1988(w), 1952(vs). ESI-MS (15 V, positive mode, m/z): calcd for $[M + H]^+$ 1385.9841; found, 1385.9738.

*Synthesis of [{M(CO)$_5$C(OEt)Fu′}PFu$_2$] (M = Cr **4a**; W **4b**), [{M(CO)$_5$ C(OEt)Fu′}$_2$PFu] (M = Cr **5a**; W **5b**), [{M(CO)$_5$ C(OEt)Fu′}$_3$P] (M = Cr 6**a**; W **6b**), [{M(CO)$_5$C(OEt)}Fu] (M = Cr **B(a)**, W **B(b)**), [{M(CO)$_5$C(OEt)}Fu′{C(OEt)M(CO)$_5$}] (M = Cr **C(a)**, W **C(b)**) and [{M(CO)$_5$C(OEt) Fu′}P(nBu)Fu}] (M = Cr **7a**; W **7b**) (Fu′ = C$_4$H$_2$O).* *n*BuLi (1.25 mL, 1.60 M, 2.00 mmol) was added to a cold solution (−78 °C) of tri(2-furyl)phosphine (0.46 g, 2.00 mmol) dissolved in dry THF (40 mL) and allowed to stir for 10 min in a cold bath, after which the solution was allowed to stir at room temperature (50 min). Upon lithiation, the reaction mixture was cooled (−60 °C), and 1 equiv of $M(CO)_6$ [($Cr(CO)_6$: 2.00 mmol, 0.44 g) ($W(CO)_6$: 2.00 mmol, 0.70 g)] was added. The mixture was removed from the cold bath and allowed to stir until all of the metal carbonyl was dissolved (45 min). The lithiation and reaction with $M(CO)_6$ steps were repeated. After the third lithiation and metal acylate formation, the solvent was removed *in vacuo* and the residue dissolved in a minimum amount of CH_2Cl_2. Et_3OBF_4 (0.48 g, 6.00 mmol) dissolved in CH_2Cl_2 (30 mL) was added to the cold (−40 °C) reaction mixture. The resulting solution was filtered through silica gel, washed with CH_2Cl_2, and the solvent removed under reduced pressure. The fractions were separated from a silica gel column using hexane and dichloromethane mixtures. The products were isolated and concentrated under reduced pressure, yielding six different products. By altering the molar equivalents of lithiation and reaction with $M(CO)_6$, the composition of the major products can be controlled (Table 6). Crystals for **4b** were isolated from a CH_2Cl_2 solution layered with hexane after slow diffusion of hexane into the solution. Scheme 7 illustrates ^1H and ^{13}C NMR numerical assignments of compounds **4**−**7**.

Table 6. Reaction Yields for *n* Subsequent Steps[a]

	n = 1		*n* = 2		*n* = 3	
	mass	yield	mass	yield	mass	yield
4a	0.68 g	71%	0.25 g	26%	0.15 g	15%
5a			0.32 g	22%	0.35 g	24%
6a			0.14 g	7%	0.23 g	12%
7a	0.08 g	9%	0.15 g	16%	0.08 g	9%
B(a)	0.05 g	8%	0.08 g	13%	0.06 g	9%
C(a)					0.04 g	4%
4b	0.91 g	74%	0.37 g	30%	0.24 g	20%
5b			0.56 g	28%	0.63 g	32%
6b			0.27 g	10%	0.38 g	14%
7b	0.18 g	15%	0.20 g	17%	0.12 g	10%
B(b)	0.11 g	12%	0.14 g	16%	0.10 g	11%
C(b)					0.10 g	6%

[a] *n*BuLi and $M(CO)_6$ were added to 2.00 mmol tri(2-furyl)phosphine under specified reaction conditions (M = Cr(a), W(b)).

Scheme 7. Numerical Proton and Carbon Assignments

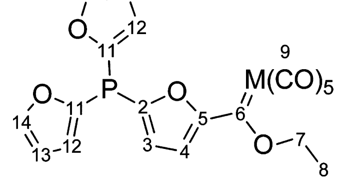

4a: $C_{20}H_{13}O_9PCr$. ^{1}H NMR ($CDCl_3$, 300 MHz) δ 7.67 (ddd, 1.9, 0.7, 0.2 Hz, 2H, H14), 6.95 (ddd, 3.3, 1.8, 0.2 Hz, 2H, H12), 6.85 (dd, 3.6, 1.3 Hz, 1H, H4), 6.64 (d, 3.5 Hz, 1H, H3), 6.44 (ddd, 3.4, 2.0, 1.8 Hz, 2H, H13), 5.10 (q, 7.1 Hz, 2H, H7), 1.60 (t, 7.1 Hz, 3H, H8). ^{13}C NMR ($CDCl_3$, 75 MHz) δ 310.6 (C6), 224.4 (C9, *trans*), 216.6 (C9, *cis*), 167.1 (d, $^{3}J_{\{P\}C}$ = 3.0 Hz, C5), 160.4 (d, $^{1}J_{\{P\}C}$ = 4.2 Hz, C2), 148.3 (d, $^{3}J_{\{P\}C}$ = 2.5 Hz, C14), 146.5 (d, $^{1}J_{\{P\}C}$ = 5.5 Hz, C11), 123.1 (d, $^{2}J_{\{P\}C}$ = 29.1 Hz, C12), 120.8 (d, $^{2}J_{\{P\}C}$ = 13.8 Hz, C3), 111.1 (d, $^{3}J_{\{P\}C}$ = 1.8 Hz, C4), 111.0 (d, $^{3}J_{\{P\}C}$ = 7.1 Hz, C13), 75.6 (C7), 15.3 (C8). ^{31}P NMR (121 MHz, $CDCl_3$): $\delta = -72.8$. IR (cm^{-1}, hexane): 2060(m), 1990(w), 1944(vs). ESI-MS (15 V, positive mode, *m/z*): calcd for $[M + H]^+$ 480.9781; found, 480.9801.

4b: $C_{20}H_{13}O_9PW$. Mp: 48 °C. ^{1}H NMR (400 MHz, $CDCl_3$): δ = 7.67 (ddd, *J* = 1.8, 0.9, 0.7 Hz, 2H, H14), 7.01 (dd, *J* = 3.7, 1.2 Hz, 1H, H4), 6.94 (ddd, *J* = 3.4, 2.4, 0.8 Hz, 2H, H12), 6.65 (dd, *J* = 3.6, 0.2 Hz, 1H, H3), 6.44 (ddd, *J* = 3.4, 2.0, 1.8 Hz, 2H, H13), 4.90 (q, *J* = 7.1 Hz, 2H, H7), 1.58 (t, *J* = 7.1 Hz, 3H, H8). ^{13}C NMR (101 MHz, $CDCl_3$): δ = 284.3 ($^{1}J_{\{W\}C}$ = 50.6 Hz, C6), 203.8 ($^{1}J_{\{W\}C}$ = 58.3 Hz, C9, *trans*), 197.8 ($^{1}J_{\{W\}C}$ = 63.6 Hz, C9, *cis*), 169.3 (d, $^{3}J_{\{P\}C}$ = 3.9 Hz, C5), 160.7 (d, $^{1}J_{\{P\}C}$ = 3.2 Hz, C2), 148.3 (d, $^{3}J_{\{P\}C}$ = 2.2 Hz, C14), 146.2 (d, $^{1}J_{\{P\}C}$ = 6.5 Hz, C11), 123.2 (d, $^{2}J_{\{P\}C}$ = 29.5 Hz, C12), 121.1 (d, $^{2}J_{\{P\}C}$ = 17.2 Hz, C3), 113.4 (C4), 111.0 (d, $^{3}J_{\{P\}C}$ = 7.7 Hz, C13), 78.1 (C7), 15.0 (C8). ^{31}P NMR (162 MHz, $CDCl_3$): $\delta = -72.7$. IR (cm^{-1}, hexane): 2070(m), 1982(w), 1954(s), 1942(vs). ESI-MS (20 V, positive mode, *m/z*): calcd for $C_{20}H_{13}O_9PW$ $[M]^+$ 611.9806; found, 611.9896.

5a: $C_{28}H_{17}O_{15}PCr_2$. ^{1}H NMR ($CDCl_3$, 400 MHz) δ 7.7.5−7.7.3 (m, 1H, H14), 7.10−7.09 (m, 1H, H12), 6.99−6.96 (m, 2H, H4), 6.85 (dd, 3.6, 1.1 Hz, 2H, H3), 6.4.9 (ddd, 3.0, 2.2, 1.7 Hz, 1H, H13), 5.11 (q, 7.0 Hz, 4H, H7), 1.61 (t, 7.0 Hz, 6H, H8). ^{13}C NMR ($CDCl_3$, 101 MHz) δ 311.6 (C6), 224.4 (C9, *trans*), 216.5 (C9, *cis*), 167.1 (d, $^{3}J_{\{P\}C}$ = 3.7 Hz, C5), 157.4 (d, $^{1}J_{\{P\}C}$ = 8.0 Hz, C2), 147.5 (d, $^{3}J_{\{P\}C}$ = 2.5 Hz, C14), 144.0 (d, $^{1}J_{\{P\}C}$ = 8.2 Hz, C11), 124.9 (d, $^{2}J_{\{P\}C}$ = 34.4 Hz, C12), 122.6 (d, $^{2}J_{\{P\}C}$ = 18.4 Hz, C3), 111.1 (d, $^{3}J_{\{P\}C}$ = 6.3 Hz, C4), 110.8 (d, $^{3}J_{\{P\}C}$ = 6.5 Hz, C13), 75.8 (C7), 15.3 (C8). ^{31}P NMR (162 MHz, $CDCl_3$): $\delta = -69.6$. IR (cm^{-1}, hexane): 2061(m), 1996(w), 1961(m), 1948(vs). ESI-MS (15 V, positive mode, *m/z*): calcd for $[M + H]^+$ 728.9194; found, 728.9195.

5b: $C_{28}H_{17}O_{15}PW_2$. ^{1}H NMR ($CDCl_3$, 400 MHz) δ 7.77 (dd, *J* = 1.8, 0.7 Hz, 1H, H14), 7.13−7.11 (m, 1H, H12), 7.04 (dd, 3.7, 1.3 Hz, 2H, H4), 6.89 (dd, *J* = 3.8, 0.5, 2H, H3), 6.51 (ddd, *J* = 3.3, 2.4, 1.8 Hz, 1H, H13), 4.93 (q, 7.1 Hz, 4H, H7), 1.62 (t, 7.1 Hz, 6H, H8). ^{13}C NMR ($CDCl_3$, 101 MHz) δ 285.1 ($^{1}J_{\{W\}C}$ = 52.0 Hz, C6), 203.7 ($^{1}J_{\{W\}C}$ = 58.8 Hz, C9, *trans*), 197.1 ($^{1}J_{\{W\}C}$ = 64.1 Hz, C9, *cis*), 169.6 (d, $^{3}J_{\{P\}C}$ = 2.8 Hz, C5), 157.2 (d, $^{1}J_{\{P\}C}$ = 8.3 Hz, C2), 149.2 (s, C14), 143.5 (d, $^{1}J_{\{P\}C}$ = 5.6 Hz, C11), 123.1 (d, $^{2}J_{\{P\}C}$ = 17.6 Hz, C12), 121.1 (d, $^{2}J_{\{P\}C}$ = 25.4 Hz, C3), 113.1 (d, $^{3}J_{\{P\}C}$ = 1.6 Hz, C4), 110.7 (d, $^{3}J_{\{P\}C}$ = 6.7 Hz, C13), 78.3 (C7), 14.9 (C8). ^{31}P NMR (162 MHz, $CDCl_3$): $\delta = -69.4$. IR (cm^{-1}, hexane): 2070(m), 1992(w), 1956(m), 1942(vs). ESI-MS (15 V, positive mode, *m/z*): calcd for $[M + H]^+$ 992.9407; found, 992.9402.

6a: $C_{36}H_{21}O_{21}PCr_3$. ^{1}H NMR ($CDCl_3$, 300 MHz) δ 7.00 (d, 3.7 Hz, 3H, H4), 6.95 (dd, 3.7, 1.4 Hz, 3H, H3), 5.13 (q, 7.0 Hz, 6H, H7), 1.63 (t, 7.0 Hz, 9H, H8). ^{13}C NMR ($CDCl_3$, 101 MHz) δ 312.0 (C6), 224.1 (C9, *trans*), 216.5 (C9, *cis*), 167.4 (d, $^{3}J_{\{P\}C}$ = 3.7 Hz, C5), 154.3 (d, $^{1}J_{\{P\}C}$ = 7.8 Hz, C2), 123.9 (d, $^{2}J_{\{P\}C}$ = 18.2 Hz, C3), 112.1 (d, $^{3}J_{\{P\}C}$ = 3.7 Hz, C4), 76.0 (s, C7), 15.2 (s, C8). ^{31}P NMR (162 MHz, $CDCl_3$): $\delta = -63.5$. IR (cm^{-1}, hexane): 2061(m), 1996(w), 1952(vs). ESI-MS (15 V, negative mode, *m/z*): calcd for $[M]^-$ 975.8620; found, 975.8605.

6b: $C_{36}H_{21}O_{21}PW_3$. ^{1}H NMR ($CDCl_3$, 400 MHz) δ 7.13 (dd, 3.7, 1.5 Hz, 3H, H4), 7.04 (dd, 3.7, 0.5 Hz, 3H, H3), 4.95 (q, 7.1 Hz, 6H, H7), 1.63 (t, 7.1 Hz, 9H, H8). ^{13}C NMR ($CDCl_3$, 101 MHz) δ 285.4 ($^{1}J_{\{W\}C}$ = 51.0 Hz, C6), 203.4 ($^{1}J_{\{W\}C}$ = 58.7 Hz, C9, *trans*), 197.0 ($^{1}J_{\{W\}C}$ = 64.1 Hz, C9, *cis*), 169.9 (d, $^{3}J_{\{P\}C}$ = 3.5 Hz, C5), 153.8 (^{1}d, $J_{\{P\}C}$ = 8.1 Hz, C2), 124.4 (d, $^{2}J_{\{P\}C}$ = 18.0, C3), 114.4 (C4), 78.5 (C7), 14.9 (C8). ^{31}P NMR (121 MHz, $CDCl_3$): $\delta = -63.2$. IR (cm^{-1}, hexane): 2070(m), 1994(w), 1948(vs). ESI-MS (15 V, positive mode, *m/z*): calcd for $[M + 2H]^{2+}$ 686.9493; found, 686.9550.

7a: $C_{20}H_{19}O_8PCr$. ^{1}H NMR ($CDCl_3$, 400 MHz) δ 7.63−7.62 (m, 1H, H14), 6.85 (ddd, 3.5, 3.0, 1.0 Hz, 1H, H12), 6.82 (dd, 3.7, 1.4 Hz, 1H, H3), 6.65 (d, 3.3 Hz, 1H, H4), 6.40 (ddd, 3.5, 2.0, 0.5 Hz, 1H, H13), 5.11 (q, 7.1 Hz, 2H, H7), 2.34−2.21 (m, 2H, H_{butyl}), 1.61 (t, 7.0 Hz, 3H, H8), 1.41−1.40 (m, 2H, H_{butyl}), 1.24 (s, 2H, H_{butyl}) 0.87 (t, 7.0 Hz, 3H, H_{butyl}). ^{13}C NMR ($CDCl_3$, 101 MHz) δ 310.1 (C6), 224.3 (C9, *trans*), 216.8 (C9, *cis*), 167.2 (C5), 164.0 (d, $^{1}J_{\{P\}C}$ = 24.4 Hz, C2), 149.0 (d, $^{1}J_{\{P\}C}$ = 19.1 Hz, C11), 147.6 (C14), 122.0 (d, $^{2}J_{\{P\}C}$ = 28.3 Hz, C3), 120.6 (d, $^{2}J_{\{P\}C}$ = 18.8 Hz, C12), 110.9 (d, $^{3}J_{\{P\}C}$ = 2.9 Hz, C4), 110.7 (d, $^{3}J_{\{P\}C}$ = 6.8 Hz, C13), 75.5 (C7), 27.9 (d, $^{2}J_{\{P\}C}$ = 15.8, C_{butyl}), 24.3 (d, $^{1}J_{\{P\}C}$ = 2.5 Hz, C_{butyl}), 23.9 (d, $^{3}J_{\{P\}C}$ = 14.0 Hz, C_{butyl}), 15.3 (C8), 13.7 (C_{butyl}). ^{31}P NMR (162 MHz, $CDCl_3$): $\delta = -55.3$. IR (cm^{-1}, hexane): 2069(m), 2000(w), 1958(m), 1952(vs). ESI-MS (15 V, positive mode, *m/z*): calcd for $[M + H]^+$ 471.0301; found, 471.0308.

7b: $C_{20}H_{19}O_8PW$. ^{1}H NMR ($CDCl_3$, 400 MHz) δ 7.69−7.68 (m, 1H, H14), 7.07 (dd, 3.7, 1.3 Hz, 1H, H4), 7.05−7.04 (m, 1H, H13), 6.88 (dd, 3.8, 1.2 Hz, 1H, H3), 6.52−6.50 (m, 1H, H12), 4.93 (q, 7.0 Hz, 2H, H7), 2.75−2.60 (m, 2H, H_{butyl}), 1.61 (t, 7.0 Hz, 3H, H8), 1.53 (s, 2H, H_{butyl}), 1.48−1.43 (m, 2H, H_{butyl}), 0.91 (t, 7.2 Hz, 3H, H_{butyl}). ^{13}C NMR ($CDCl_3$, 101 MHz) δ 285.5 (C6), 203.1 ($^{1}J_{\{W\}C}$ = n.o., C9, *trans*), 196.9 ($^{1}J_{\{W\}C}$ = 62.4 Hz, C9, *cis*), 169.0 (^{3}C5), 158.6 (d, $^{1}J_{\{P\}C}$ = 45.4 Hz, C2), 148.4 (d, $^{3}J_{\{P\}C}$ = 4.1 Hz, C14), 146.9 (d, $^{1}J_{\{P\}C}$ = 53.1 Hz, C11), 122.6 (d, $^{2}J_{\{P\}C}$ = 19.3 Hz, C3), 121.8 (d, $^{2}J_{\{P\}C}$ = 16.8 Hz, C12), 113.7 (d, $^{3}J_{\{P\}C}$ = 5.9 Hz, C4), 111.4 (d, $^{3}J_{\{P\}C}$ = 6.8 Hz, C13), 78.5 (C7), 29.3 (d, $^{1}J_{\{P\}C}$ = 31.8 Hz, C_{butyl}), 26.3 (C_{butyl}), 23.7 (C_{butyl}), 15.0 (C8), 13.5 (C_{butyl}). ^{31}P NMR (162 MHz, $CDCl_3$): $\delta = -55.0$. IR (cm^{-1}, hexane): 2070(m), 1988(w), 1948(vs). ESI-MS (15 V, positive mode, *m/z*): calcd for $[M]^+$ 602.0327; found, 602.0326.

8b: $C_{25}H_{13}O_{14}PW_2$. ^{1}H NMR (400 MHz, $CDCl_3$): δ = 7.72−7.72 (m, 2H, H14), 7.19−7.18 (m, 1H, H4), 7.00−6.99 (m, 2H, H12), 6.82−6.79 (m, 1H, H3), 6.57−6.55 (m, 2H, H13), 4.93 (q, *J* = 7.0 Hz, 2H, H7), 1.62 (t, *J* = 7.1 Hz, 3H, H8). ^{13}C NMR (101 MHz, $CDCl_3$): δ = 285.1 ($^{1}J_{\{W\}C}$ = n.o., C6), 203.7 ($^{1}J_{\{W\}C}$ = n.o., C9, *trans*), 197.1 ($^{1}J_{\{W\}C}$ = 62.3 Hz, C9, *cis*), 169.6 (d, $^{3}J_{\{P\}C}$ = 3.5 Hz, C5), 157.2 (d, $^{1}J_{\{P\}C}$ = 8.1 Hz, C2), 147.4 (d, $^{3}J_{\{P\}C}$ = 2.5 Hz, C14), 146.2 (d, $^{1}J_{\{P\}C}$ = 6.5 Hz, C11), 125.1 (d, $^{2}J_{\{P\}C}$ = 34.8 Hz, C12), 122.6 (d, $^{2}J_{\{P\}C}$ = 18.8 Hz, C3), 111.6 (d, $^{3}J_{\{P\}C}$ = 6.9 Hz, C4), 111.3 (d, $^{3}J_{\{P\}C}$ = 6.6 Hz, C13), 78.3 (C7), 14.9 (C8).^{31}P NMR (162 MHz, $CDCl_3$): $\delta = -11.7$ ppm. IR (cm^{-1}, hexane): 2080(m), 1990(w), 1962(vs). ESI-MS (20 V, positive mode, *m/z*): calcd for $[M]^+$ 935.9067; found, 935.9070.

The synthesis and characterization of **B** and **C** have been reported.[30]

*Synthesis of [({W(CO)$_5$C(OEt)Fu′}PFu$_2$)$_2$PtCl$_2$] (**9**).* [Pt(COD)Cl_2] (0.24 g, 0.64 mmol) was dissolved in 20 mL of CH_2Cl_2 and added to a solution of **4b** (0.78 g, 1.3 mmol) dissolved in 10 mL of CH_2Cl_2. The reaction mixture was allowed to stir for 18 h at room temperature after which the solvent was removed under reduced pressure. The red-brown product was isolated from a silica gel column by eluting with CH_2Cl_2. Crystals were isolated from CH_2Cl_2 by slow diffusion of hexane into the solution. Yield: 0.80 g (84.3%).

9b: $C_{40}H_{26}O_{18}P_2W_2PtCl_2$. ^{1}H NMR (400 MHz, $CDCl_3$): δ = 7.53 (ddd, *J* = 1.7, 0.9, 0.8 Hz, 4H, H14), 7.09 (ddd, *J* = 3.7, 1.3, 1.0 Hz, 4H, H12), 7.08 (dd, *J* = 3.8, 2.1 Hz, 2H, H4), 6.96 (dd, *J* = 3.8, 1.8 Hz, 2H, H3), 6.42 (ddd, *J* = 5.2, 3.7, 1.8 Hz, 4H, H13), 4.88 (q, *J* = 7.1 Hz, 4H, H7), 1.59 (t, *J* = 7.1 Hz, 6H, H8). ^{13}C NMR (101 MHz, $CDCl_3$): δ = 286.4 ($^{1}J_{\{W\}C}$ = 52.6 Hz, C6), 203.7 ($^{1}J_{\{W\}C}$ = 57.2 Hz, C9, *trans*), 196.6 ($^{1}J_{\{W\}C}$ = 63.1 Hz, C9, *cis*), 169.3 (d, $^{4}J_{\{P\}C}$ = 5.2 Hz, C5), 149.2 (d, $^{4}J_{\{P\}C}$ = 3.2 Hz, C14), 138.3 (d, $^{1}J_{\{P\}C}$ = 3.7 Hz, C2), 137.2 (d, $^{1}J_{\{P\}C}$ = 3.2 Hz, C11), 126.4 (d, $^{2}J_{\{P\}C}$ = 19.8 Hz, C12), 126.3 (d, $^{2}J_{\{P\}C}$ = 10.5 Hz, C3), 112.2 (d, $^{3}J_{\{P\}C}$ = 3.8 Hz, C4), 111.6 (d, $^{3}J_{\{P\}C}$ = 4.2 Hz, C13), 78.5 (C7), 15.0 (C8). ^{31}P NMR (162 MHz, $CDCl_3$): $\delta = -35.3$ ($^{1}J_{\{Pt\}P}$ = 1847 Hz). IR (cm^{-1}, CH_2Cl_2): 2069(m), 1990(w), 1944(vs). ESI-MS (20 V, positive mode, *m/z*): calcd for $[M + Na]^+$ 1511.8542; found, 1511.8587.

COMPUTATIONAL DETAILS

All of the calculations reported in this article were obtained with the Gaussian 09 suite of programs.[60] All species were optimized at the DFT level using the B3LYP[61,62] functional with the triple-ξ valence plus polarization basis set def2-TZVP[63] for all atoms. This protocol is denoted B3LYP/def2-TZVP. All compounds were characterized by frequency calculations[64] and have a positive defined Hessian matrix indicating that they are minima on the potential energy surface. Calculations of absorption spectra were accomplished by using the TD-DFT[65,66] method at the same level. TD-DFT calculations were performed in dichloromethane as solvent using the polarizable continuum model (PCM) method.[67−69] This protocol is denoted PCM(CH_2Cl_2)-TD-B3LYP/def2-TZVP. The assignment of the excitation energies to the experimental bands was performed on the basis of the energy values and oscillator strengths. The B3LYP Hamiltonian was chosen because it was proven to provide reasonable UV/vis spectra for a variety of chromophores[70] including Fischer carbene complexes[44,47] and other organometallic species.[71−73]

Donor−acceptor interactions and WBI have been computed using the NBO method.[74−77] The energies associated with these two-electron interactions have been computed according to the following equation:

$$\Delta E^{(2)}_{\phi\phi^*} = -n_\phi \frac{\langle \phi^* | \hat{F} | \phi \rangle^2}{\varepsilon_{\phi^*} - \varepsilon_\phi}$$

where $\hat{F}$ is the DFT equivalent of the Fock operator, and ϕ and ϕ^* are two filled and unfilled NBOs having ε_ϕ y $\varepsilon_\phi{}^*$ and energies, respectively; n_ϕ stands for the occupation number of the filled orbital.

AUTHOR INFORMATION

Corresponding Authors

*(I.F.) E-mail: israel@quim.ucm.es.
*(S.L.) E-mail: simon.lotz@up.ac.za.

Notes

The authors declare no competing financial interest.

ACKNOWLEDGMENTS

We are grateful for assistance by Mr. E. R. Palmer (NMR), Dr. M. Landman (full crystallographic data set of compound **B(b)**,[49] and Dr. D. Koot (MS analysis). We gratefully acknowledge the financial support from the National Research Foundation (NRF) of South Africa under grant number 73679, the Spanish MINECO grant CTQ2013-44303-P, and European FEDER.

DEDICATION

This work is dedicated to Professor Cedric Holzapfel on the occasion of his 80th birthday.

REFERENCES

(1) Fischer, E. O.; Maasböl, A. *Angew. Chem., Int. Ed.* **1964**, *3*, 580−581.

(2) Wu, Y.-T.; Kurahashi, T.; Meijere, A. de. *J. Organomet. Chem.* **2005**, *690*, 5900−5911.

(3) Sierra, M. A.; Gómez-Gallego, M.; Martínez-Alvarez, R. *Chem.—Eur. J.* **2007**, *13*, 736−744.

(4) Waters, M. L.; Wulff, W. D. *Org. React.* **2008**, *70*, 121−623.

(5) Dötz, K. H.; Stendel, J., Jr. *Chem. Rev.* **2009**, *109*, 3227−3274.

(6) Herndon, J. W. *Coord. Chem. Rev.* **2010**, *254*, 103−194.

(7) Fernández, I.; Cossío, F. P.; Sierra, M. A. *Acc. Chem. Res.* **2011**, *44*, 479−490.

(8) Aguilar, E.; Lopez, L. A. *Sci. Synth., Knowl. Updates* **2014**, *2*, 1−137.

(9) Leininger, S.; Olenyuk, B.; Stang, P. J. *Chem. Rev.* **2000**, *100*, 853−908.

(10) Tranchemontagne, D. J.; Mendoza-Cortés, J. L.; O'Keeffe, M.; Yaghi, O. M. *Chem. Soc. Rev.* **2009**, *38*, 1257−1283.

(11) Chakrabarty, R.; Mukherjee, P. S.; Stang, P. J. *Chem. Rev.* **2011**, *111*, 6810−6918.

(12) Kim, S. B.; Sweigart, D. A.; Lotz, S. Nanomaterials: Inorganic and Bioinorganic Perspectives. In *Encyclopedia of Inorganic Chemistry*; Lukehart, C. M., Scott, R. A., Eds.; J. Wiley & Sons: New York, 2008; p 775.

(13) Ulrich, K.; Guerchais, V.; Dötz, K.-H.; Toupet, L.; Le Bozec, H. *Eur. J. Inorg. Chem.* **2001**, *2001*, 725−732.

(14) Lotz, S.; Crause, C.; Olivier, A. J.; Liles, D. C.; Görls, H.; Landman, M.; Bezuidenhout, D. I. *Dalton Trans.* **2009**, 697−710.

(15) Hartbaum, C.; Mauz, E.; Roth, G.; Weissenbach, K.; Fischer, H. *Organometallics* **1999**, *18*, 2619−2627.

(16) Landman, M.; Görls, H.; Lotz, S. *J. Organomet. Chem.* **2001**, *617−618*, 280−287.

(17) Dovesi, S.; Solari, E.; Scopelliti, R.; Floriani, C. *Angew. Chem., Int. Ed.* **1999**, *38*, 2388−2391.

(18) Bezuidenhout, D. I.; Lotz, S.; Landman, M.; Liles, D. C. *Inorg. Chem.* **2011**, *50*, 1521−1533.

(19) Bezuidenhout, D. I.; Van der Watt, E.; Liles, D. C.; Landman, M.; Lotz, S. *Organometallics* **2008**, *27*, 2447−2456.

(20) Shieh, M.; Chen, H.-S.; Lai, Y.-W. *Organometallics* **2004**, *23*, 4018−4025.

(21) Bezuidenhout, D. I.; Barnard, W.; van der Westhuizen, B.; van der Watt, E.; Liles, D. C. *Dalton Trans.* **2011**, *40*, 6711−6721.

(22) Werner, M.; Lis, T.; Bruhn, C.; Linder, R.; Steinborn, D. *Organometallics* **2006**, *25*, 5946−5954.

(23) Bezuidenhout, D. I.; Lotz, S.; Liles, D. C.; van der Westhuizen, B. *Coord. Chem. Rev.* **2012**, *256*, 479−524.

(24) Bernasconi, C. F. *Chem. Soc. Rev.* **1997**, *26*, 299−307.

(25) Ning, Z.; Tian, H. *Chem. Commun.* **2009**, 5483−5495.

(26) Wu, G.; Kong, F.; Zhang, Y.; Zhang, X.; Li, J.; Chen, W.; Liu, W.; Ding, Y.; Zhang, C.; Zhang, B.; Yao, J.; Dai, S. *J. Phys. Chem. C* **2014**, *118*, 8756−8765.

(27) Tang, S.; Li, W.; Shen, F.; Liu, D.; Yang, B.; Ma, Y. *J. Mater. Chem.* **2012**, *22*, 4401−4408.

(28) Polit, W.; Exner, T.; Wuttke, E.; Winter, R. F. *BioInorg. React. Mech.* **2012**, *8*, 85−105.

(29) Lotz, S.; van den Berg, M.; Dillen, J. L. M. *Trans. Met. Chem.* **1988**, *13*, 170−175.

(30) Crause, C.; Görls, H.; Lotz, S. *Dalton Trans.* **2005**, 1649−1657.

(31) Ackermann, M.; Pascariu, A.; Höcher, T.; Siehl, H.-U.; Berger, S. *J. Am. Chem. Soc.* **2006**, *128*, 8434−8440.

(32) Andersen, N. G.; Keay, B. A. *Chem. Rev.* **2001**, *101*, 997−1030.

(33) Fernández, I.; Sierra, M. A.; Cossío, F. P. *J. Org. Chem.* **2006**, *71*, 6178−6184.

(34) Fernández, I.; Sierra, M. A.; Cossío, F. P. *J. Org. Chem.* **2008**, *73*, 2083−2089.

(35) Andrada, D. M.; Granados, A. M.; Solá, M.; Fernández, I. *Organometallics* **2011**, *30*, 466−476.

(36) Raubenheimer, H. G. *Dalton Trans.* **2014**, *43*, 16959−16973.

(37) Seidel, G.; Fürstner, A. *Angew. Chem., Int. Ed.* **2014**, *53*, 4807−4811.

(38) Schrage, H.; Vögtle, F.; Steckhan, E. *J. Inclusion Phenom. Macrocyclic Chem.* **1988**, *6*, 157−165.

(39) Eberson, L.; Hartshorn, M. P.; Svensson, J. O. *Acta Chem. Scand.* **1997**, *51*, 279−288.

(40) Mills, O. S.; Redhouse, A. D. *J. Chem. Soc. A* **1968**, 642−647.

(41) See computational details.

(42) Chu, G. M.; Fernández, I.; Sierra, M. A. *Chem.—Eur. J.* **2013**, *19*, 5899−5908.

(43) Hegedus, L. S. *Tetrahedron* **1997**, *53*, 4105−4128.

(44) Lage, M. L.; Fernández, I.; Mancheño, M. J.; Sierra, M. A. *Inorg. Chem.* **2008**, *47*, 5253−5258.

(45) Block, T. F.; Fenske, R. F.; Casey, C. P. *J. Am. Chem. Soc.* **1976**, *98*, 441−443.

(46) Foley, H. C.; Strubinger, L. M.; Targos, T. S.; Geoffroy, G. L. *J. Am. Chem. Soc.* **1983**, *105*, 3064.

(47) Chu, G. M.; Guerrero-Martínez, A.; Fernández, I.; Sierra, M. Á. *Chem.—Eur. J.* **2014**, *20*, 1367−1375.

(48) Monkowius, U. V.; Nogai, S.; Schmidbaur, H. *Dalton Trans.* **2004**, 1610−1617.

(49) Landman, M.; Pretorius, R.; Buitendach, B. E.; van Rooyen, P. H.; Conradie, J. *Organometallics* **2013**, *32*, 5491−5503.

(50) Bernasconi, C. F. *Adv. Phys. Org. Chem.* **2002**, *37*, 137−237.

(51) ALQaisi, S. M.; Galat, K. J.; Minghui, C.; Ray, D. G., III; Rinaldi, P. L.; Tessier, C. A.; Youngs, W. J. *J. Am. Chem. Soc.* **1998**, *120*, 12149−12150.

(52) Kumazawa, K.; Biradha, K.; Kusukawa, T.; Okano, T.; Fujita, M. *Angew. Chem., Int. Ed.* **2003**, *42*, 3909−3913.

(53) Schmidtendorf, M.; Pape, T.; Hahn, F. E. *Angew. Chem., Int. Ed.* **2012**, *51*, 2195−2198.

(54) Smulders, M. M. J.; Riddell, I. A.; Browne, C.; Nitschke, J. R. *Chem. Soc. Rev.* **2013**, *42*, 1728−1754.

(55) Gómez-Gallego, M.; Mancheño, M. J.; Sierra, M. A. *Acc. Chem. Res.* **2005**, *38*, 44−53.

(56) Fernández, I.; Mancheño, M. J.; Vicente, R.; López, L. A.; Sierra, M. A. *Chem.—Eur. J.* **2008**, *14*, 11222−11230.

(57) Chu, G. M.; Fernández, I.; Sierra, M. A. *J. Org. Chem.* **2013**, *78*, 865−871.

(58) Clark, H. C.; Manzer, L. E. *J. Organomet. Chem.* **1973**, *59*, 411−428.

(59) Meerwein, H. *Org. Synth.* **1966**, *46*, 113−114.

(60) Frisch, M. J.; Trucks, G. W.; Schlegel, H. B.; Scuseria, G. E.; Robb, M. A.; Cheeseman, J. R.; Scalmani, G.; Barone, V.; Mennucci, B.; Petersson, G. A.; Nakatsuji, H.; Caricato, M.; Li, X.; Hratchian, H. P.; Izmaylov, A. F.; Bloino, J.; Zheng, G.; Sonnenberg, J. L.; Hada, M.; Ehara, M.; Toyota, K.; Fukuda, R.; Hasegawa, J.; Ishida, M.; Nakajima, T.; Honda, Y.; Kitao, O.; Nakai, H.; Vreven, T.; Montgomery, J. A. Jr.; Peralta, J. E.; Ogliaro, F.; Bearpark, M.; Heyd, J. J.; Brothers, E.; Kudin, K. N.; Staroverov, V. N.; Kobayashi, R.; Normand, J.; Raghavachari, K.; Rendell, A.; Burant, J. C.; Iyengar, S. S.; Tomasi, J.; Cossi, M.; Rega, N.; Millam, M. J.; Klene, M.; Knox, J. E.; Cross, J. B.; Bakken, V.; Adamo, C.; Jaramillo, J.; Gomperts, R.; Stratmann, R. E.; Yazyev, O.; Austin, A. J.; Cammi, R.; Pomelli, C.; Ochterski, J. W.; Martin, R. L.; Morokuma, K.; Zakrzewski, V. G.; Voth, G. A.; Salvador, P.; Dannenberg, J. J.; Dapprich, S.; Daniels, A. D.; Farkas, Ö.; Foresman, J. B.; Ortiz, J. V.; Cioslowski, J.; Fox, D. J. *Gaussian 09*, revision D.01; Gaussian, Inc.: Wallingford CT, 2009.

(61) Becke, A. D. *J. Chem. Phys.* **1993**, *98*, 5648−5652.

(62) Lee, C.; Yang, W.; Parr, R. G. *Phys. Rev. B* **1988**, *37*, 785−789.

(63) Weigend, F.; Ahlrichs, R. *Phys. Chem. Chem. Phys.* **2005**, *7*, 3297−3305.

(64) McIver, J. W., Jr.; Komornicki, A. *J. Am. Chem. Soc.* **1972**, *94*, 2625−2633.

(65) Casida, M. E. In *Recent Developments and Applications of Modern Density Functional Theory*; Seminario, J. M., Ed.; Elsevier: Amsterdamm, The Netherlands, 1996; p 391.

(66) Chong, D. P. In *Recent Advances in Density Functional Methods, Part 1*; Chong, D. P., Ed.; World Scientific: Singapore, 1995; p 155.

(67) Miertuš, S.; Scrocco, E.; Tomasi, J. *Chem. Phys.* **1981**, *55*, 117−129.

(68) Pascual-Ahuir, J. L.; Silla, E.; Tuñón, I. *J. Comput. Chem.* **1994**, *15*, 1127−1138.

(69) Barone, V.; Cossi, M. *J. Phys. Chem. A* **1998**, *102*, 1995−2001.

(70) Dreuw, A.; Head-Gordon, M. *Chem. Rev.* **1995**, *105*, 4009−4037.

(71) Nemykin, V. N.; Makarova, E. A.; Grosland, J. O.; Hadt, R. G.; Koposov, A. Y. *Inorg. Chem.* **2007**, *46*, 9591−9601.

(72) Braunschweig, H.; Herbst, T.; Rais, D.; Ghosh, S.; Kupfer, T.; Radacki, K.; Crawford, A. G.; Ward, R. M.; Marder, T. B.; Fernández, I.; Frenking, G. *J. Am. Chem. Soc.* **2009**, *131*, 8989−8999.

(73) López-Alberca, M. P.; Mancheño, M. J.; Fernández, I.; Gómez-Gallego, M.; Sierra, M. A.; Torres, R. *Chem.—Eur. J.* **2009**, *15*, 3595−3603.

(74) Foster, J. P.; Weinhold, F. *J. Am. Chem. Soc.* **1980**, *102*, 7211−7218.

(75) Reed, A. E.; Weinhold, F. *J. Chem. Phys.* **1985**, *83*, 1736−1740.

(76) Reed, A. E.; Weinstock, R. B.; Weinhold, F. *J. Chem. Phys.* **1985**, *83*, 735−746.

(77) Reed, A. E.; Curtiss, L. A.; Weinhold, F. *Chem. Rev.* **1988**, *88*, 899−926.

SUPPLEMENTARY INFORMATION

Contents

NMR Spectra

1a′ ^{1}H NMR spectrum

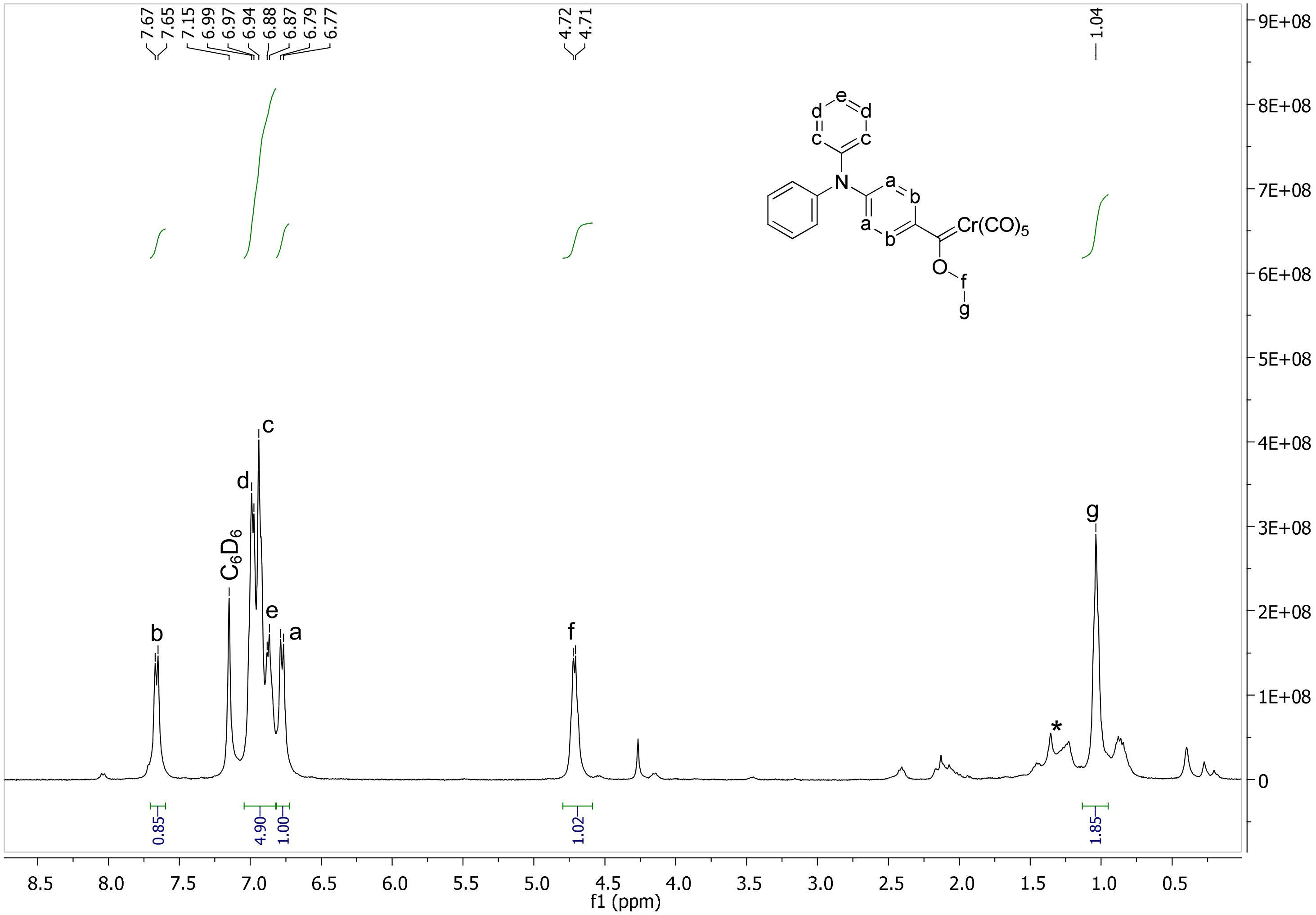

*Solvent contaminant

1a′ ^{13}C NMR spectrum

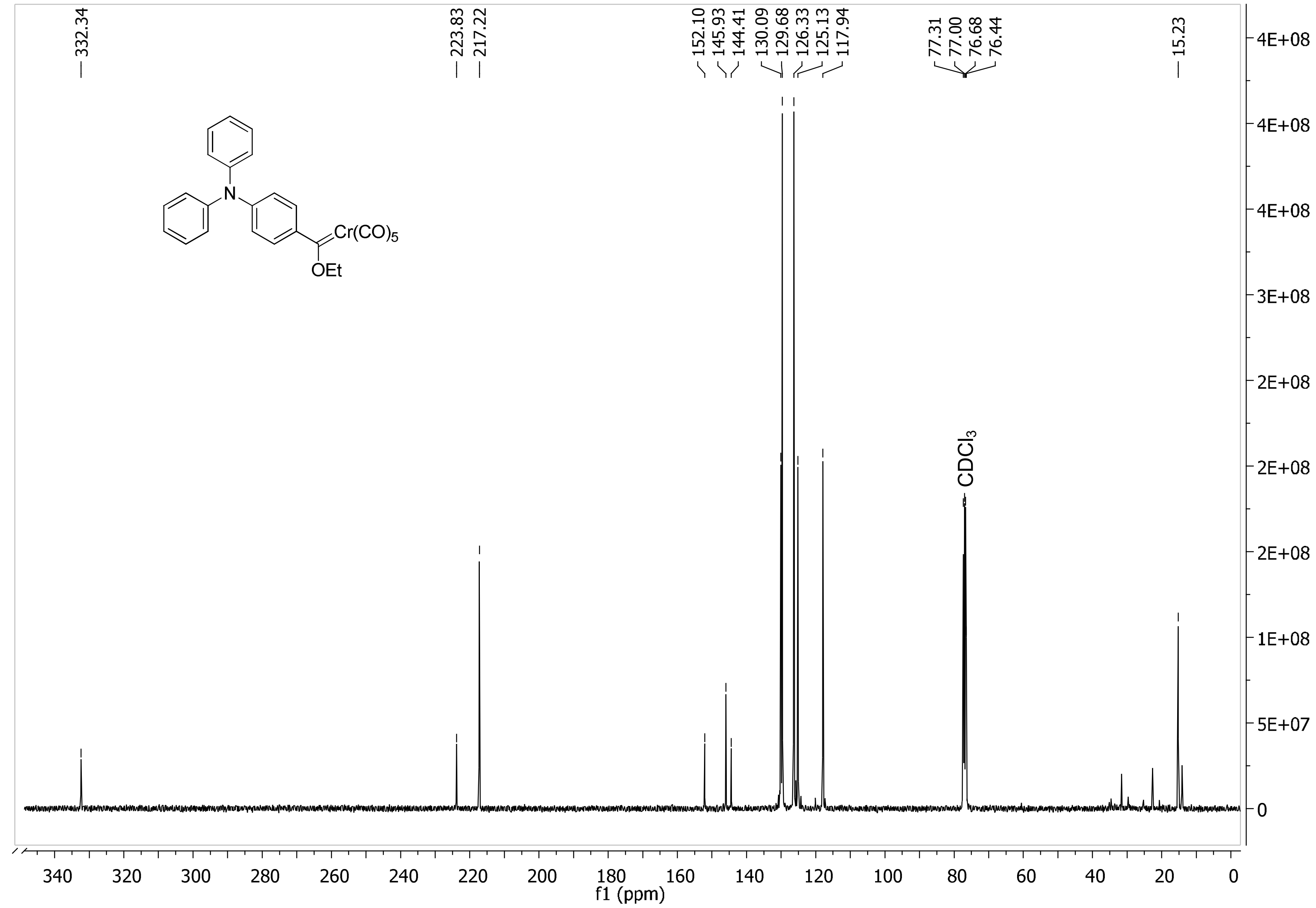

1a ^{1}H NMR spectrum

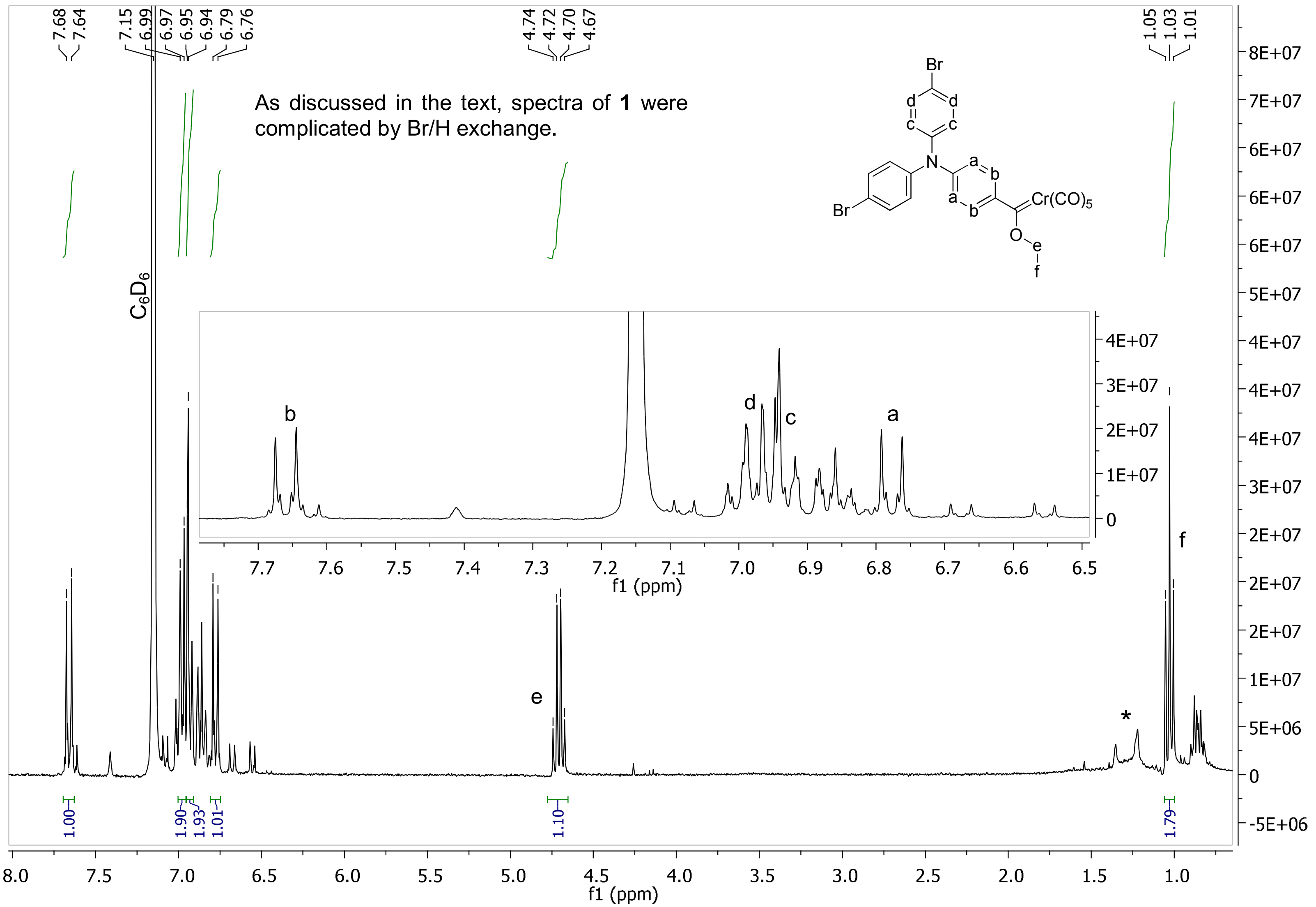
As discussed in the text, spectra of **1** were complicated by Br/H exchange.

* Solvent contaminant

1a ^{13}C NMR spectrum

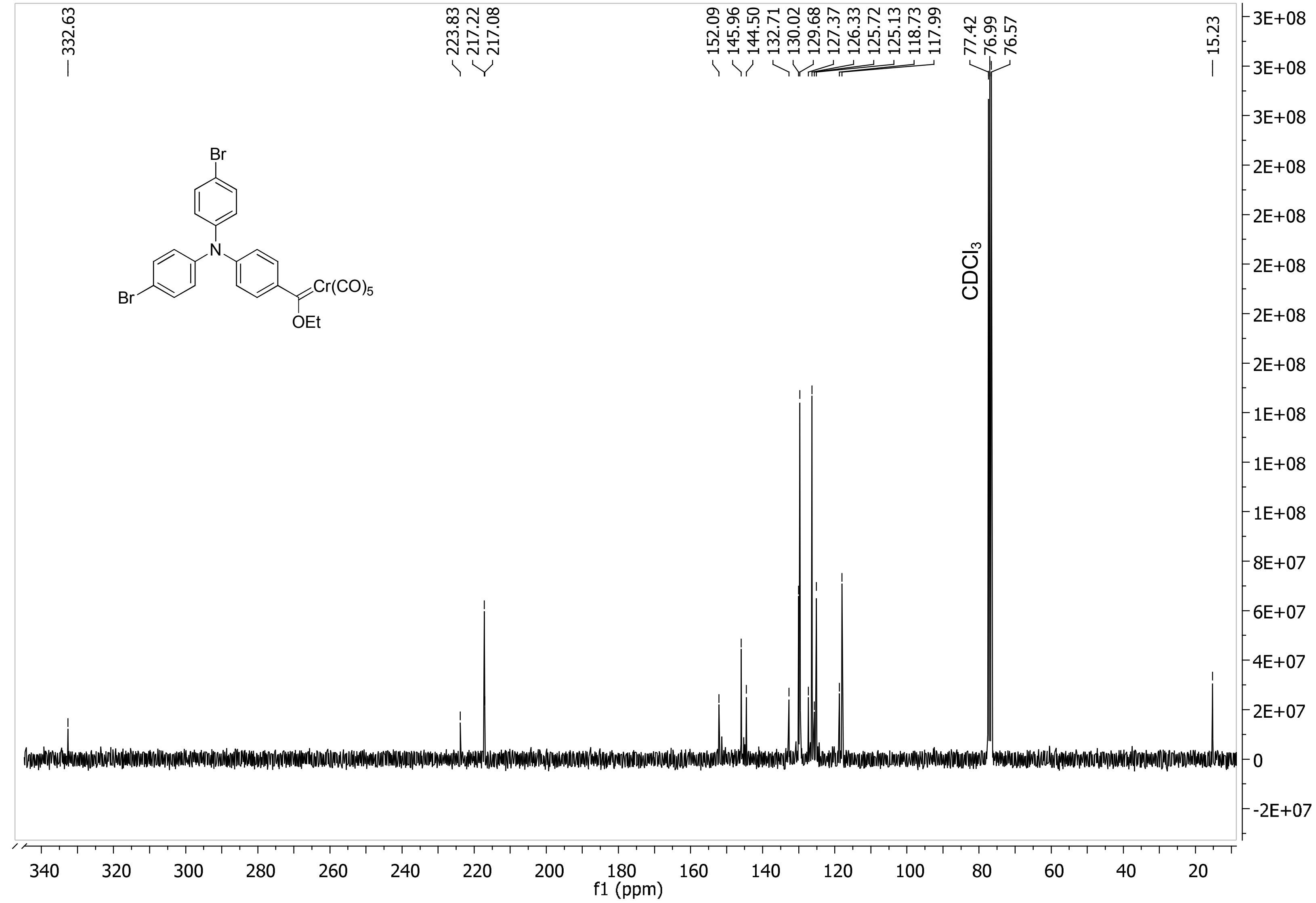

1b ^{1}H NMR spectrum

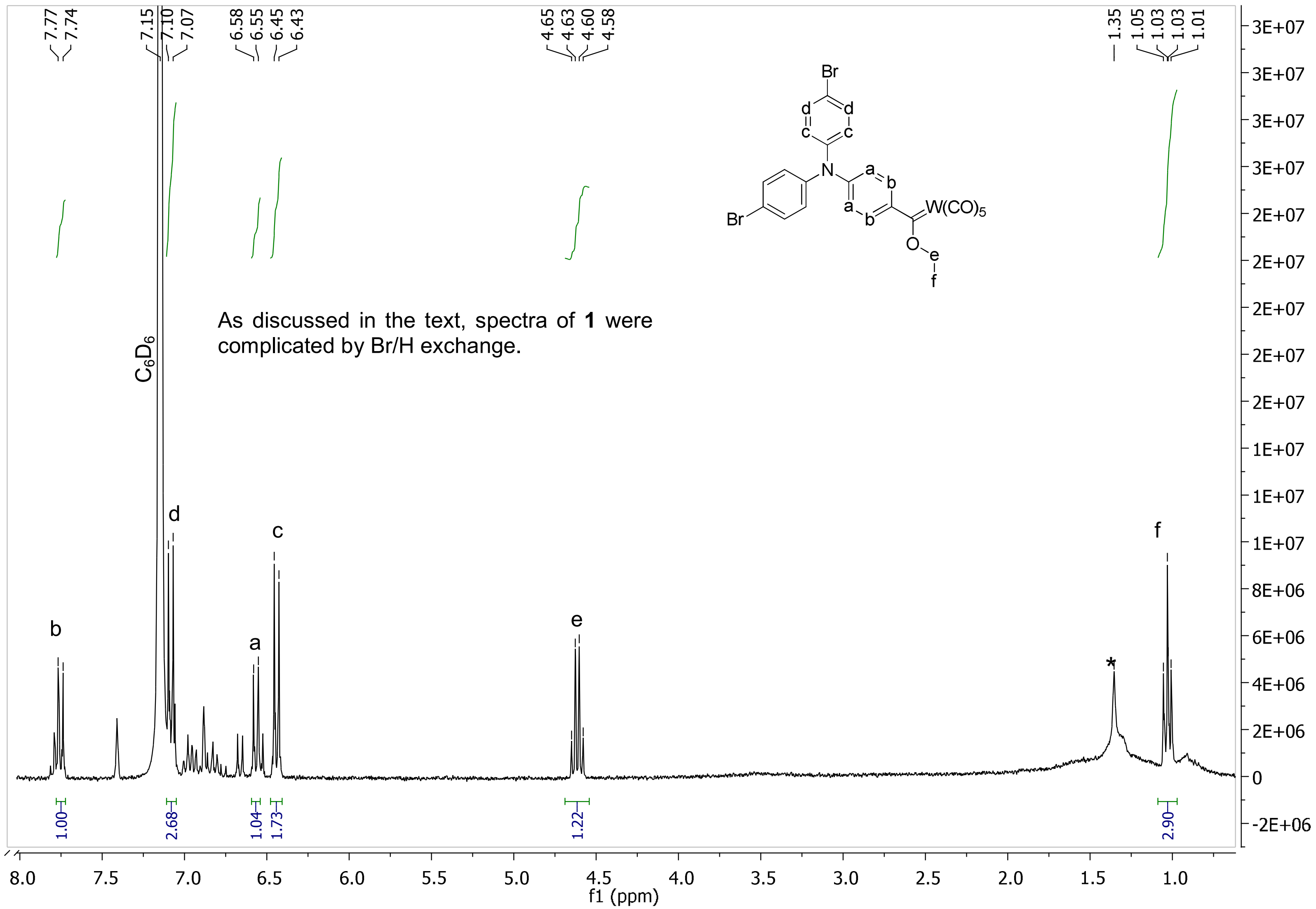

As discussed in the text, spectra of **1** were complicated by Br/H exchange.

*Solvent contaminant

1b ^{13} C NMR spectrum

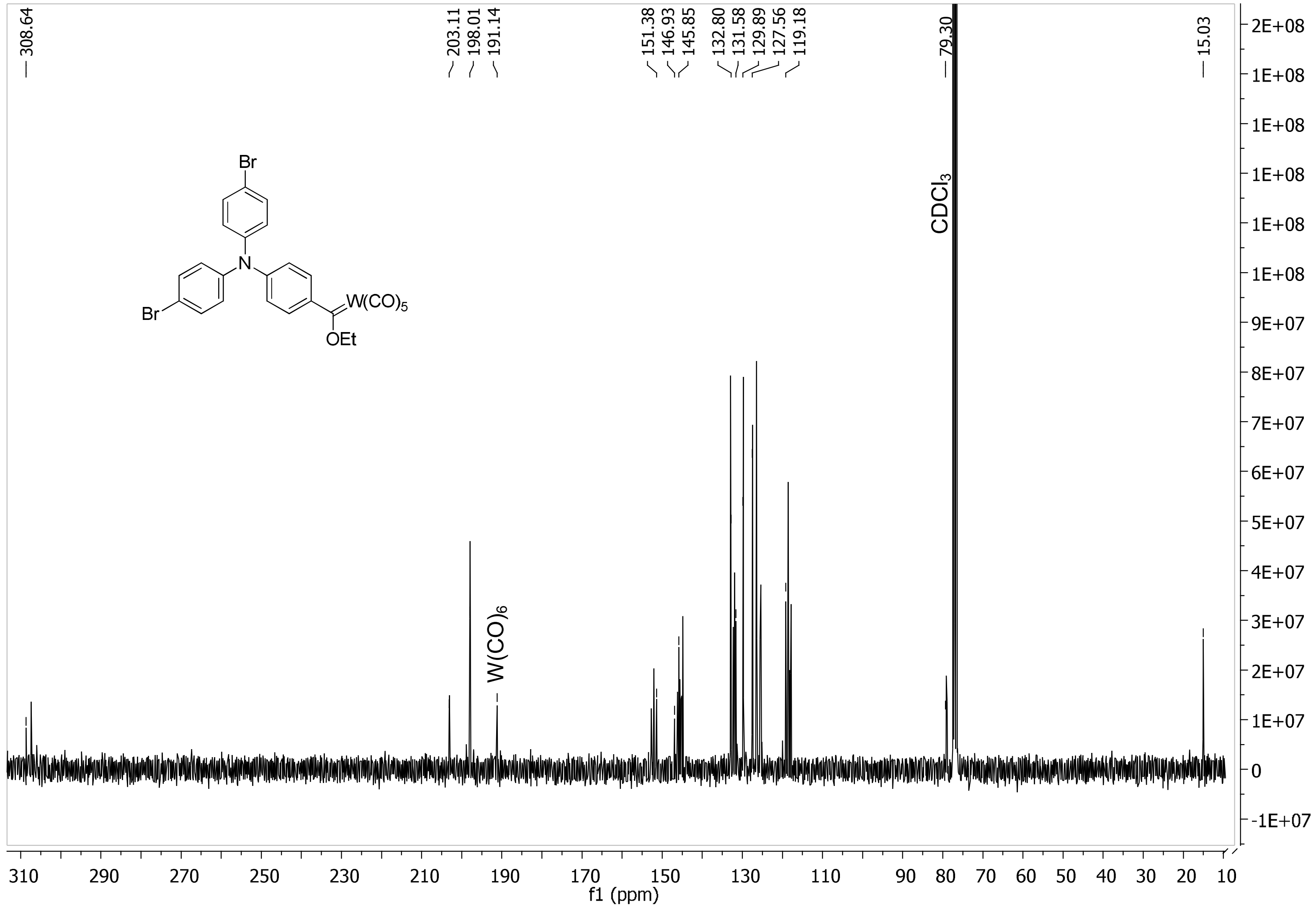

2a ^{1}H NMR spectrum

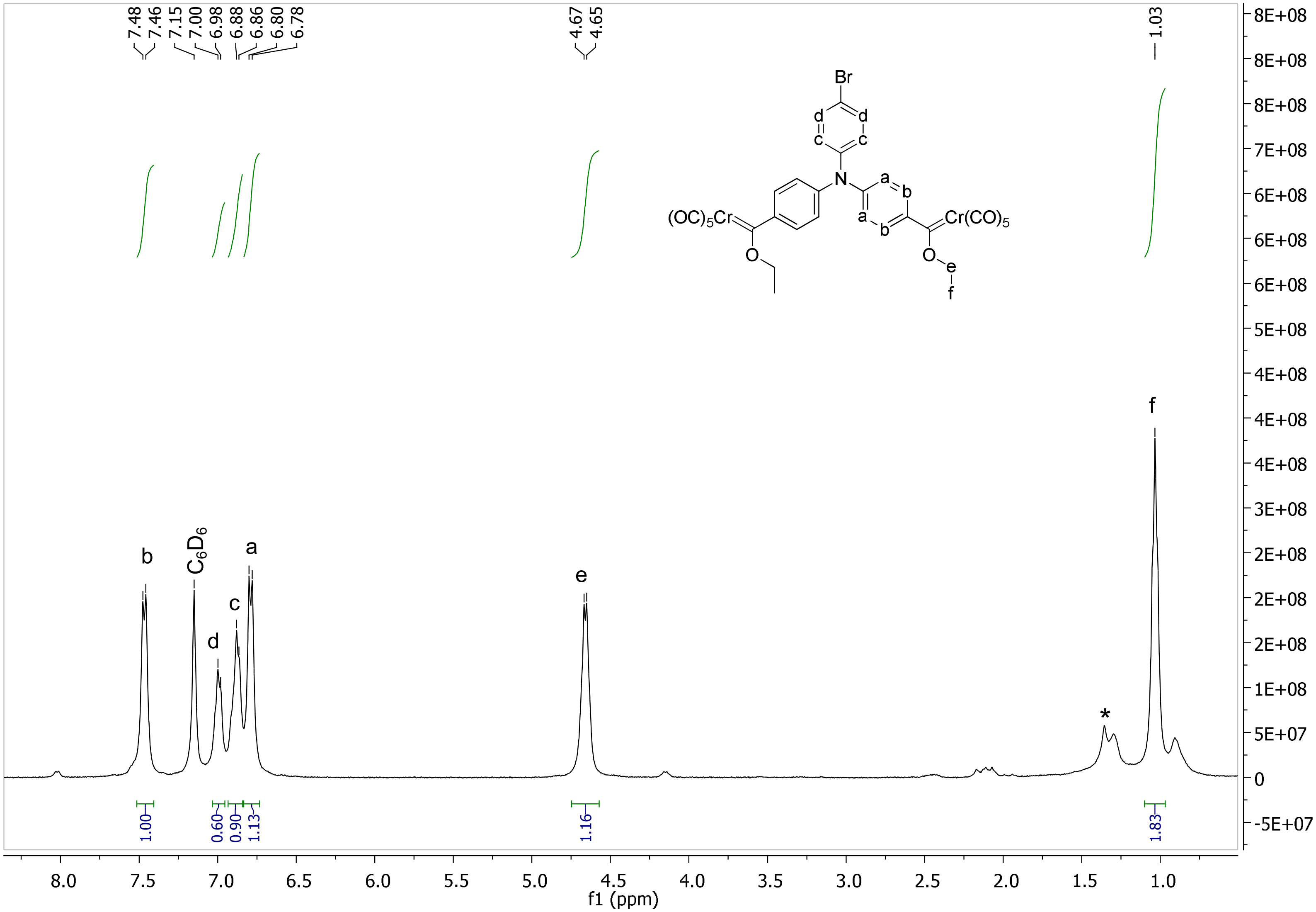

*Solvent contaminant

2a ^{13}C NMR spectrum

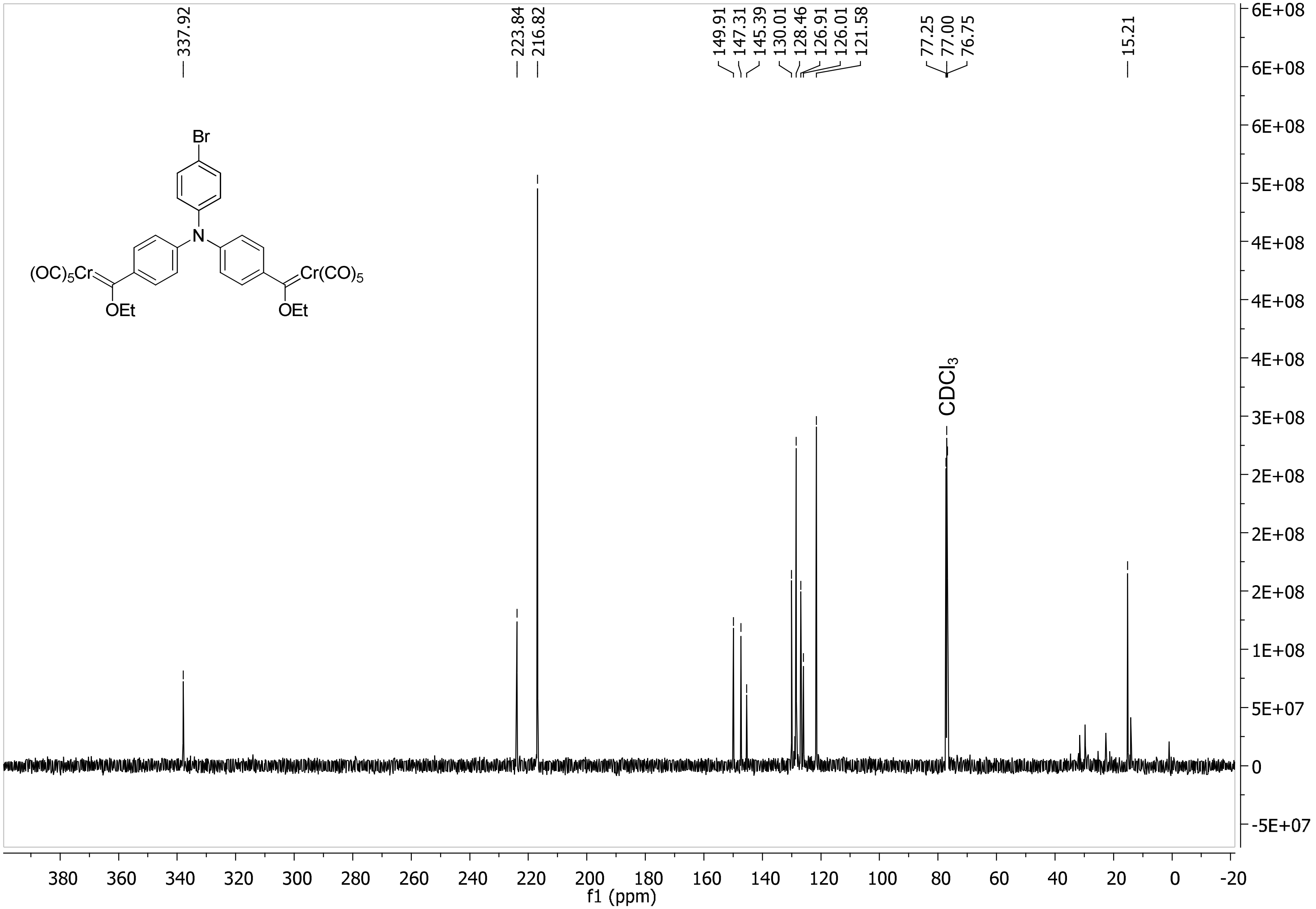

2b ^{1}H NMR spectrum

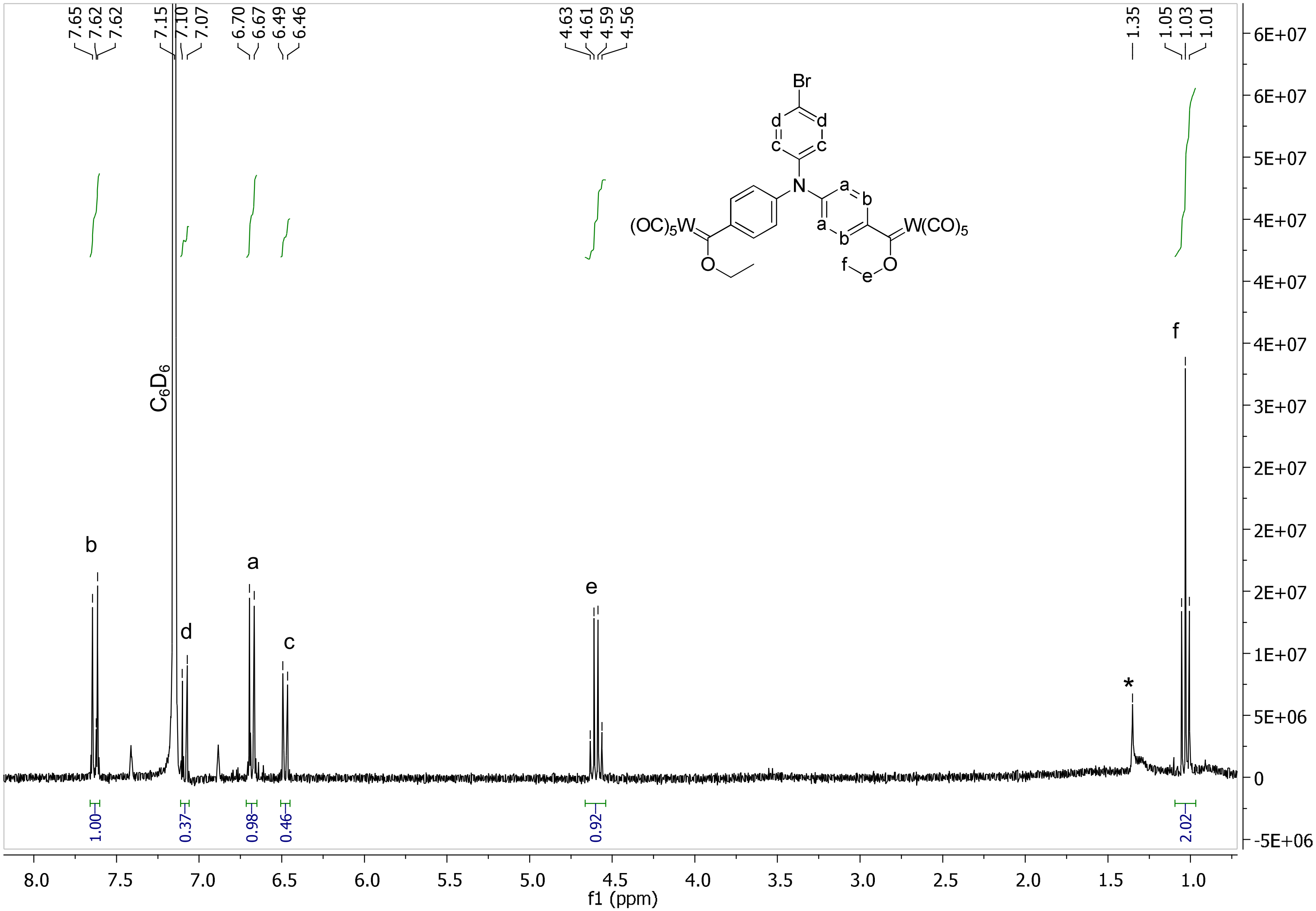

*Solvent contaminant

2b ^{13}C NMR spectrum

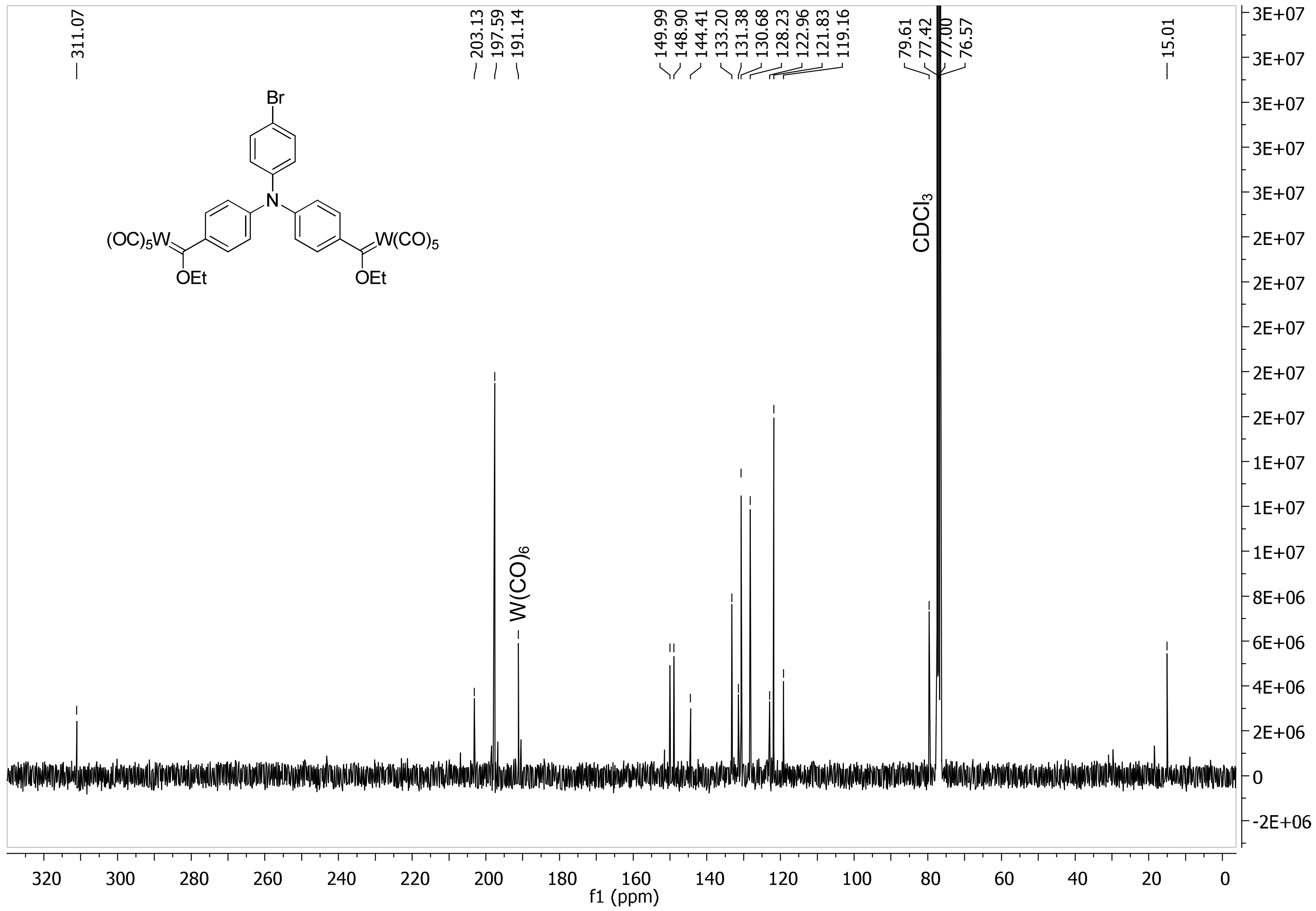

3a ^{1}H NMR spectrum

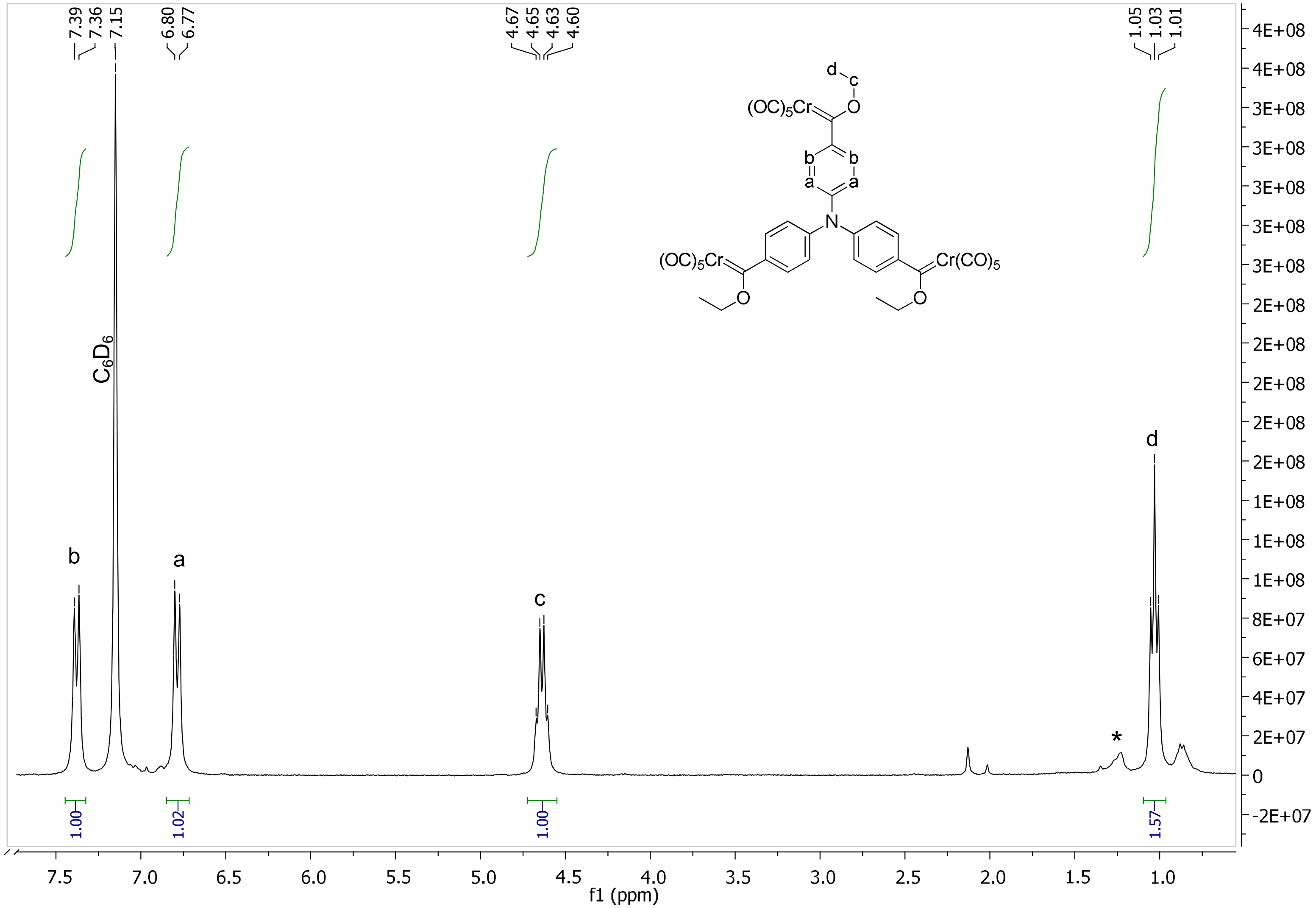

*Solvent contaminant

3a ^{13}C NMR spectrum

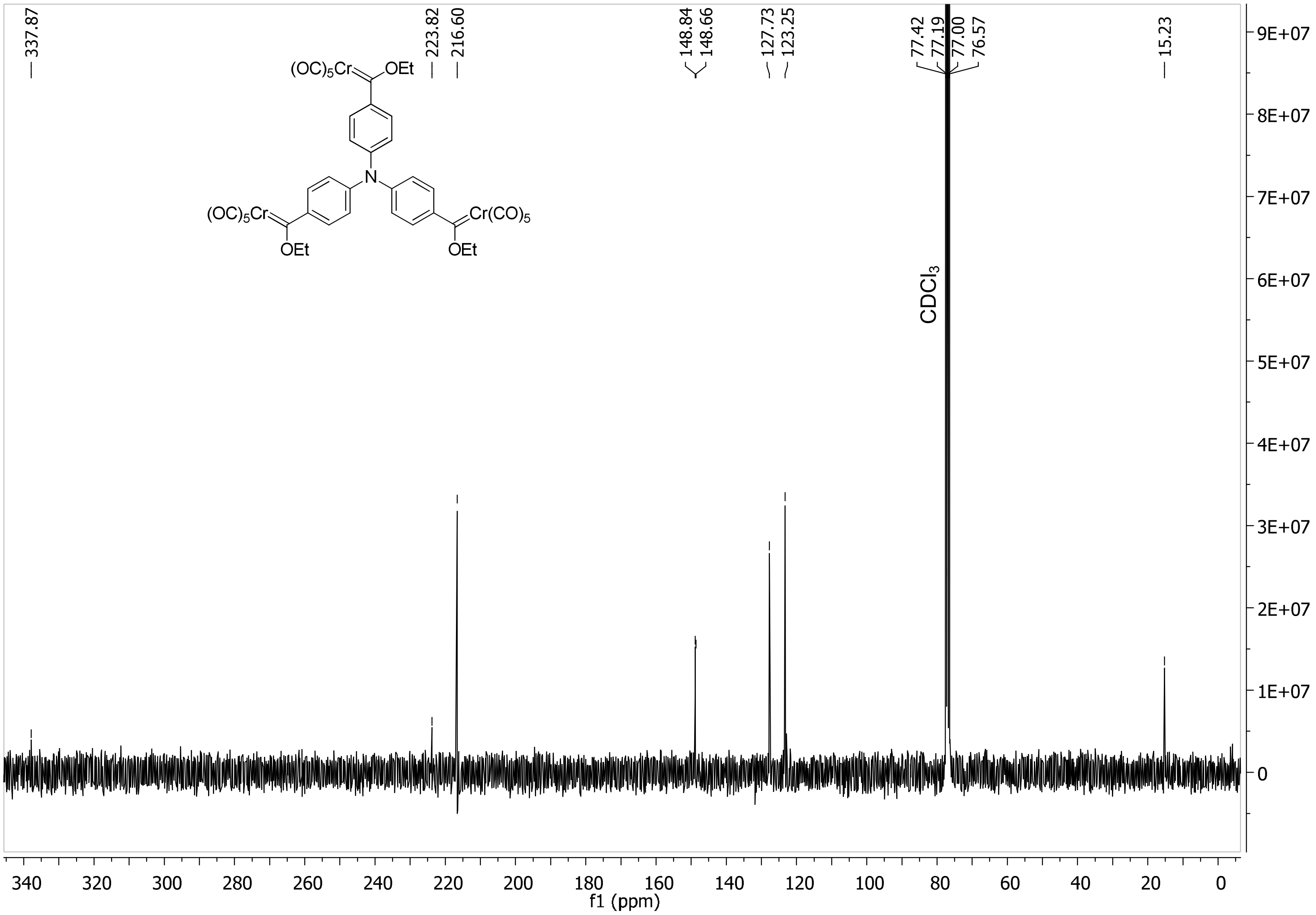

3b ^{1}H NMR spectrum

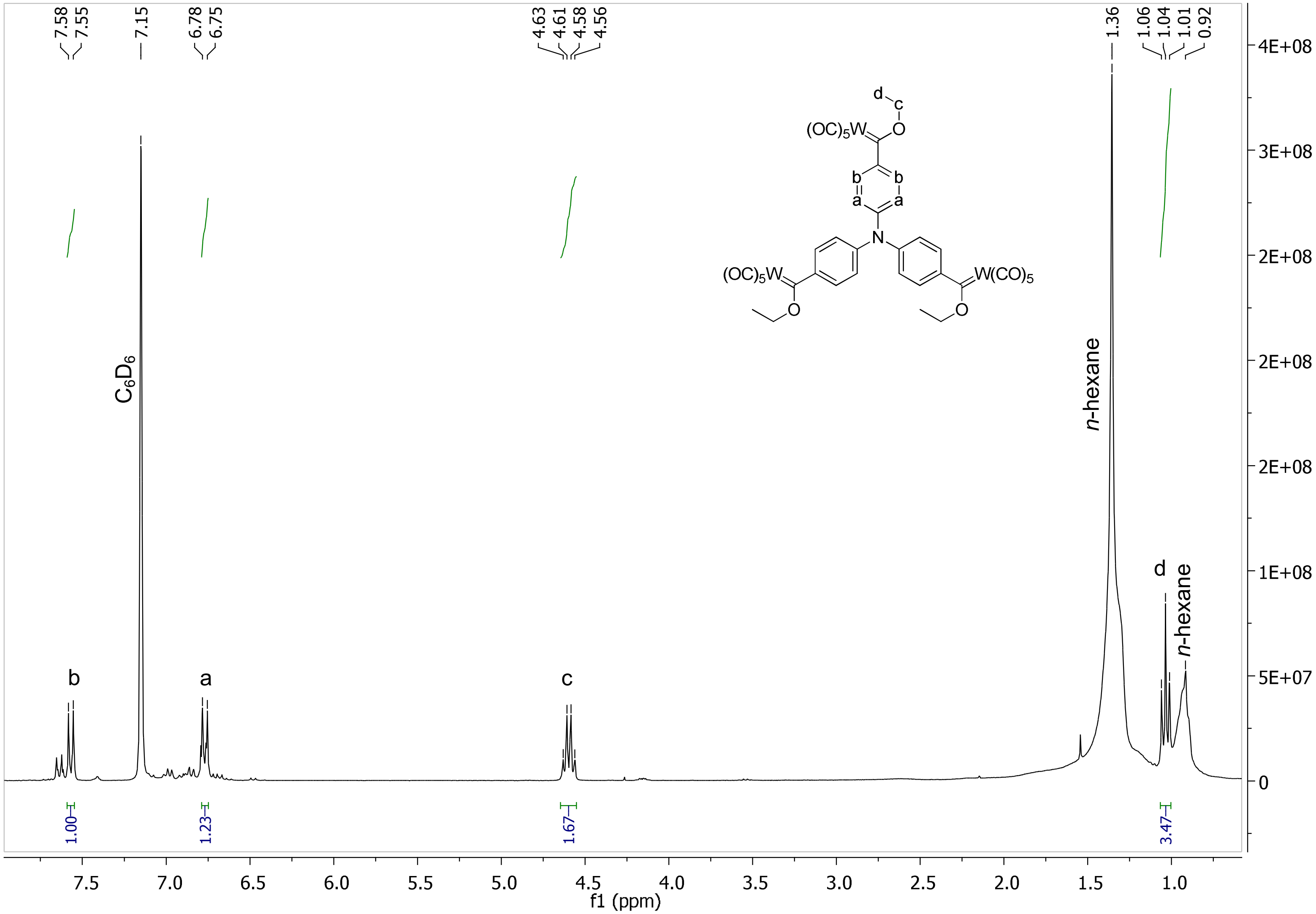

* Solvent contaminant

3b ^{13}C NMR spectrum

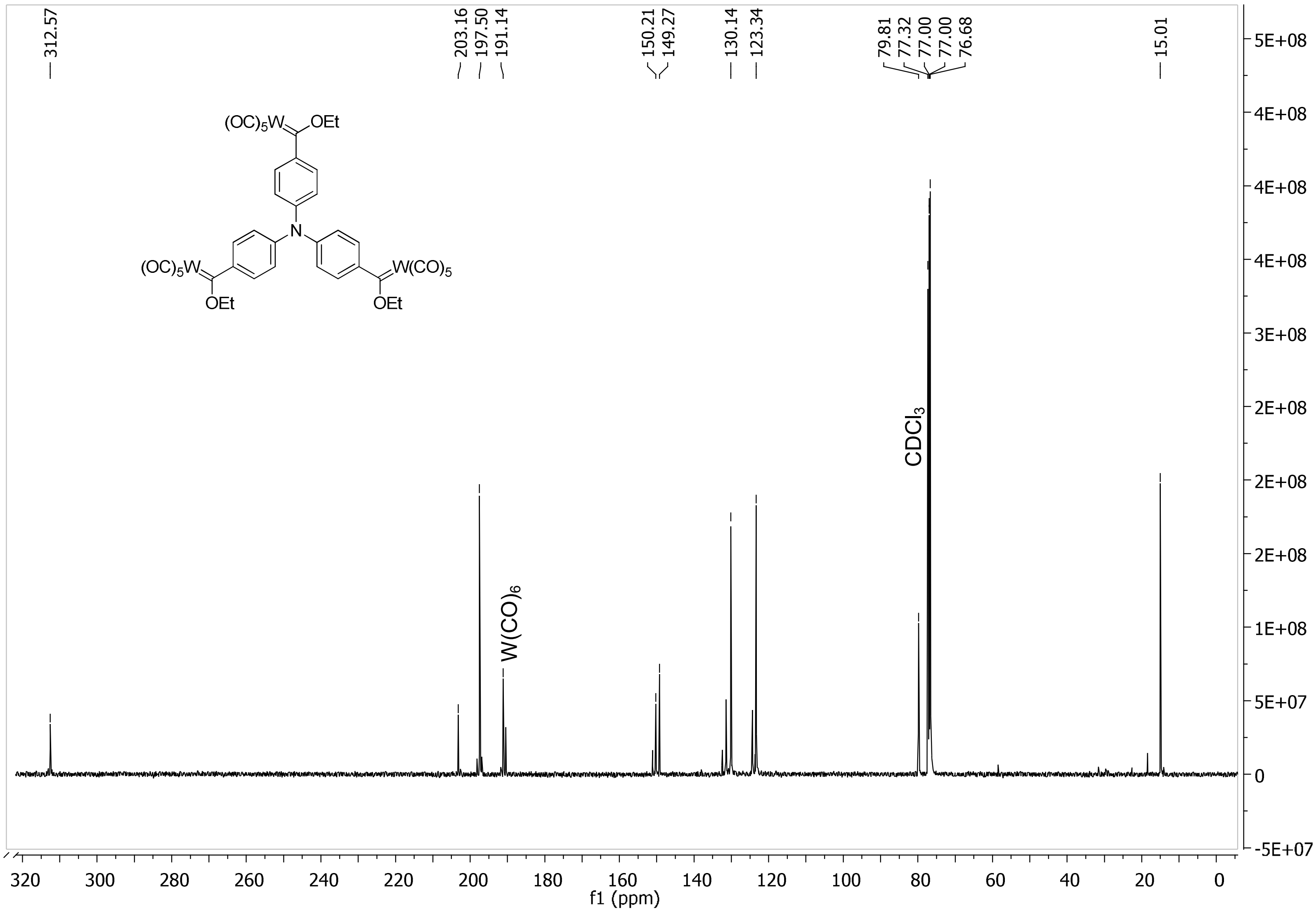

4a ^{1}H NMR spectrum

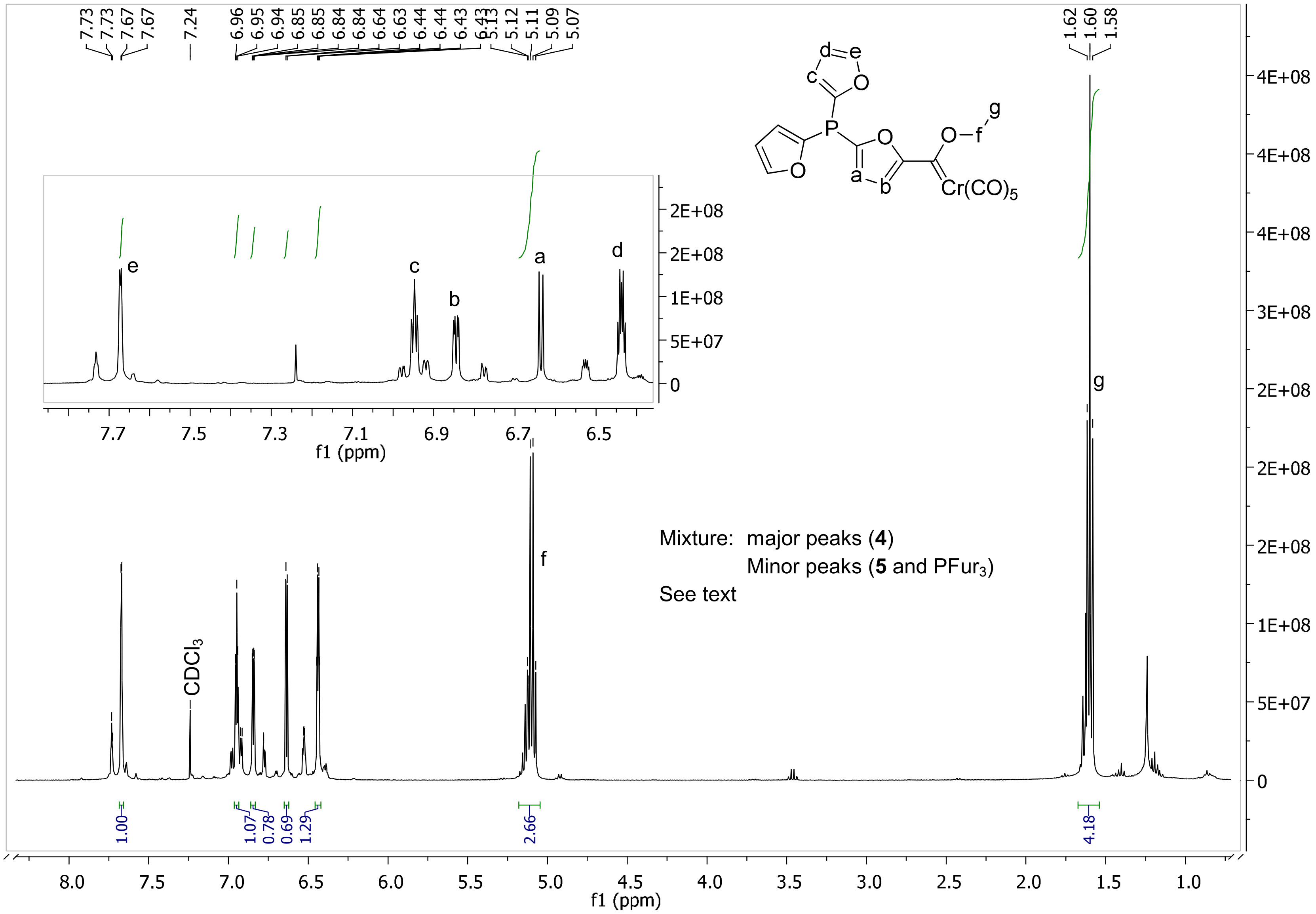

Mixture: major peaks (**4**)
Minor peaks (**5** and PFur$_3$)
See text

4a ^{13}C NMR spectrum

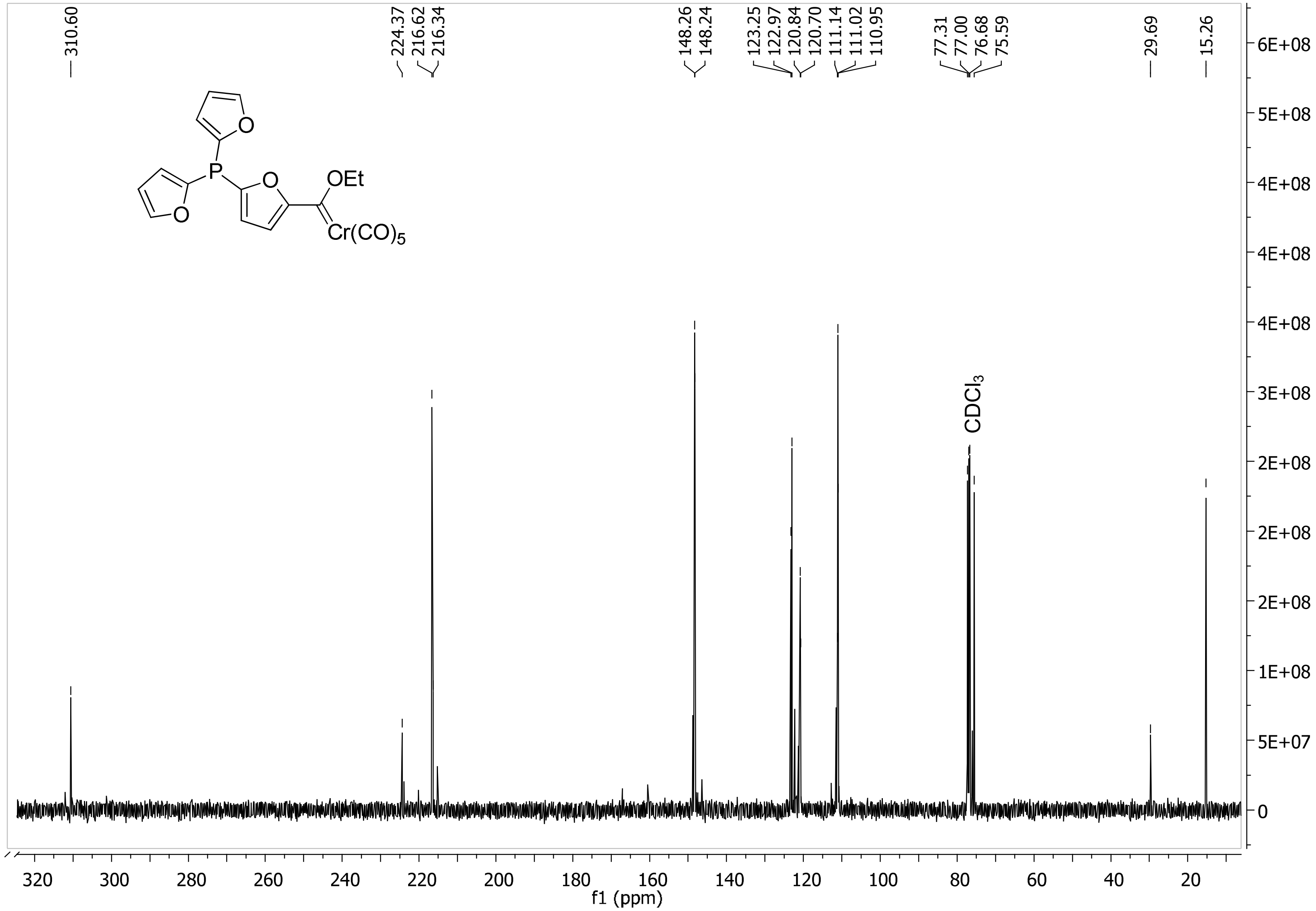

4a ^{1}P NMR spectrum

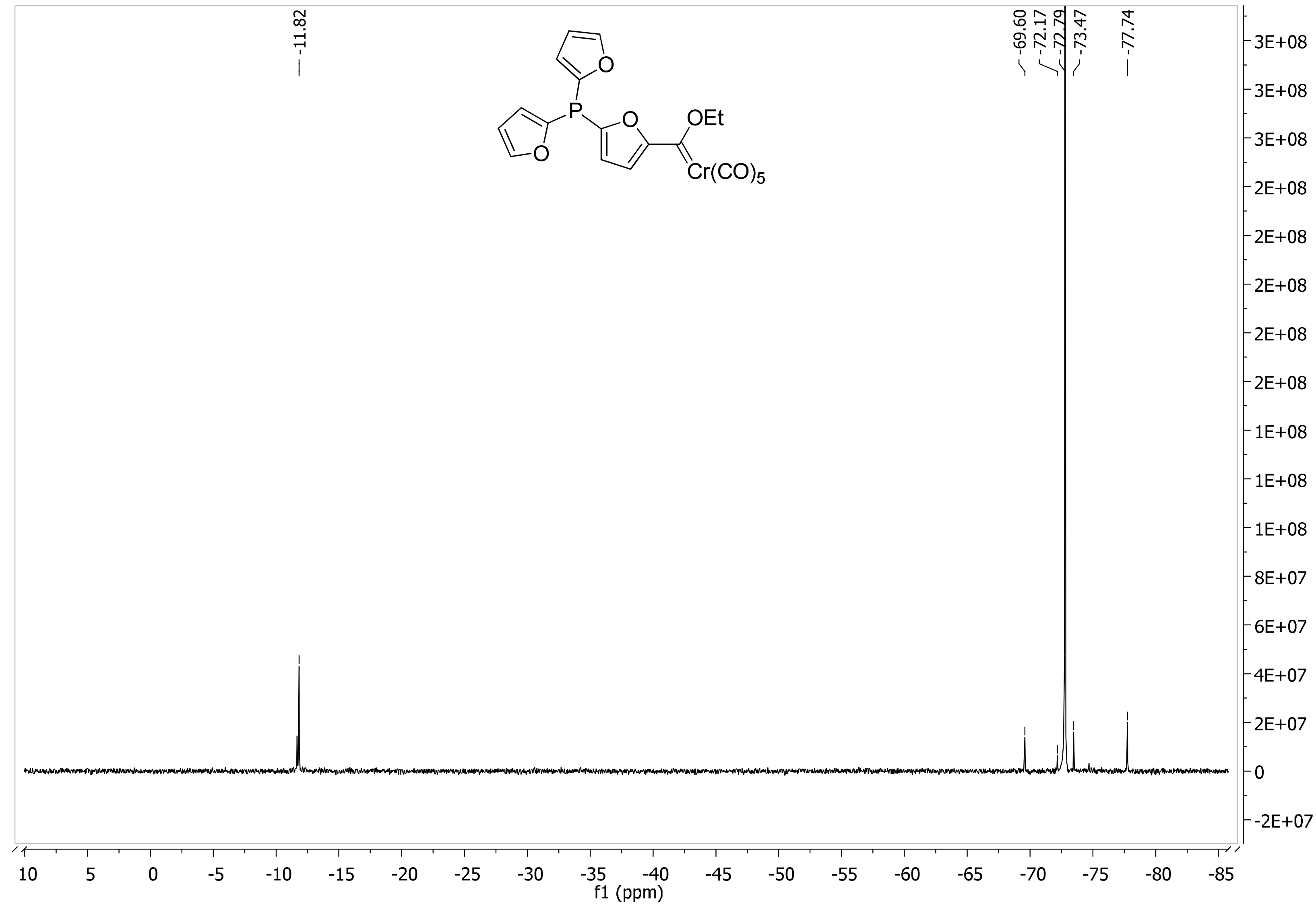

4b ^{1}H NMR spectrum

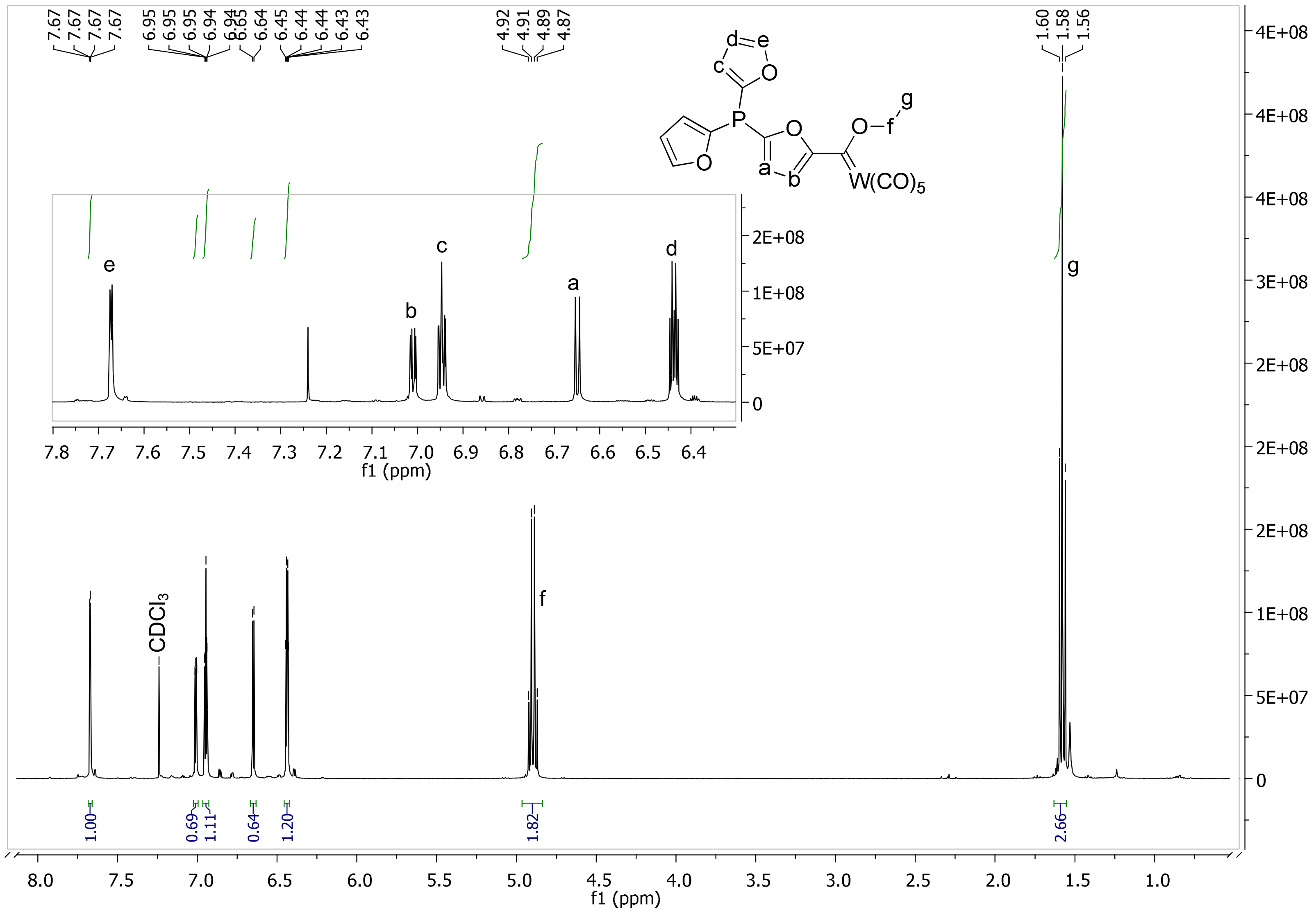

4b ^{13}C NMR spectrum

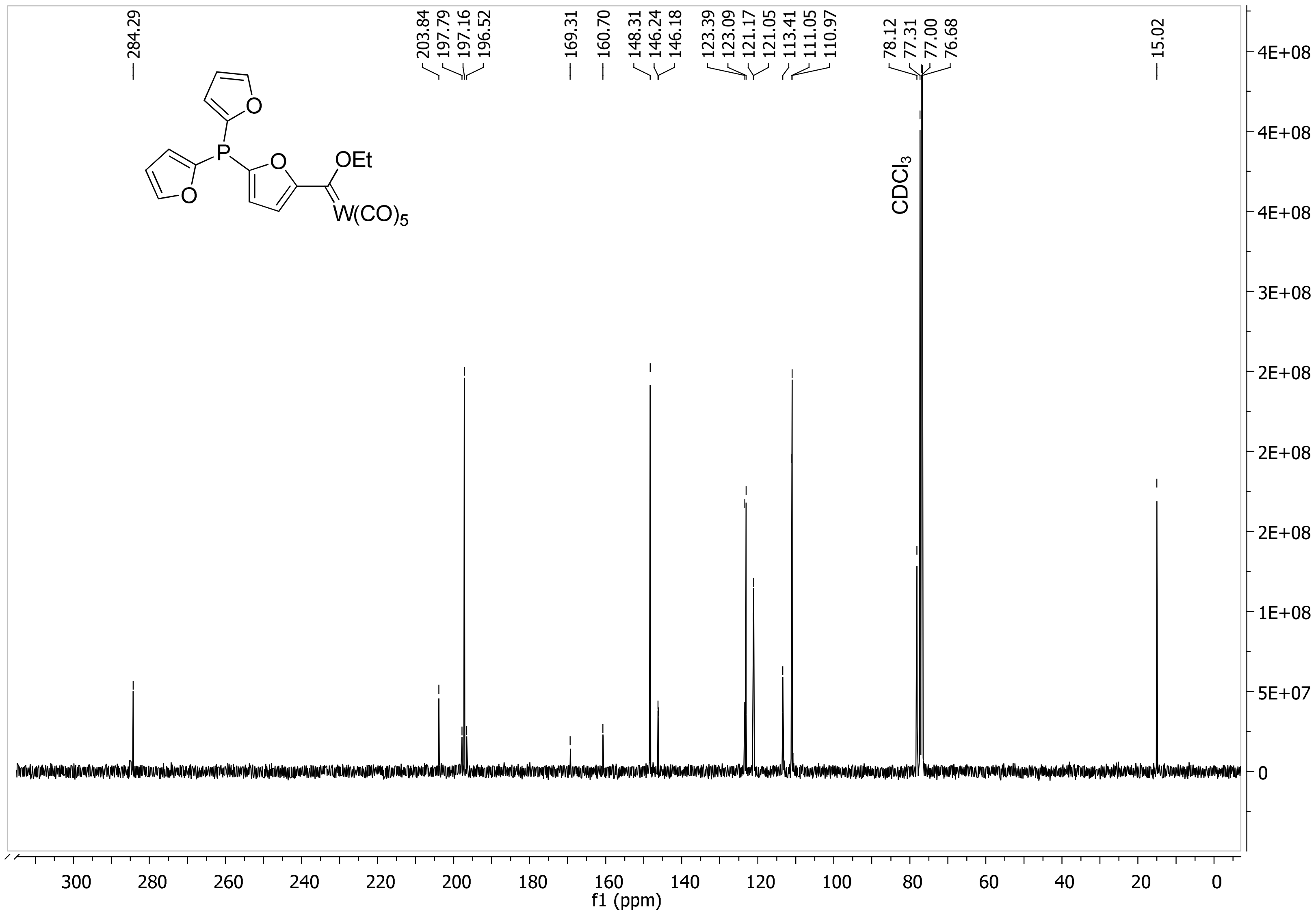

4b ^{31}P NMR spectrum

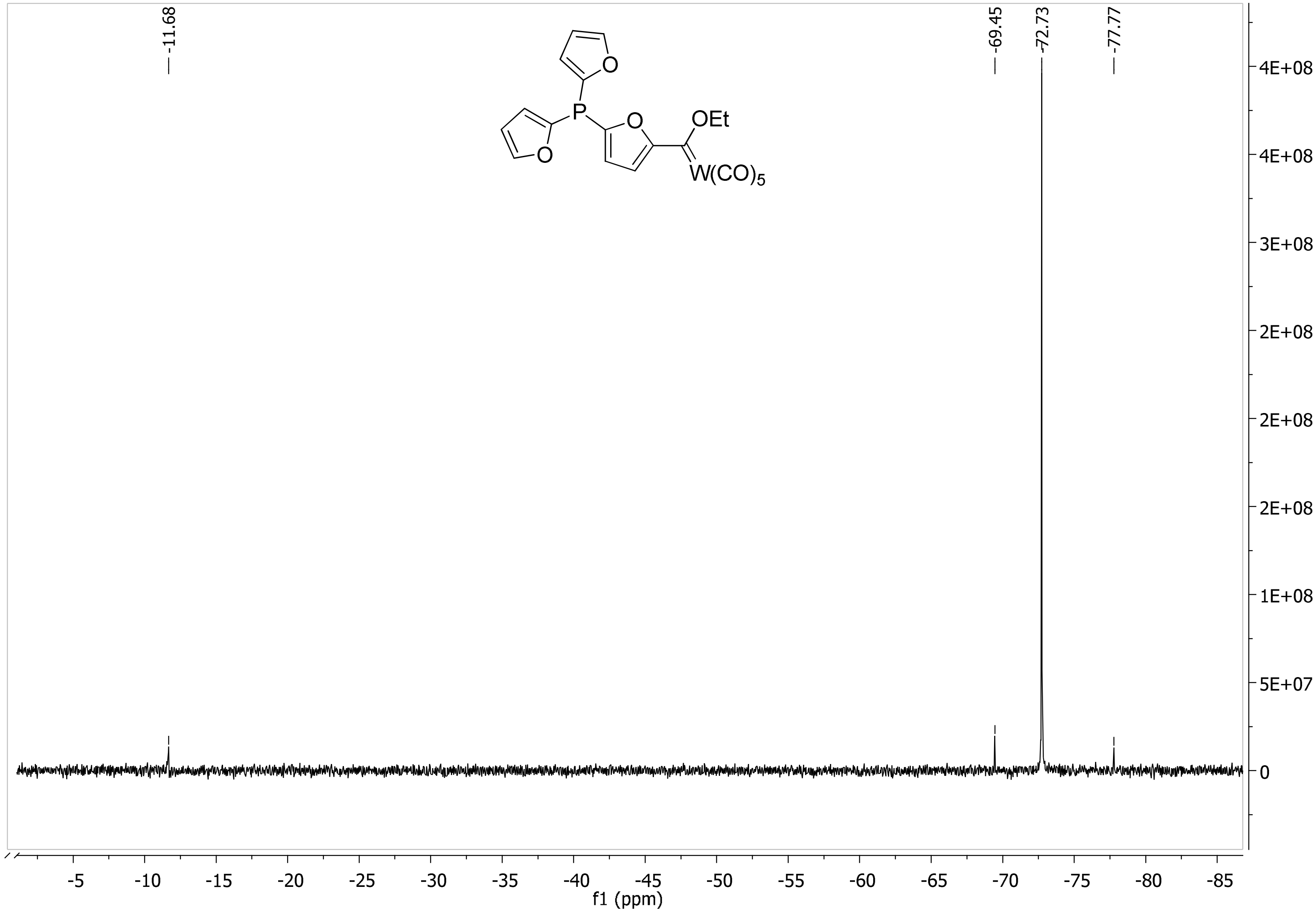

5a ^{1}H NMR spectrum

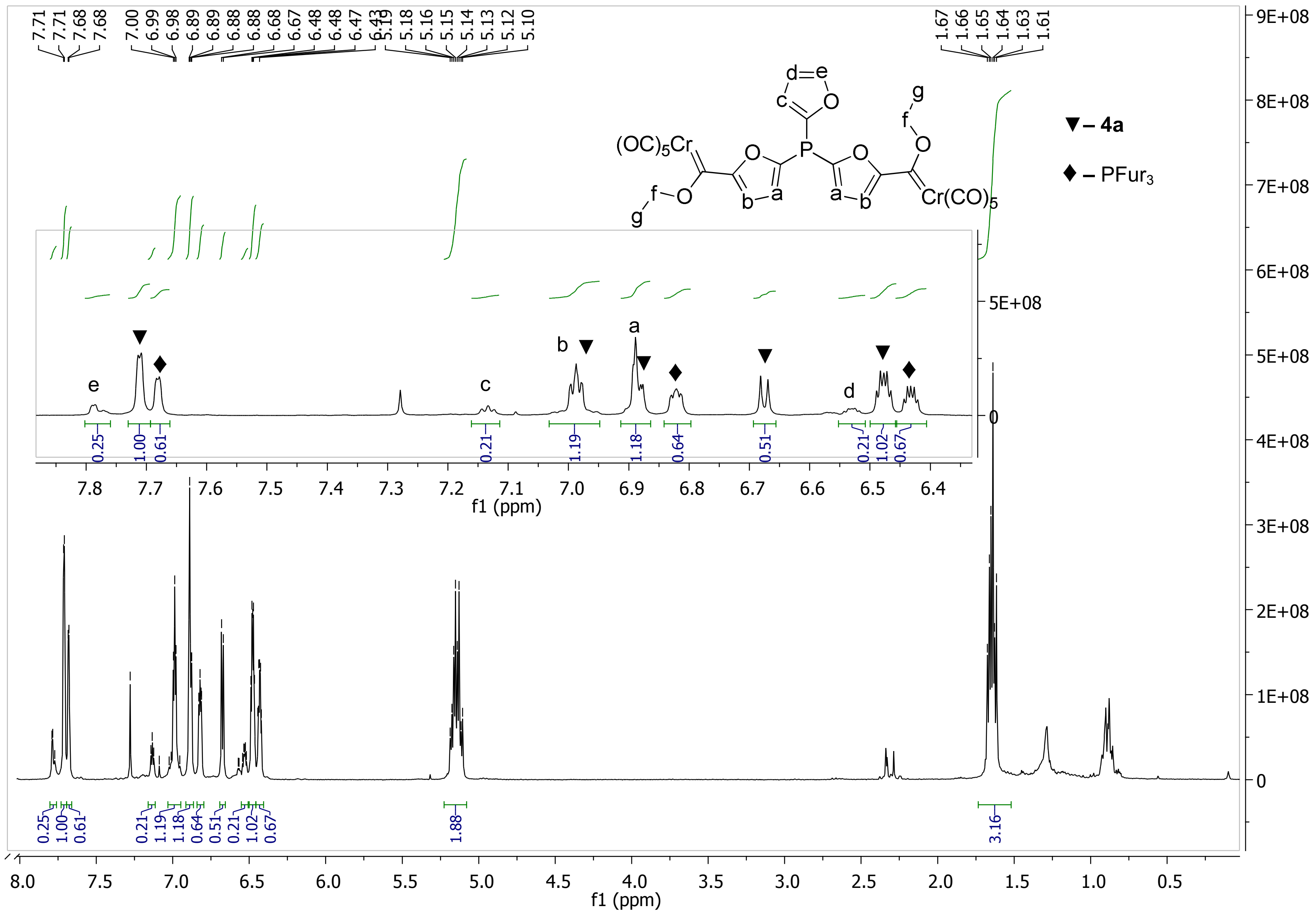

5a ^{13}C NMR spectrum

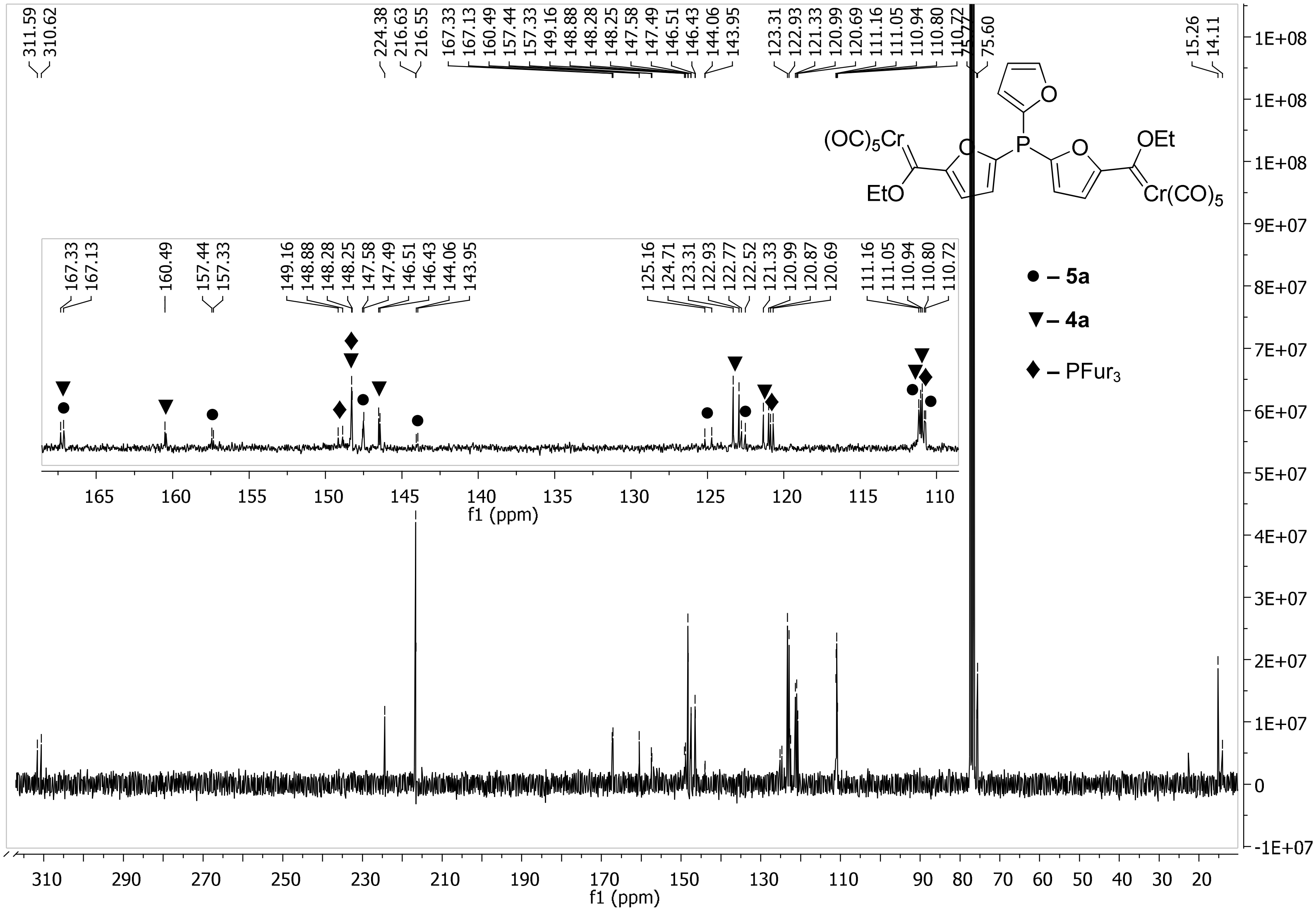

5a ^{31}P NMR spectrum

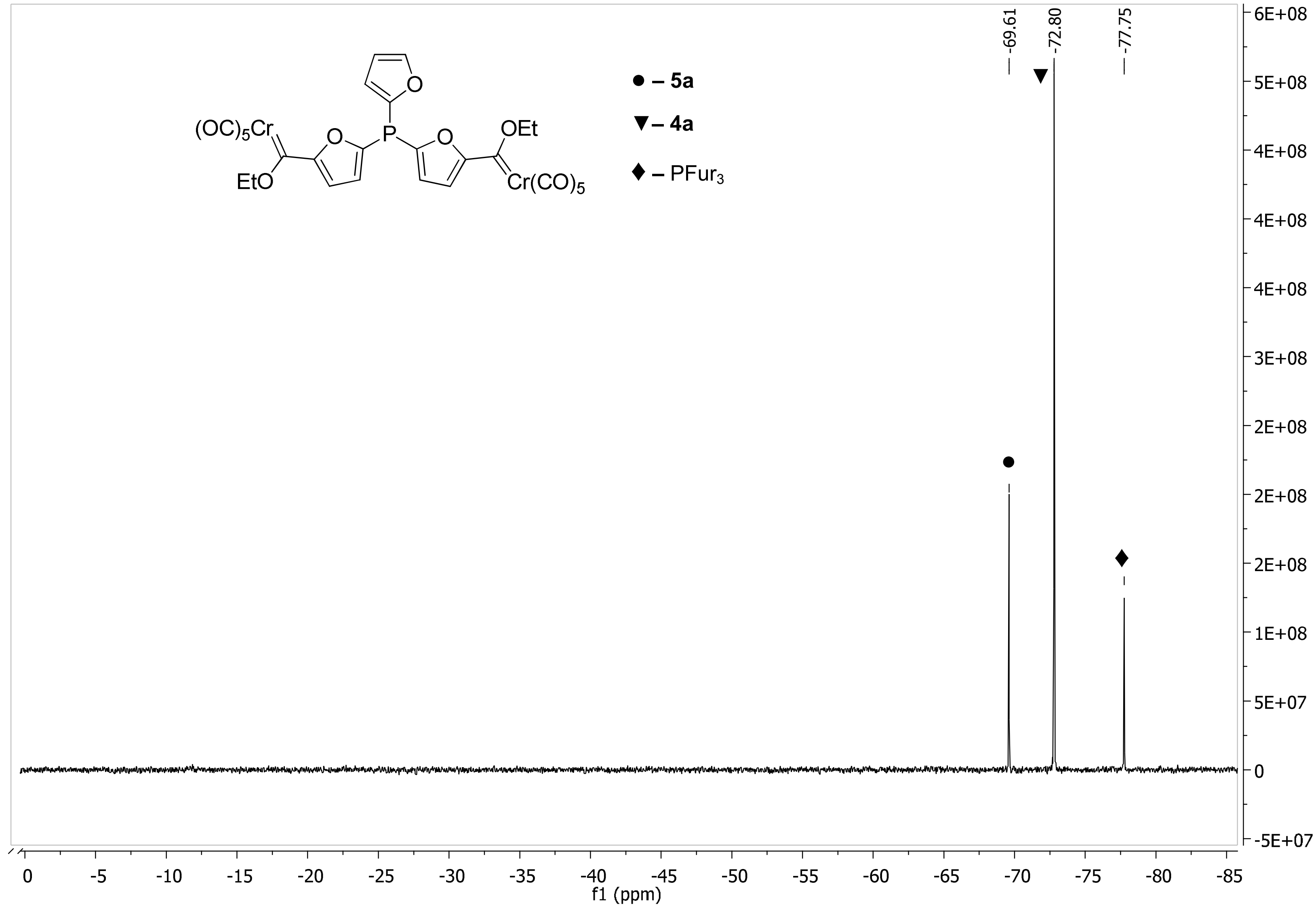

5b ^{1}H NMR spectrum

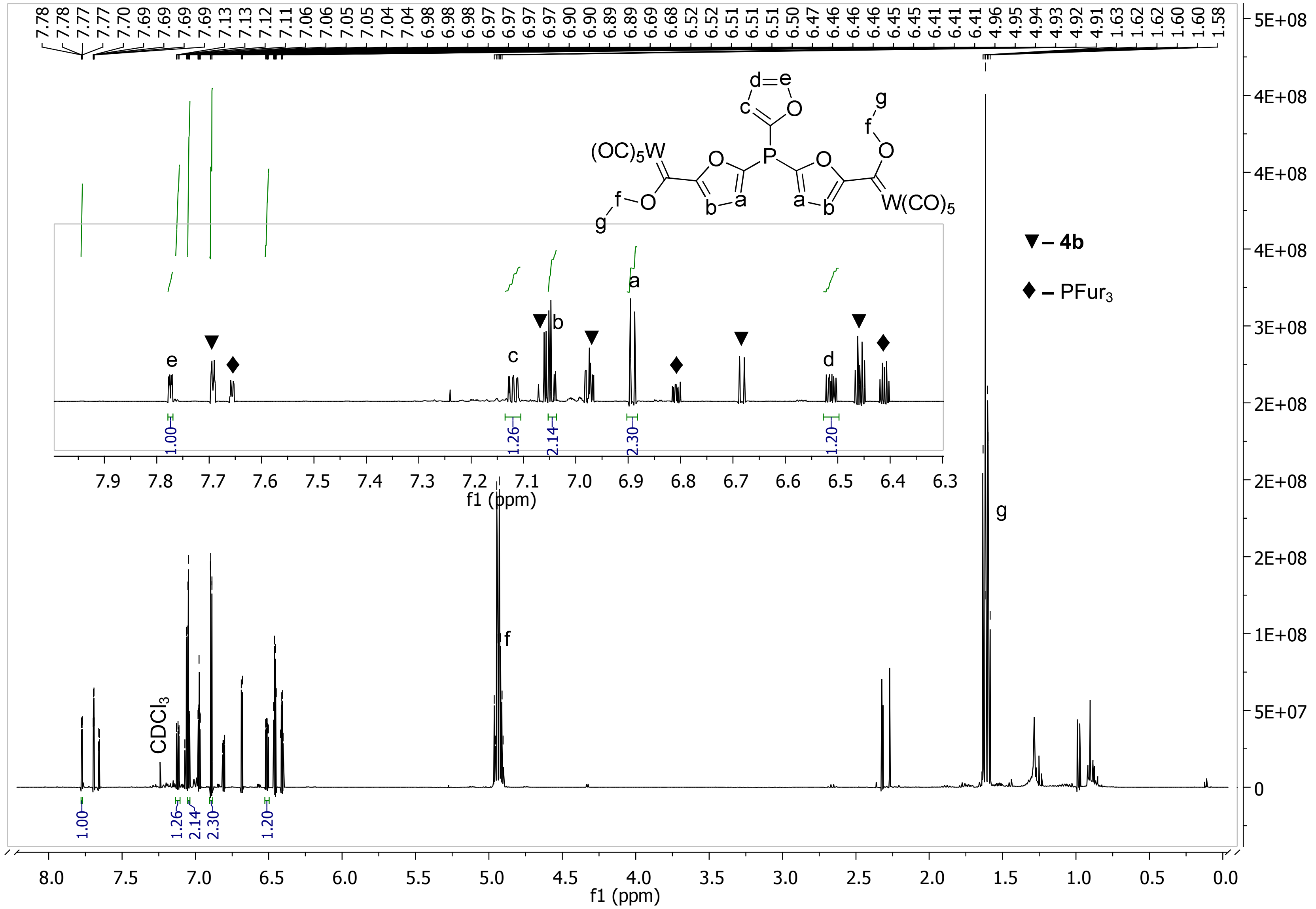

5b ^{13}C NMR spectrum

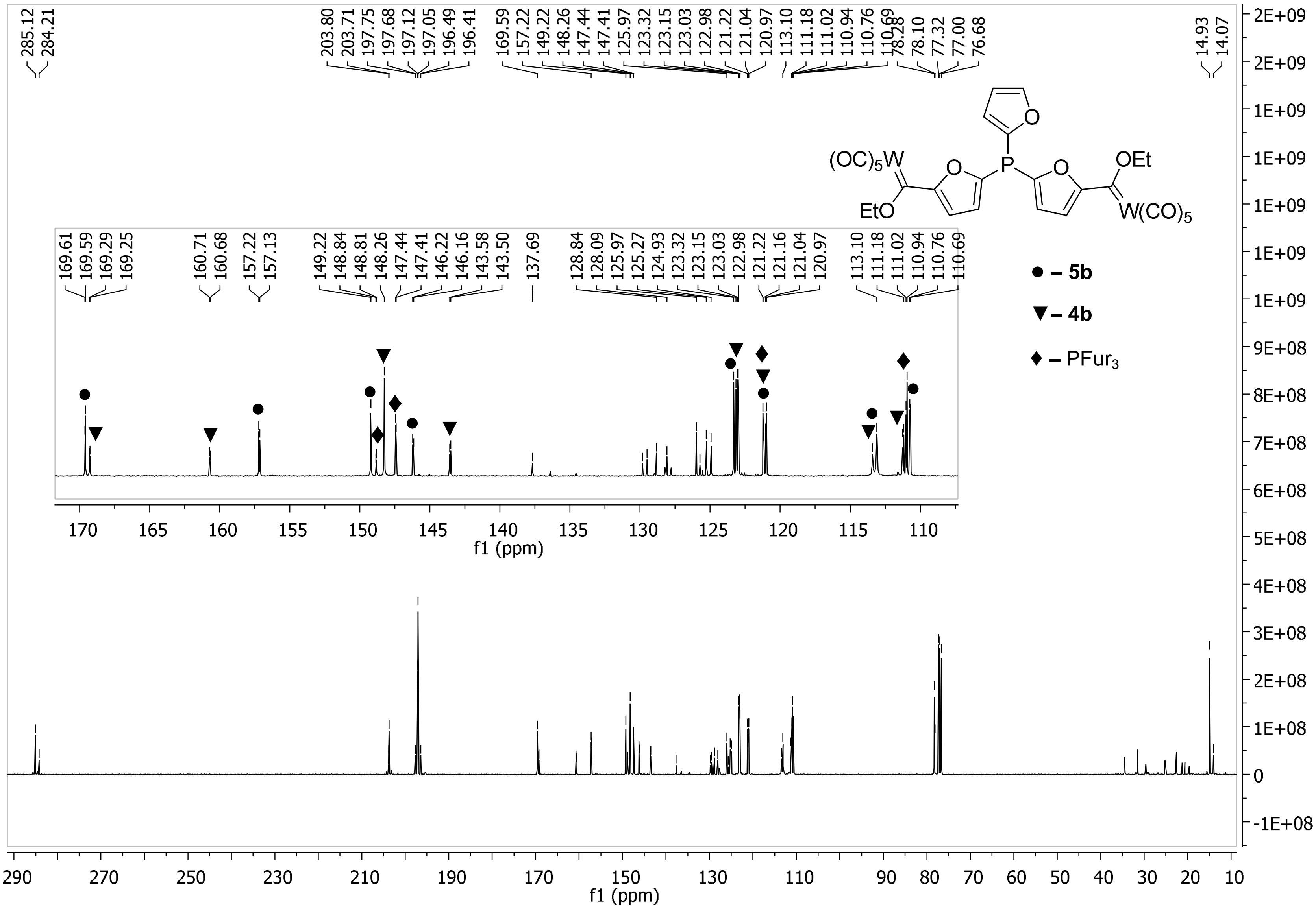

6a ^{1}H NMR spectrum

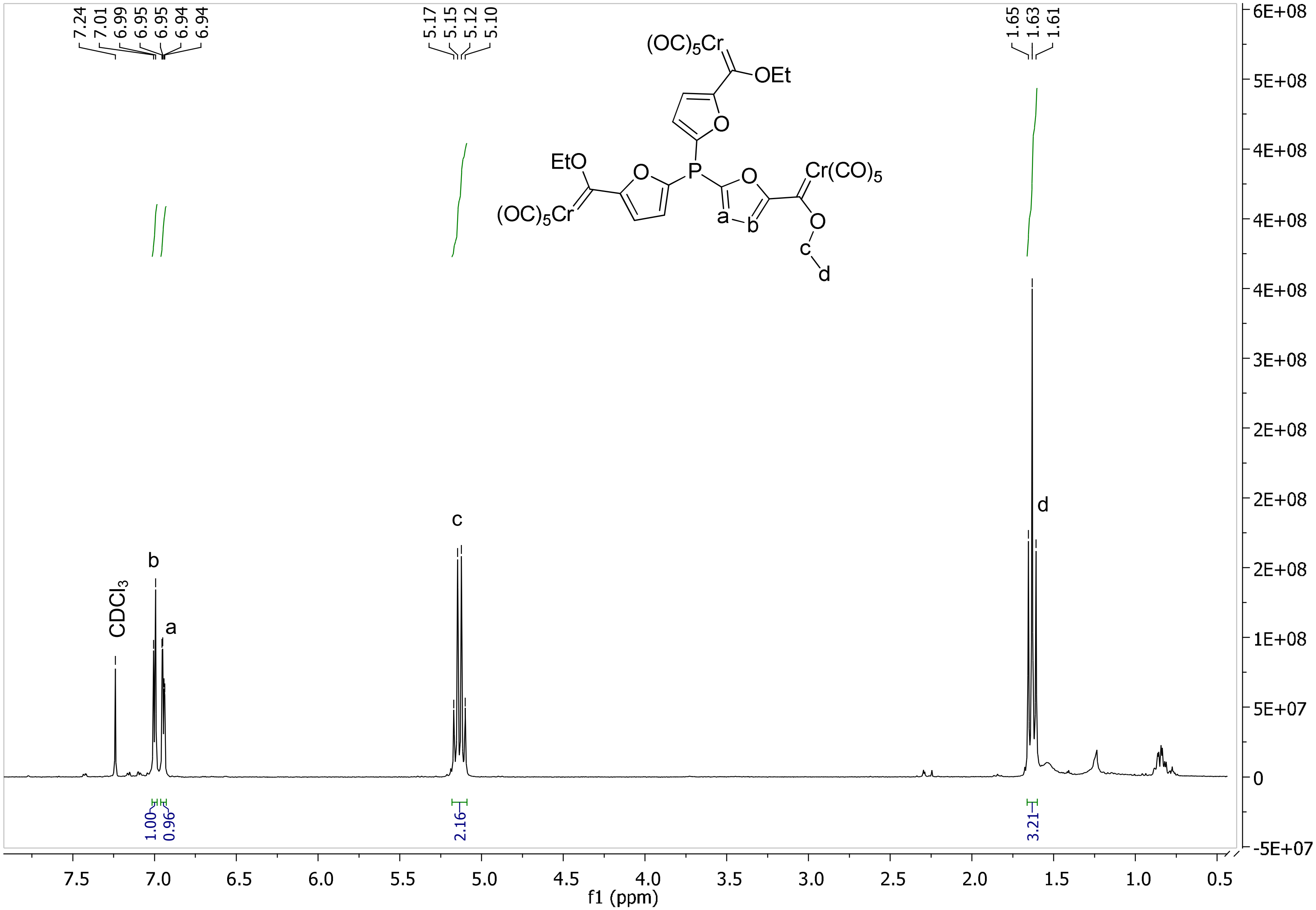

6a ^{13}C NMR spectrum

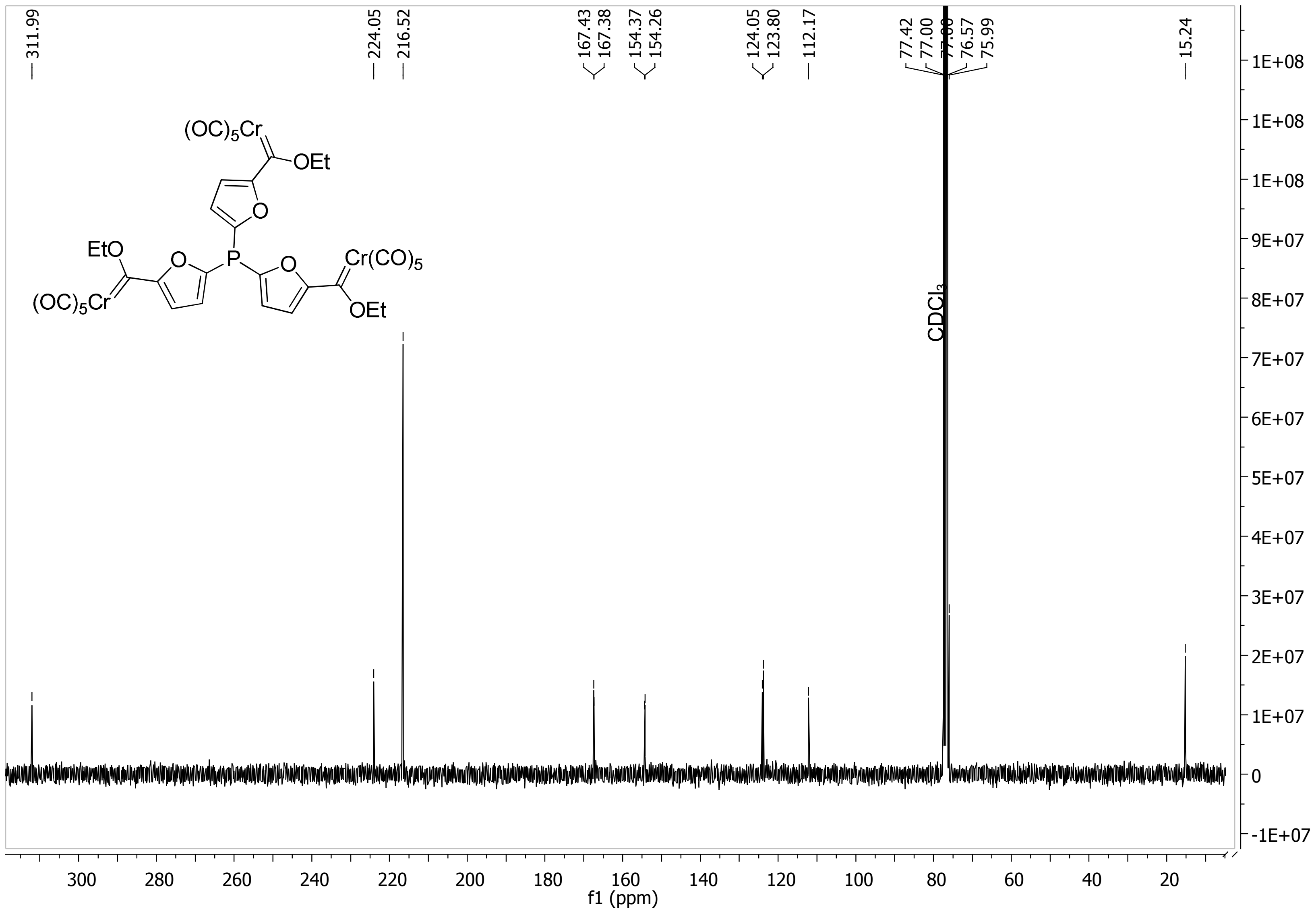

6a ^{31}P NMR spectrum

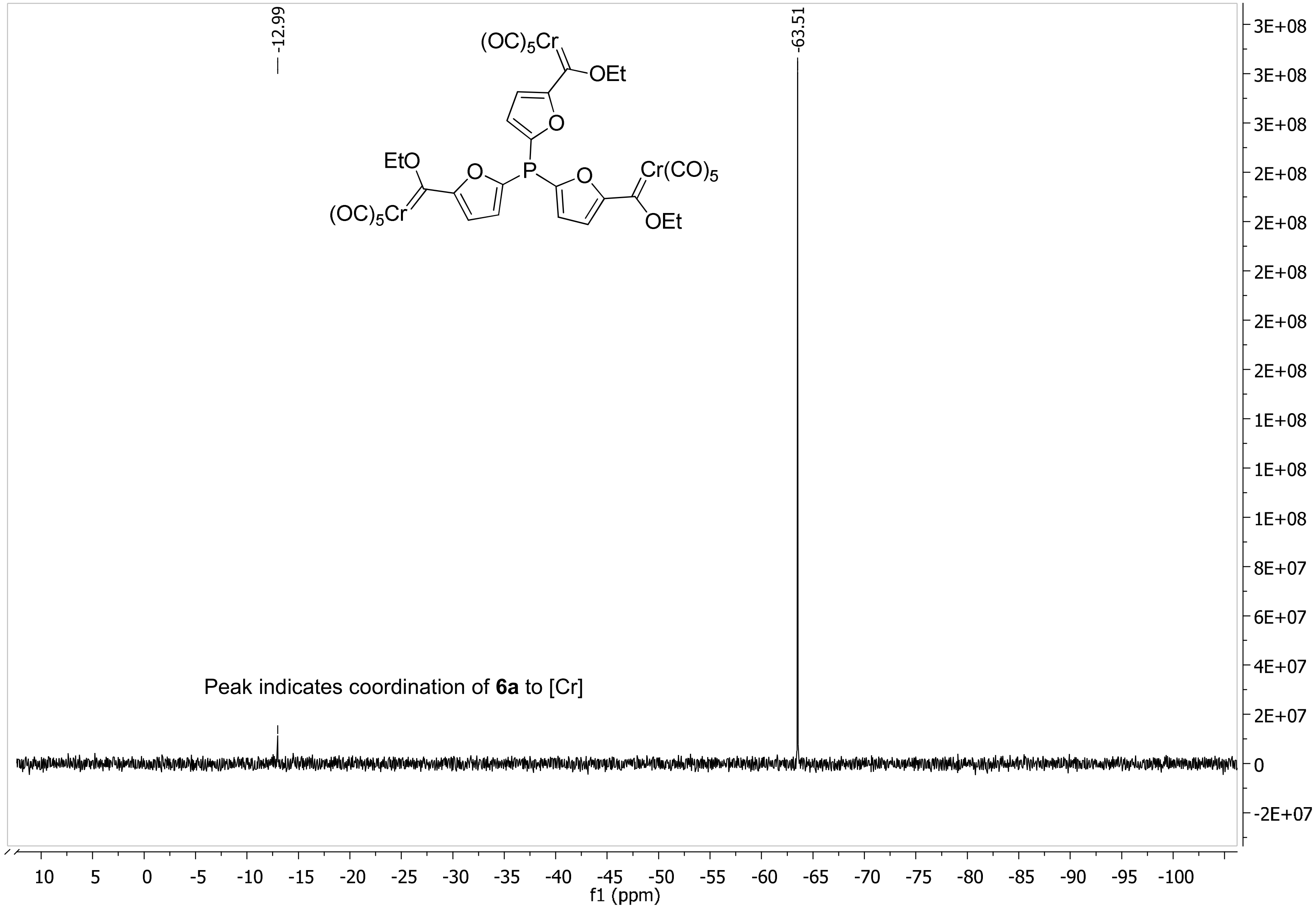

Peak indicates coordination of **6a** to [Cr]

6b ^{1}H NMR spectrum

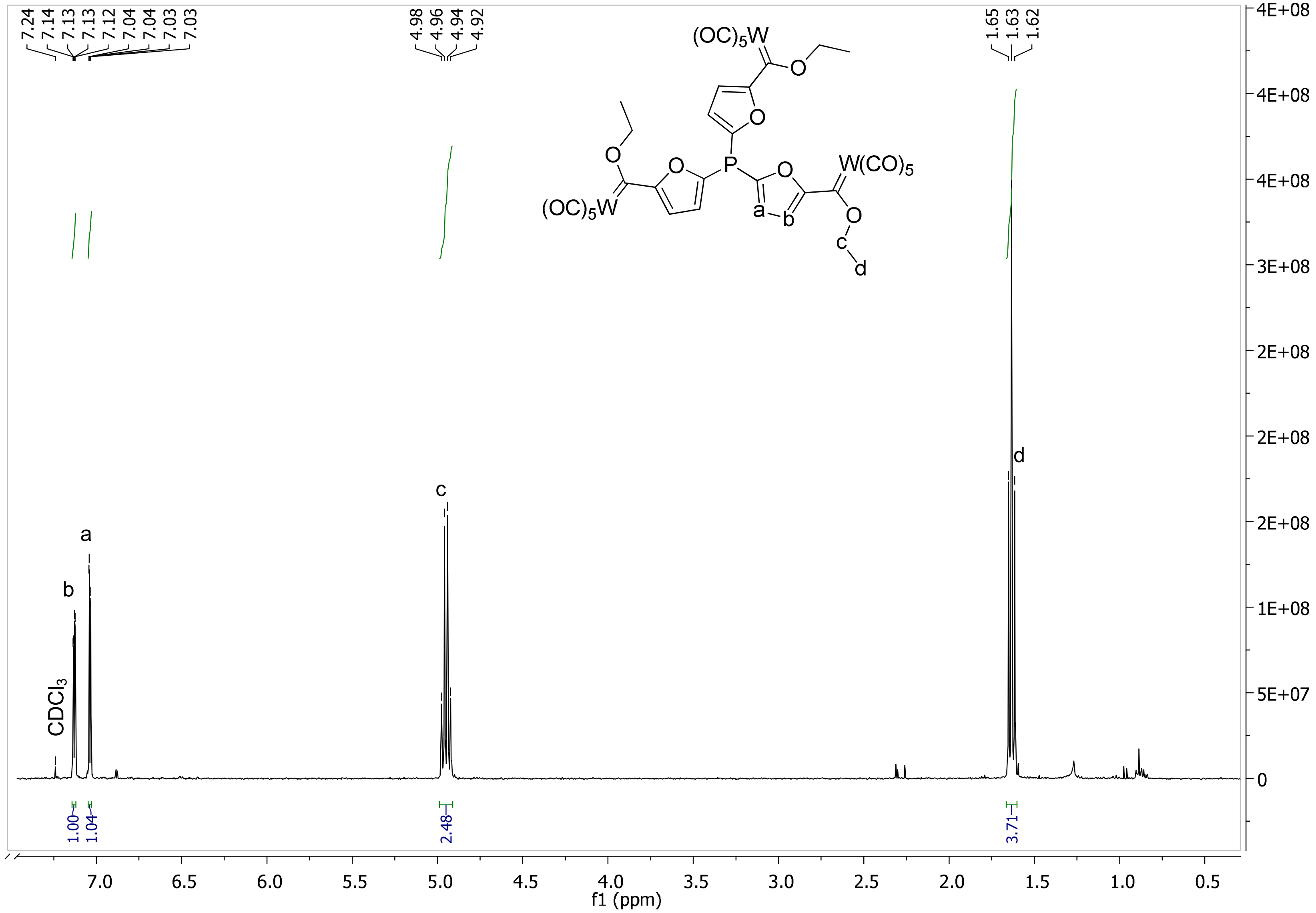

6b ^{13}C NMR spectrum

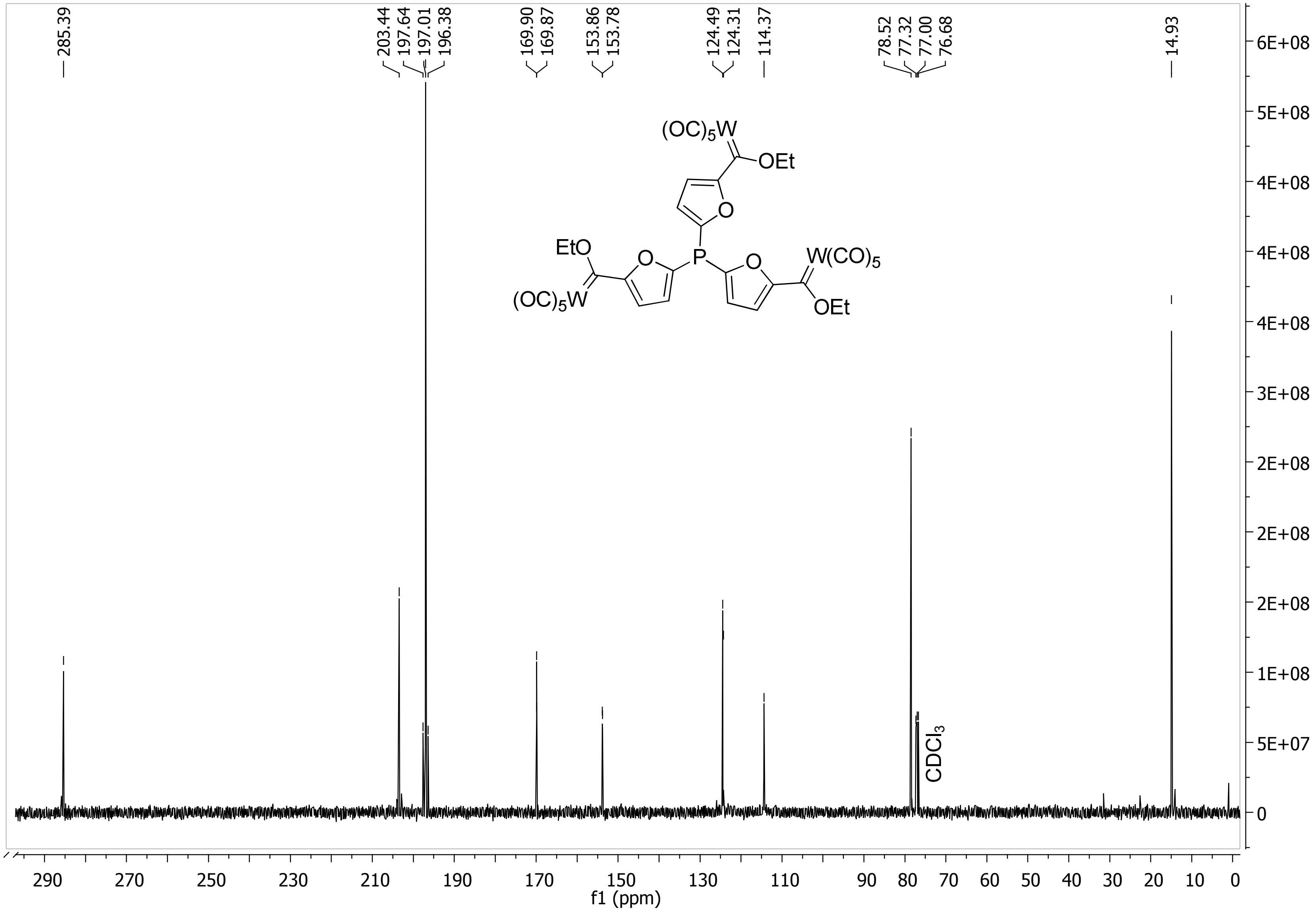

6b ^{31}P NMR spectrum

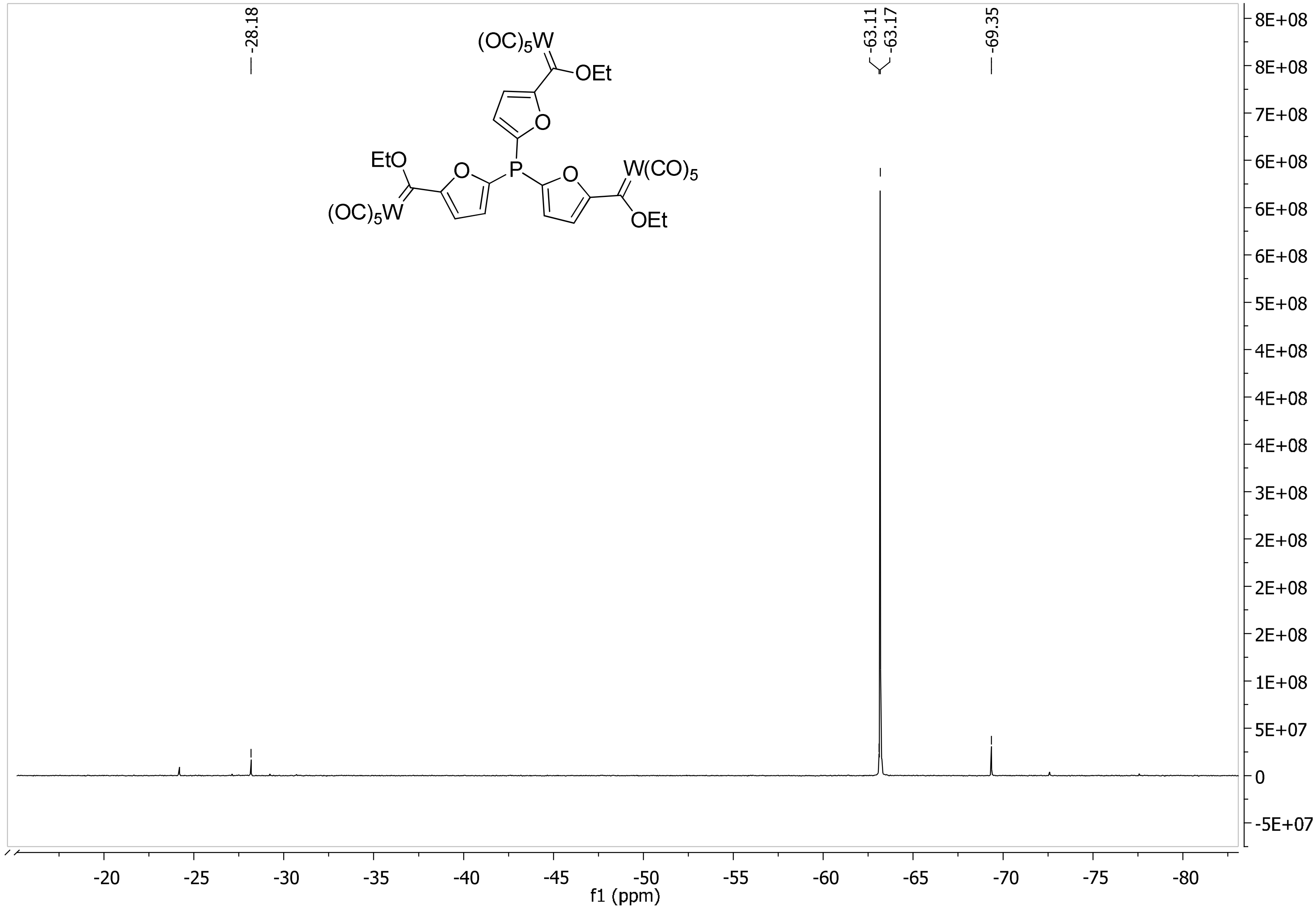

Compounds **7a** and **7b** are oils. Poor resolution of butyl peaks are caused by $^{2}J_{PH}$ coupling and the chirality of P when coordinated.

7a ^{1}H NMR spectrum

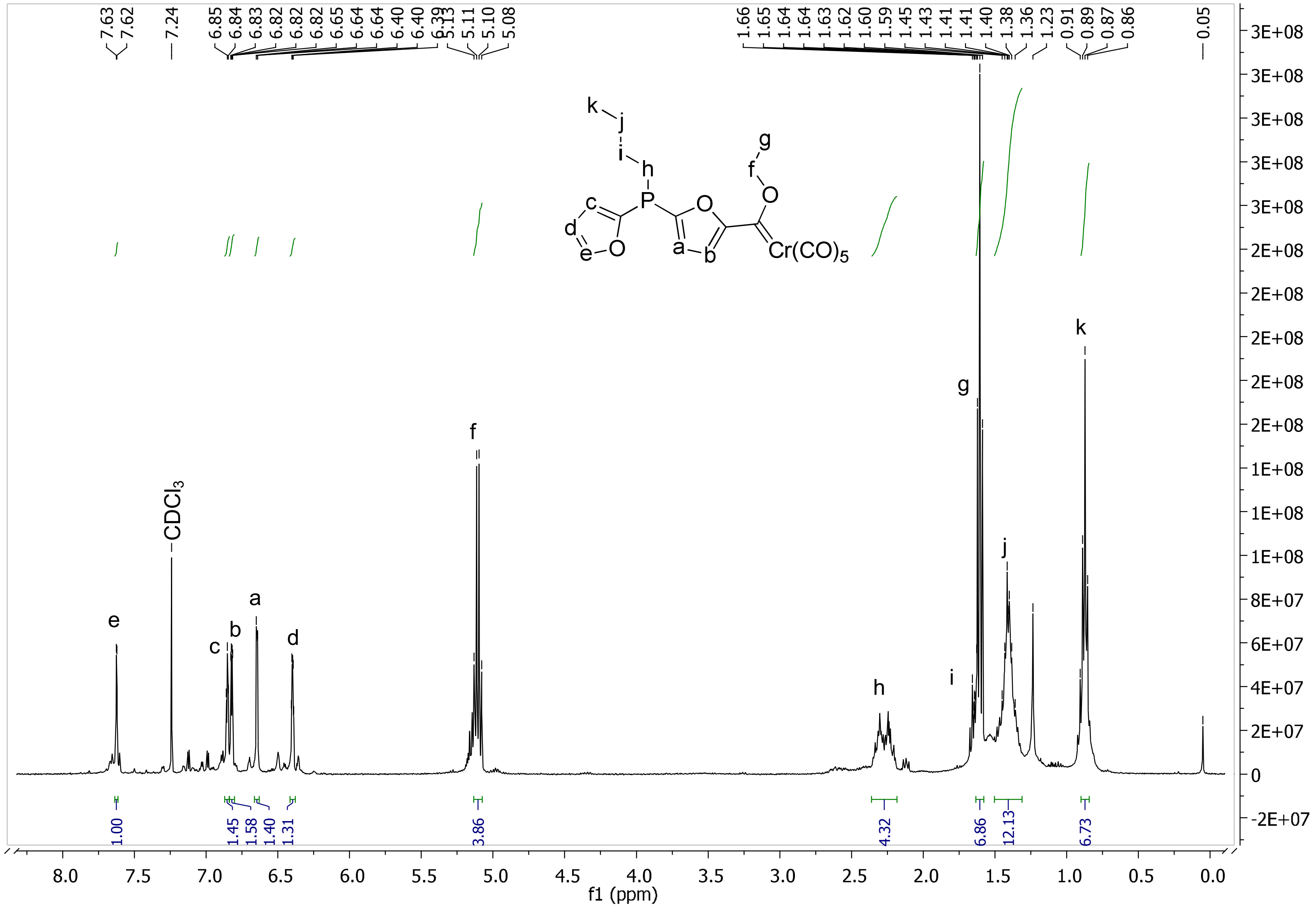

7a ^{13}C NMR spectrum

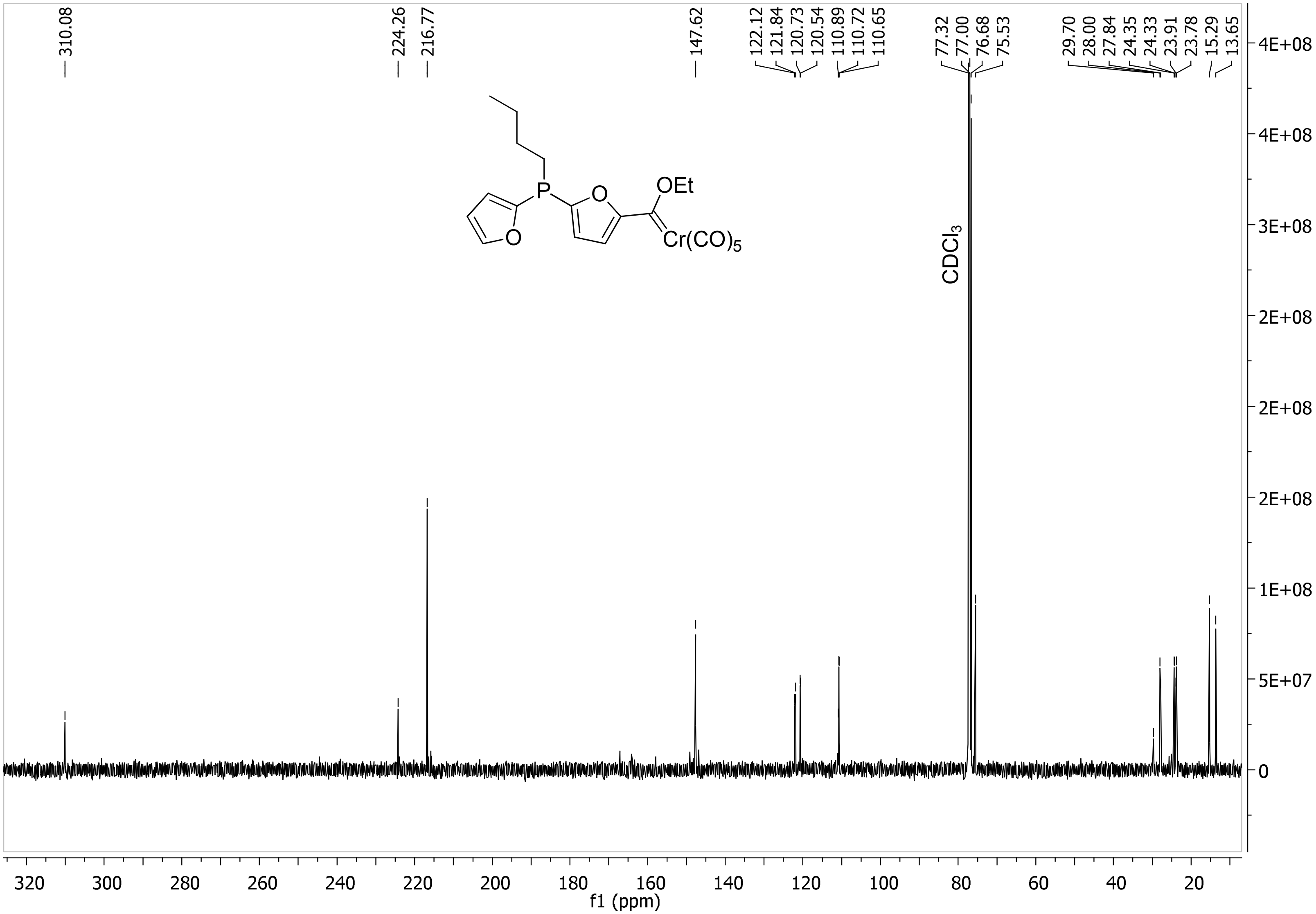

7a ^{31}P NMR spectrum

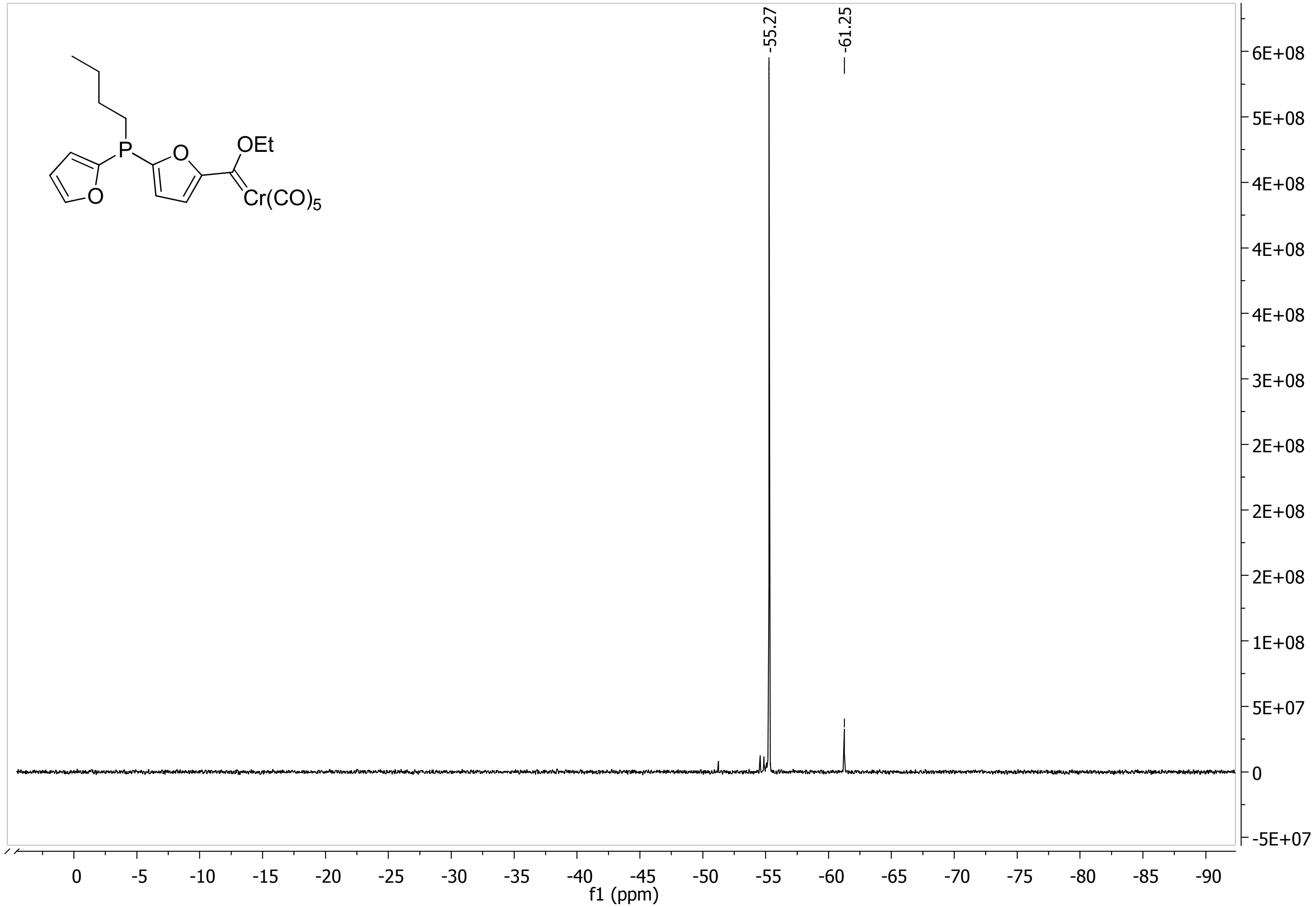

7b ^{1}H NMR spectrum

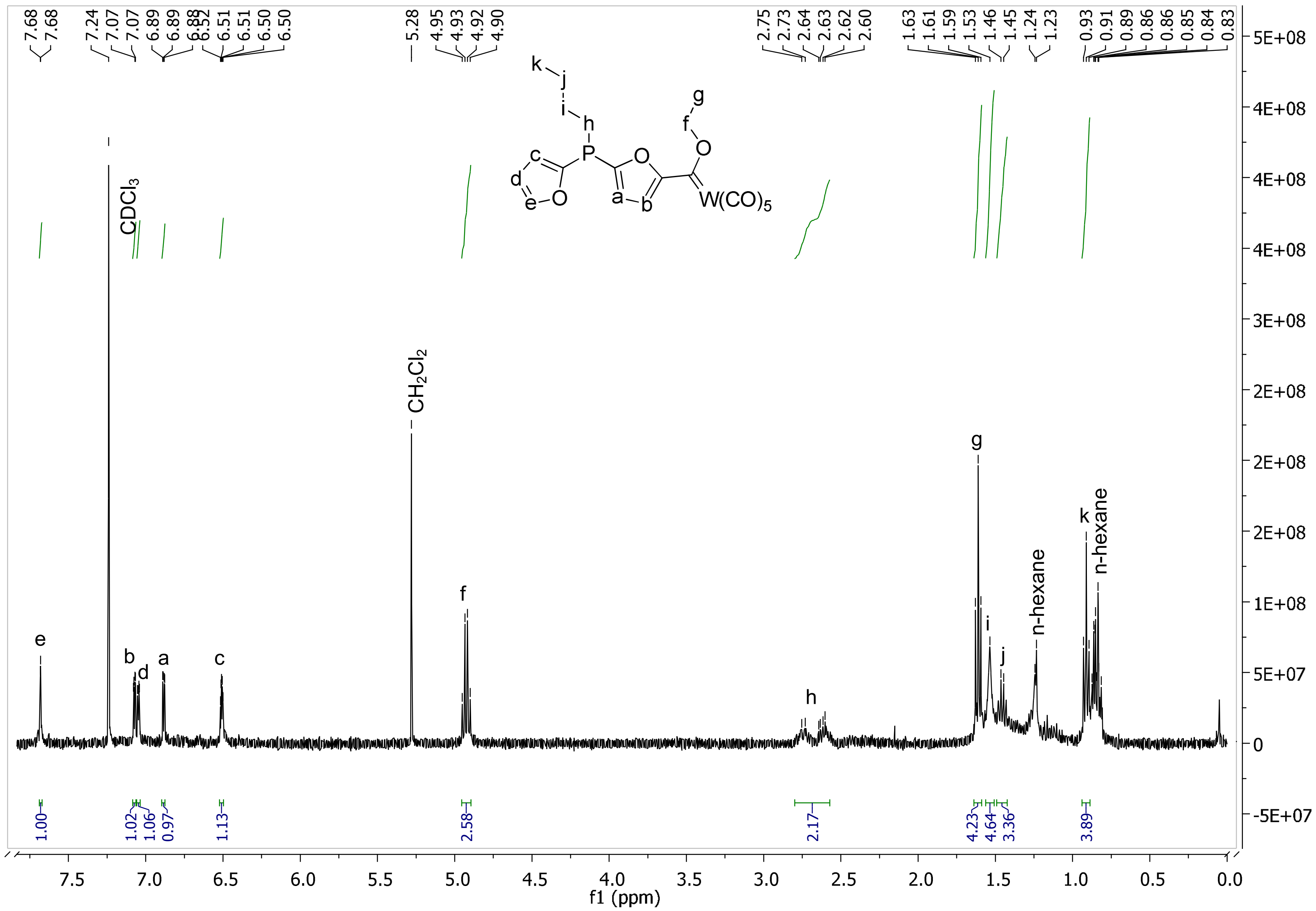

7b ^{13}C NMR spectrum

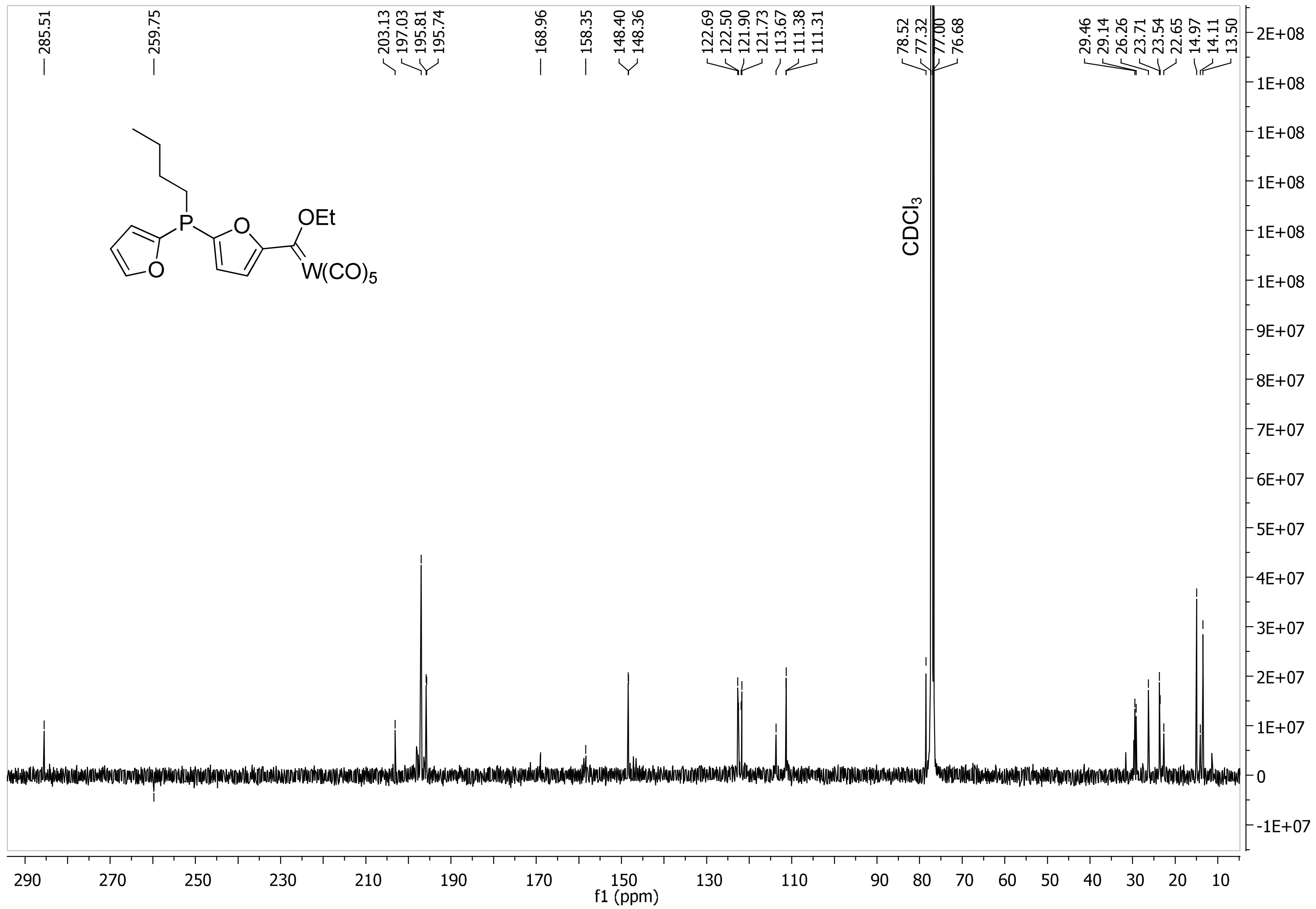

8b ^{1}H NMR spectrum

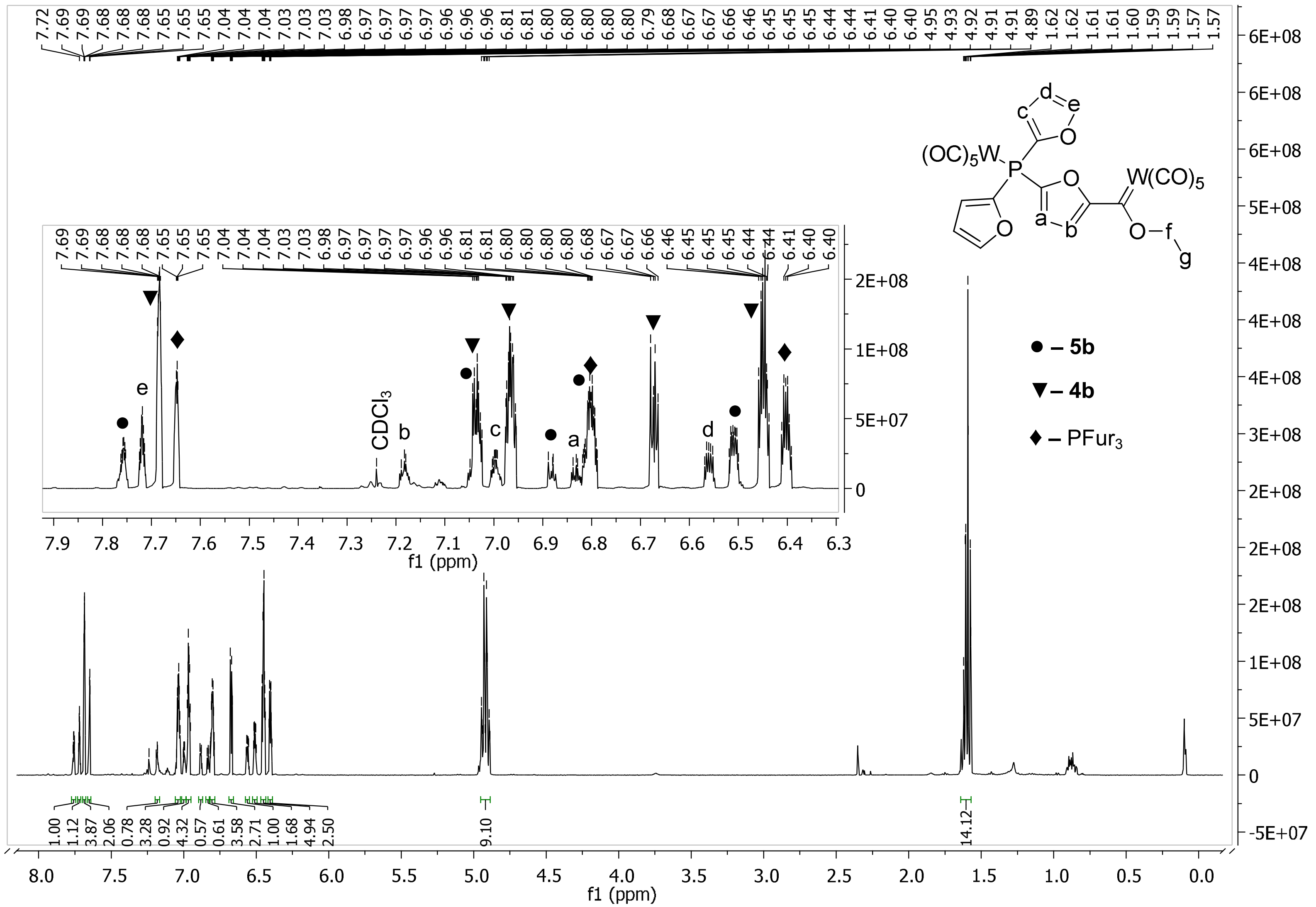

8b ^{13}C NMR spectrum

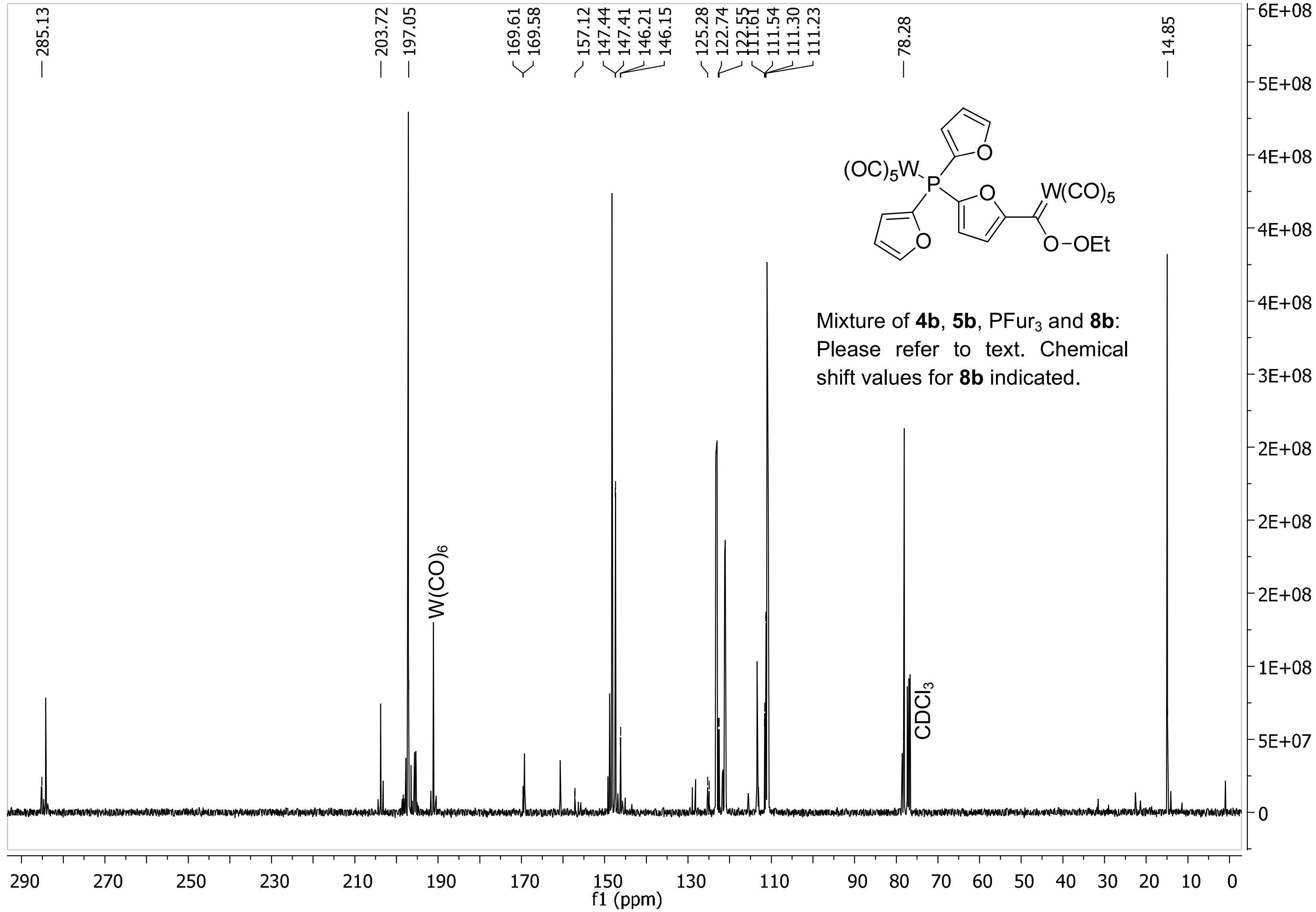
Mixture of **4b**, **5b**, $PFur_3$ and **8b**: Please refer to text. Chemical shift values for **8b** indicated.

9b ^{1}H NMR spectrum

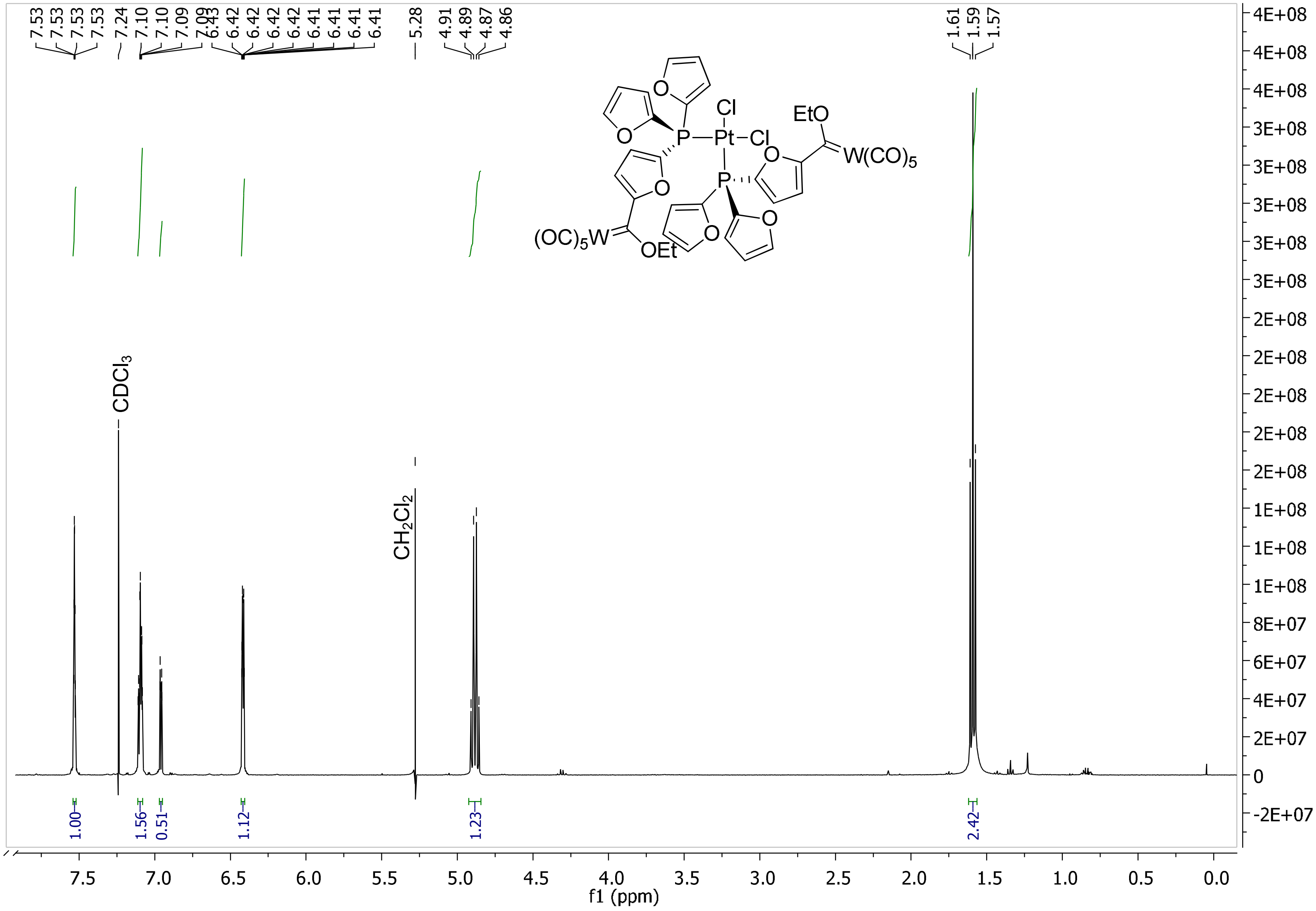

9b ^{13}C NMR spectrum

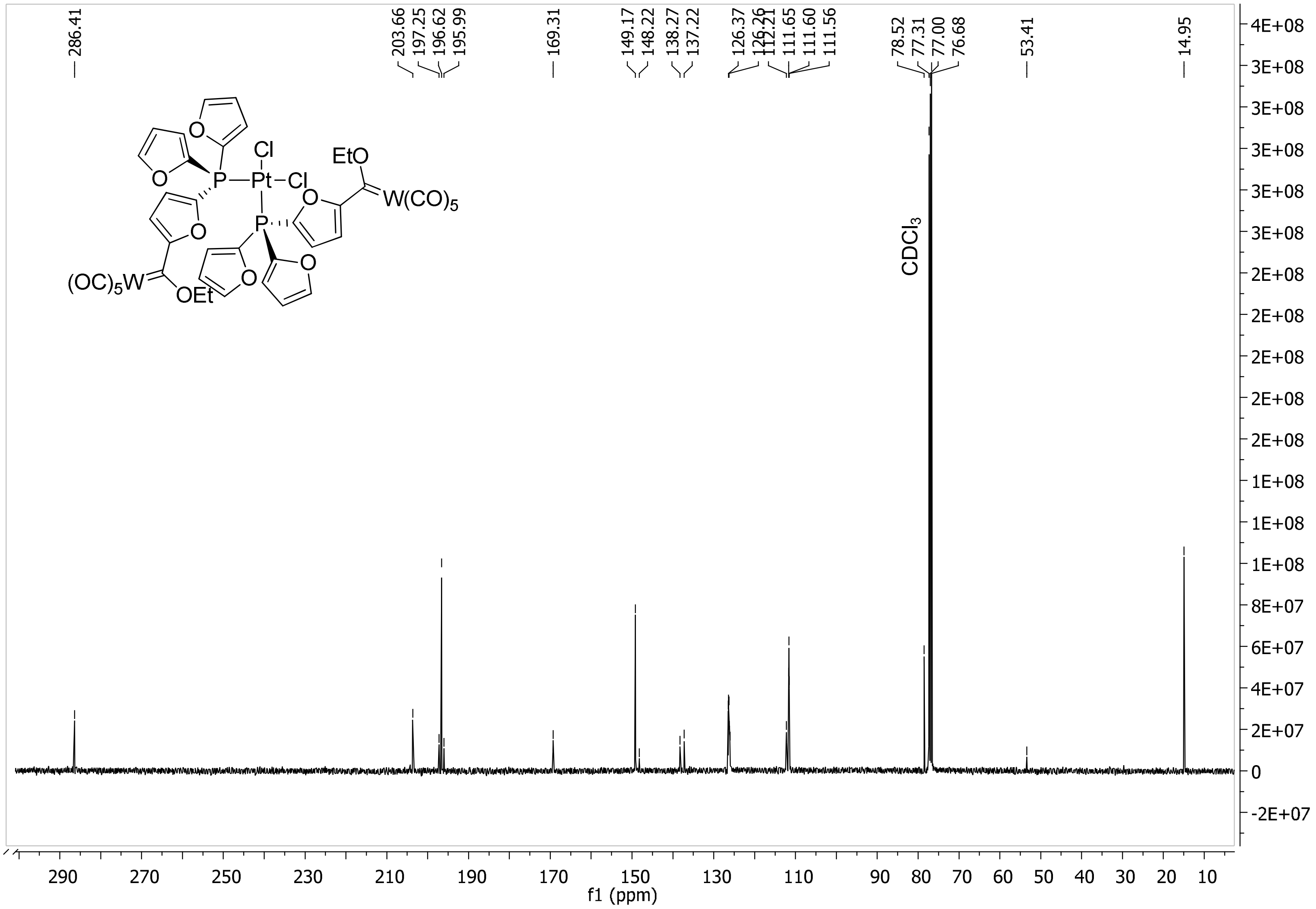

9b ^{31}P NMR spectrum

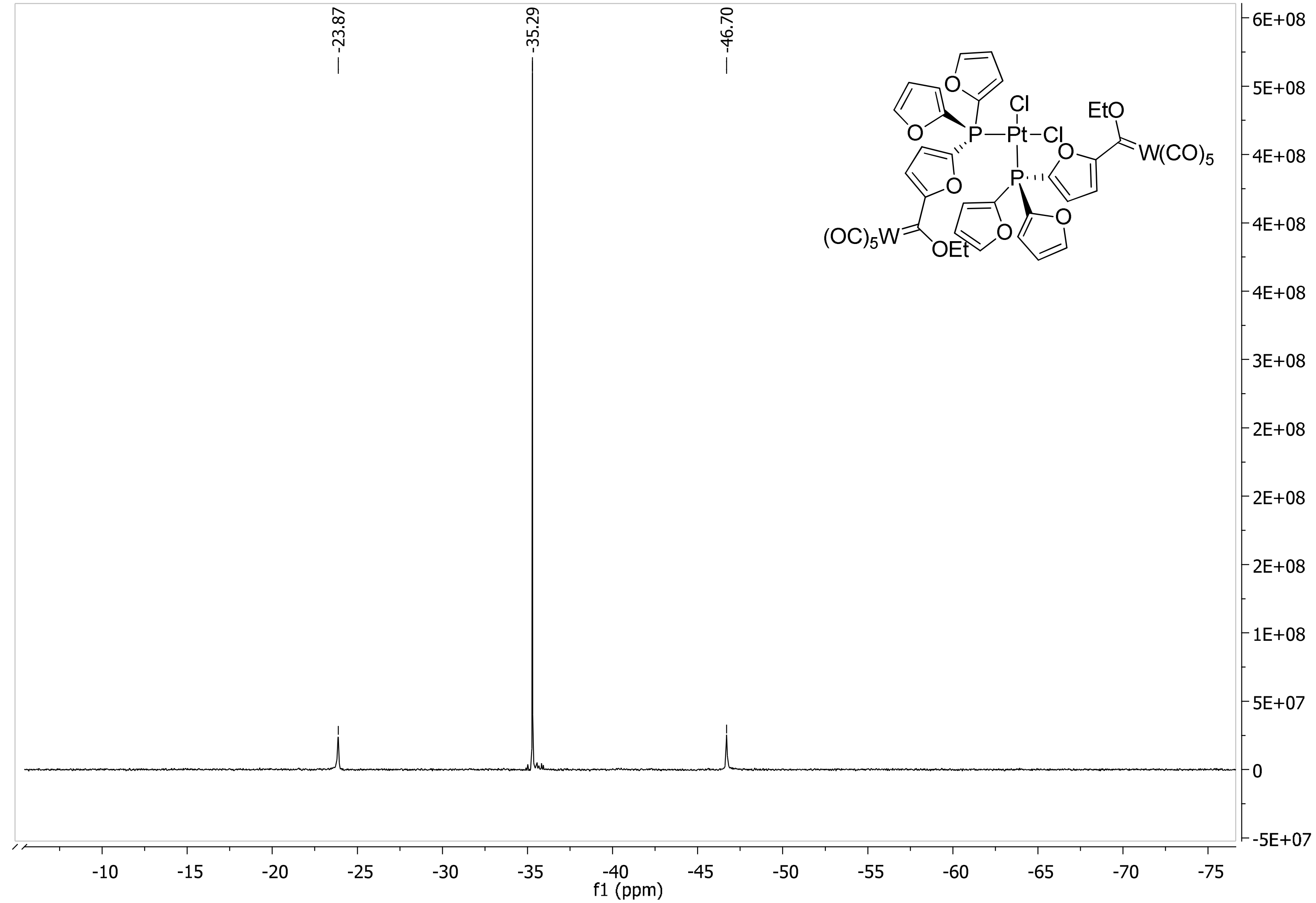

B(a)[1] ^{1}H NMR spectrum

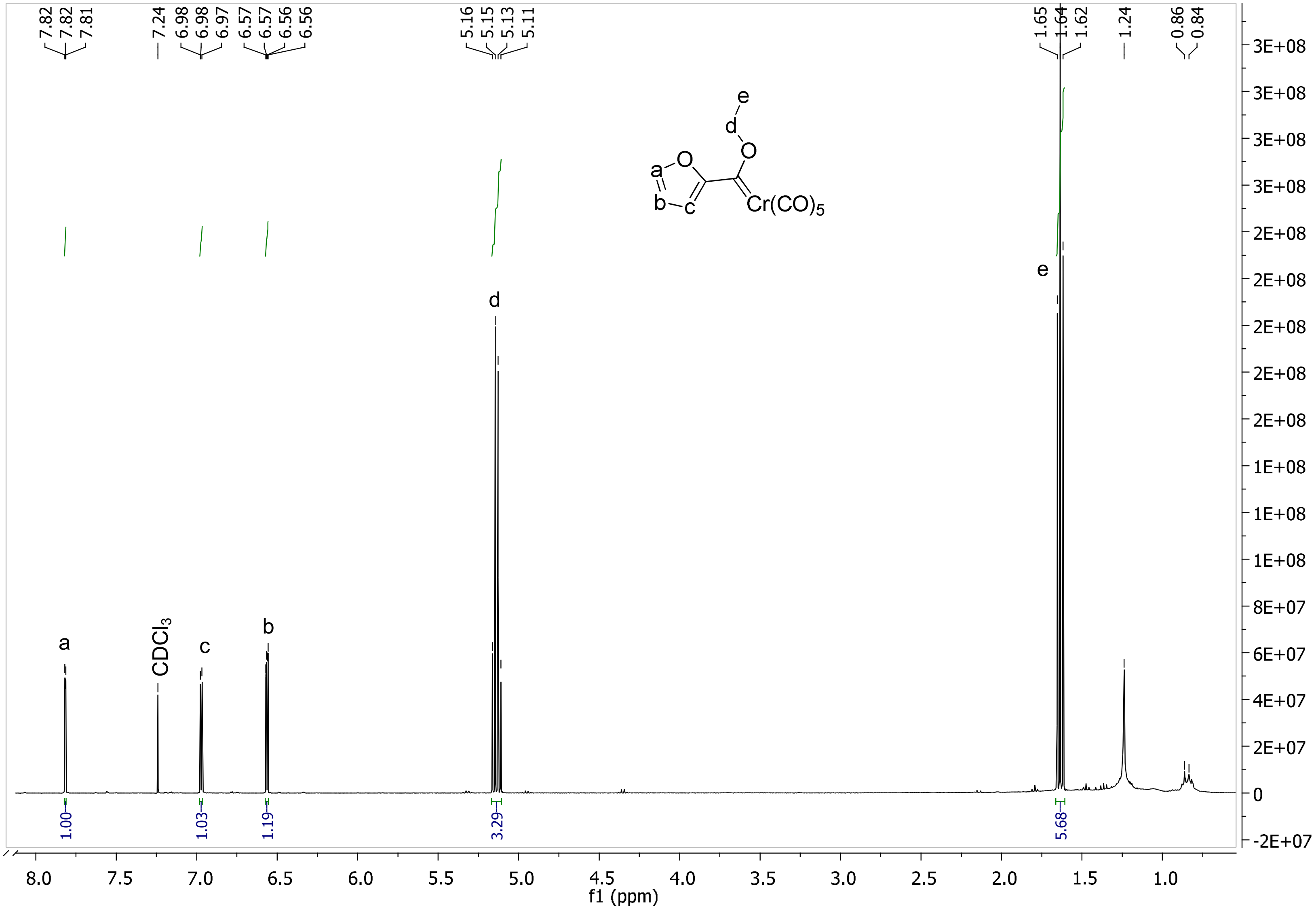

B(a)[1] ^{13}C NMR spectrum

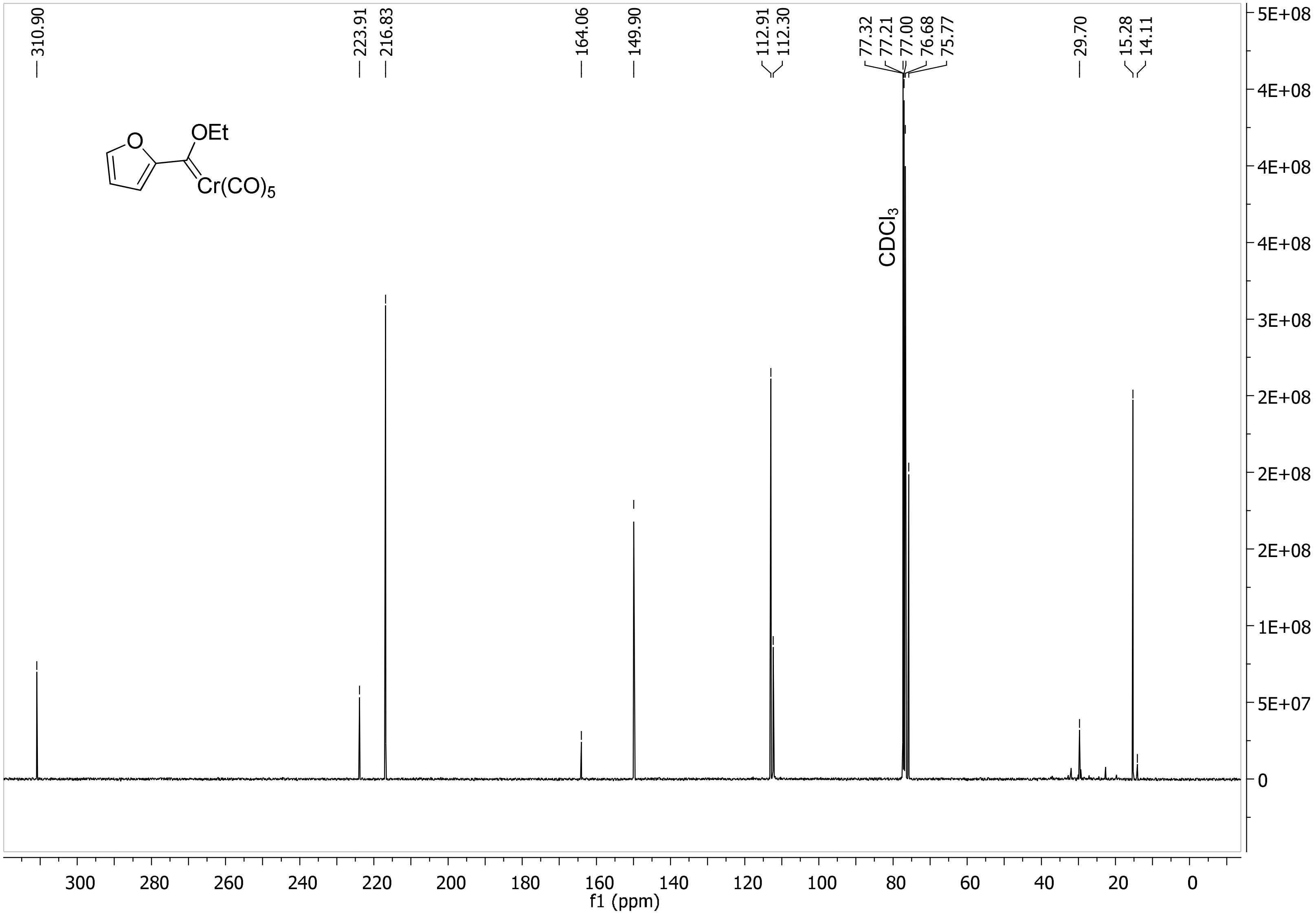

B(b)[1] ^{1}H NMR spectrum

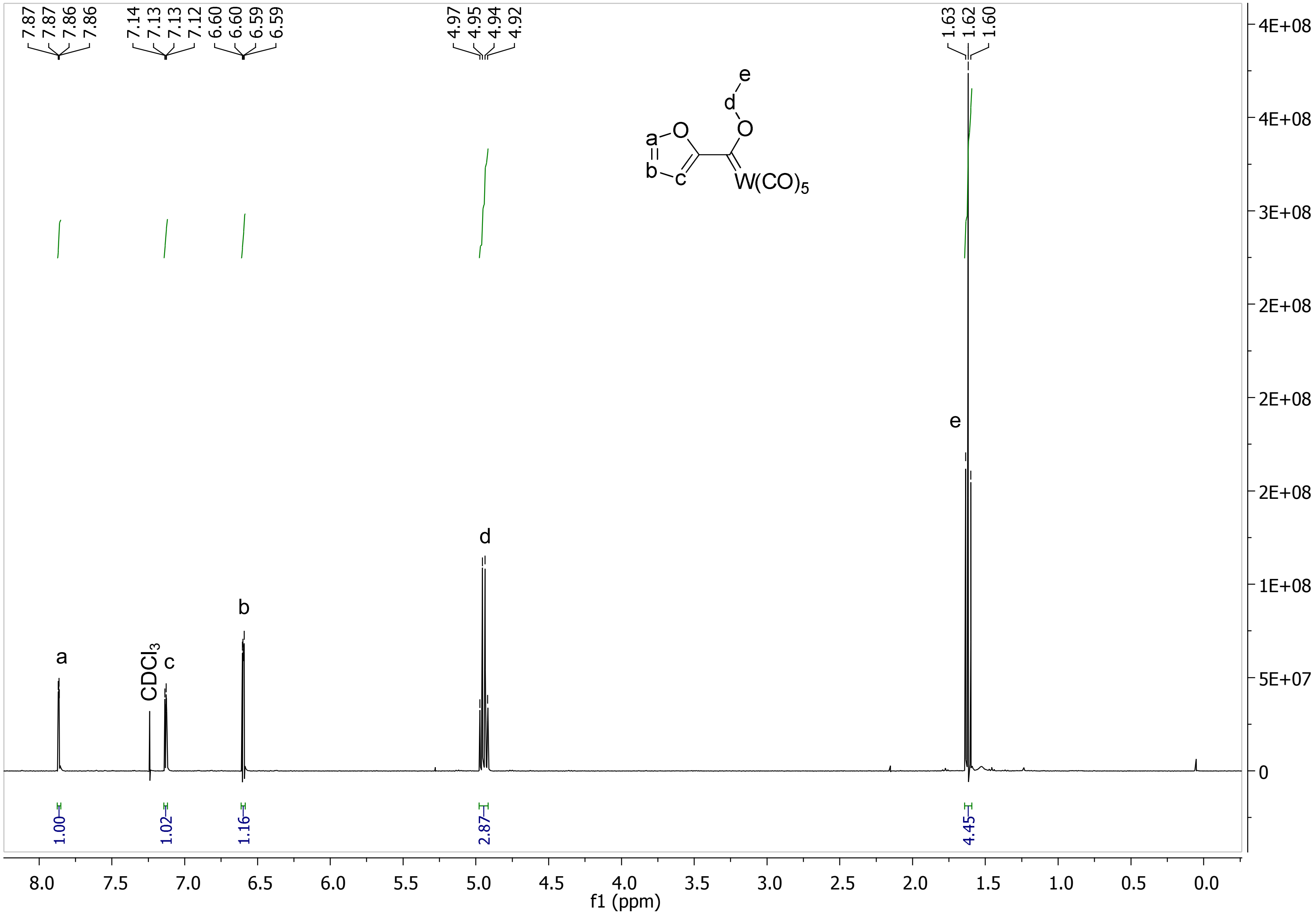

B(b)[1] ^{13}C NMR spectrum

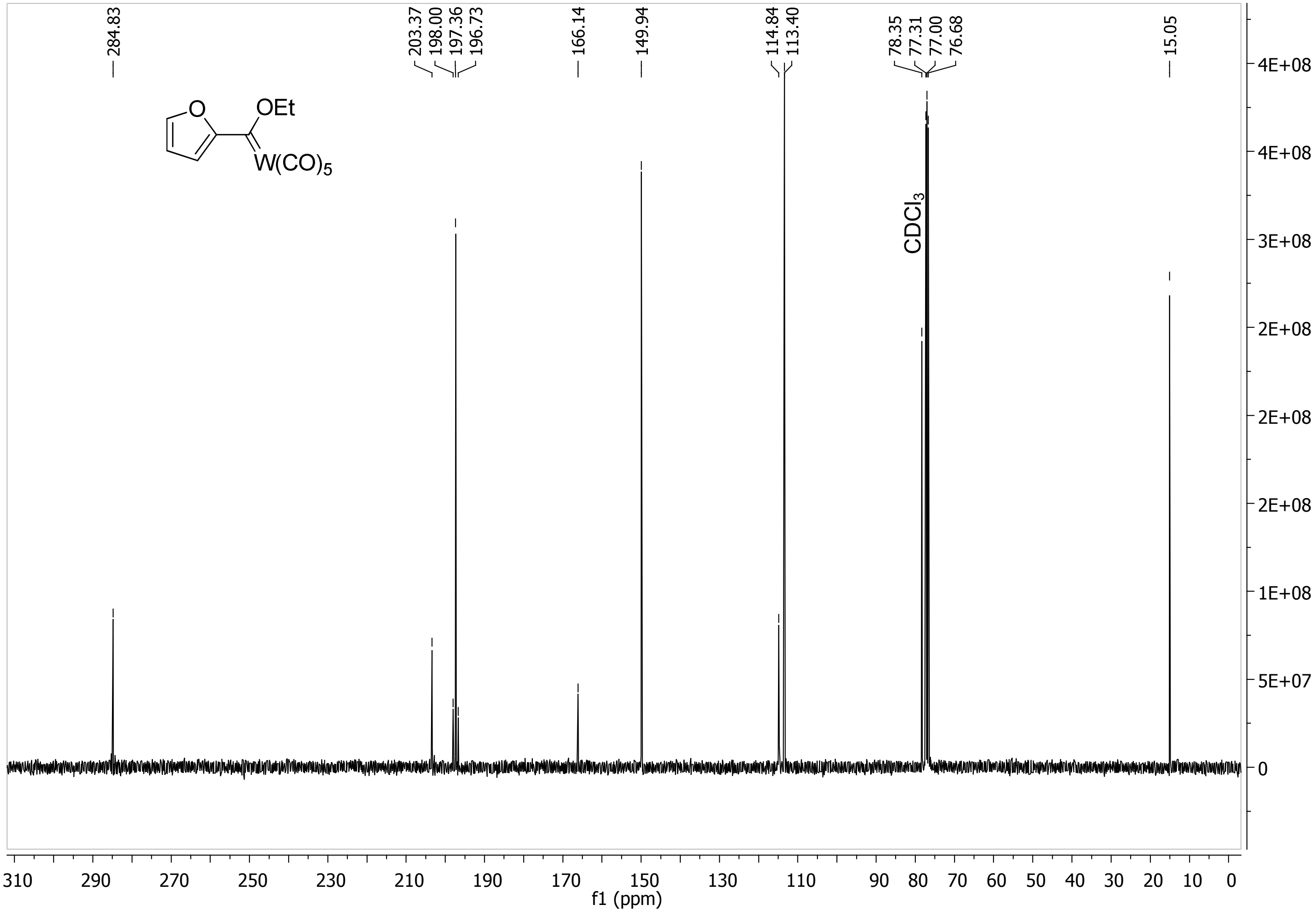

C(a)[1] ^{1}H NMR spectrum

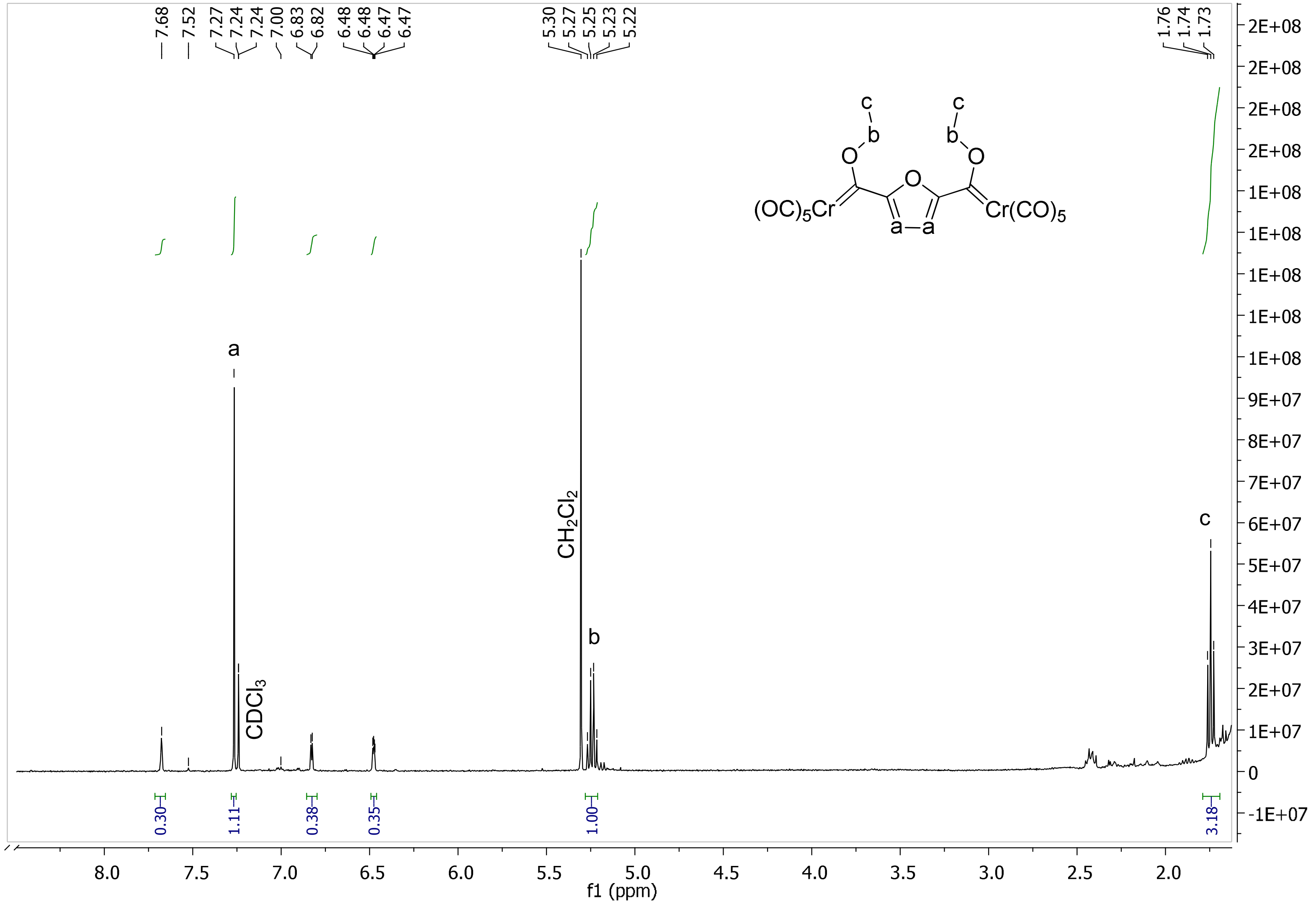

XRD Data and Parameters

Table S1. Crystal data for complexes **1a’**, **1b** and **2b**.

		1a’	**1b**	**2b**
Empirical formula		$C_{26}H_{19}CrNO_6$	$C_{26}H_{17}Br_2NO_6W$	$C_{34}H_{22}BrNO_{12}W_2$
Formula weight (g/mol)		493.42	783.07	1084.13
Temperature (K)		100(2)	150(2)	150(2)
Colour		Orange	Orange	Red-black
Wavelength (Å)		0.71073	0.71073	0.71073
Crystal system		triclinic	monoclinic	monoclinic
Space group		*P -1*	*C 2/c*	$P\ 2_1/c$
Unit cell dimensions (Å, º)	*a*	9.2423(6)	51.9931(16)	19.5309(13)
	b	9.7790(7)	6.4100(2)	22.5776(15)
	c	13.6276(9)	15.6570(5)	7.9946(5)
	α	82.9800(10)	90	90
	β	71.6530(10)	95.9360(12)	90.262(2)
	γ	82.6000(10)	90	90
Volume ($Å^3$)		1154.95(14)	5190.1(3)	3525.3(4)
Z		2	8	4
Density (calculated) (Mg/m^3)		1.419	2.004	2.043
Absorption coefficient (mm^{-1})		0.538	7.572	7.717
F(000)		508	2976	2048
Crystal size (mm^3)		0.36 x 0.26 x 0.18	0.370 x 0.149 x 0.022	0.433 x 0.095 x 0.048
θ range for data collection		2.77 to 28.34	2.363 to 30.507	2.272 to 30.520
Index ranges	*h*	-12 – 12	-74 – 74	-27 – 27
	k	-12 – 12	-9 – 9	0 – 32
	l	-18 – 17	-22 – 22	0 – 11
Reflections collected		13933	124024	15782
Independent reflections		5513 [*R*(int) = 0.0256]	7933 [*R*(int) = 0.0539]	13593 [*R*(int) = 0.0436]
Completeness to θ = 25.242°		99.80%	100.00%	99.90%
Refinement method		Full-matrix least squares on F^2	Full-matrix least squares on F^2	Full-matrix least squares on F^2
Data / restraints / parameters		5513 / 0 / 308	7933 / 0 / 326	15782 / 0 / 454
Goodness of fit on F^2		1.053	1.056	1.104
R indices [$I>2\sigma(I)$]		$R1 = 0.0369$, $wR2 = 0.0889$	$R1 = 0.0288$, $wR2 = 0.0719$	$R1 = 0.0377$, $wR2 = 0.0784$
R indices (all data)		$R1 = 0.0457$, $wR2 = 0.0929$	$R1 = 0.0375$, $wR2 = 0.0767$	$R1 = 0.0493$, $wR2 = 0.0829$
Largest diff. peak and hole ($e.Å^{-3}$)		0.353 and -0.379	1.973 and -1.820	3.201 and -1.701

Full crystallographic structure details for complexes **4b** and **9b** may be obtained in electronic *CIF* format from the Cambridge Crystallographic Data Centre as CCDC 967603 and CCDC 967604 respectively.

Table S2. Crystal data for complexes **4b** and **9b**.

		4b	**9b**
Empirical formula		$C_{20}H_{13}O_9PW$	$C_{40}H_{26}Cl_2O_{18}P_2PtW_2$
Formula weight (g/mol)		613.13	1490.24
Temperature (K)		150(2)	150(2)
Colour		Red	Red-black
Wavelength (Å)		0.71073	0.71073
Crystal system		monoclinic	monoclinic
Space group		*C*2/*c*	$P2_1/n$
Unit cell dimensions (Å, º)	*a*	40.3819(18)	12.209(3)
	b	7.6045(3)	10.307(3)
	c	13.7313(6)	37.771(11)
	α	90	90
	β	93.651(3)	97.669(5)
	γ	90	90
Volume ($Å^3$)		4208.1(3)	4170(2)
Z		8	4
Density (calculated) (Mg/m^3)		1.932	2.101
Absorption coefficient (mm^{-1})		5.616	8.088
F(000)		2360	2800
Crystal size (mm^3)		0.264 x 0.088 x 0.071	0.445 x 0.166 x 0.052
θ range for data collection		2.726 to 36.317	2.049 to 28.697
Index ranges	*h*	-67 – 67	-16 – 16
	k	-12 – 12	-13 – 13
	l	-22 – 22	-51 – 51
Reflections collected		153596	131301
Independent reflections		10217 [*R*(int) = 0.0548]	12011 [*R*(int) = 0.0816]
Completeness to θ = 25.242°		99.90%	99.30%
Refinement method		Full-matrix least squares on F^2	Full-matrix least squares on F^2
Data / restraints / parameters		10217 / 0 / 281	12011 / 558 / 599
Goodness of fit on F^2		1.112	1.044
R indices [$I>2\sigma(I)$]		$R1 = 0.0231$, $wR2 = 0.0506$	$R1 = 0.0385$, $wR2 = 0.0714$
R indices (all data)		$R1 = 0.0342$, $wR2 = 0.0541$	$R1 = 0.0667$, $wR2 = 0.0790$
Largest diff. peak and hole (e.$Å^{-3}$)		2.425 and -0.606	2.120 and -1.079

References

(1) Crause, C.; Görls, H.; Lotz, S. *Dalton Trans.* **2005**, 1649–1657.